Design and Study of Nanomaterial-Based Flexible Antennas for Sensing Applications

THESIS

Submitted in partial fulfillment
of the requirements for the degree of
DOCTOR OF PHILOSOPHY

by

Battina Sindhu
ID No. **2019PHXF0029H**

Under the Supervision of

Dr. Sourav Nandi
&
Under the Co-Supervision of

Dr. Parikshit Sahatiya

BITS Pilani
Pilani | Dubai | Goa | Hyderabad

BIRLA INSTITUTE OF TECHNOLOGY AND SCIENCE, PILANI
2024

Birla Institute of Technology and Science, Pilani

Certificate

This is to certify that the thesis entitled, "*Design and Study of Nanomaterial-Based Flexible Antennas for Sensing Applications*" is submitted by **Battina Sindhu** ID No. **2019PHXF0029H** in partial fulfillment of the requirements of **DOCTOR OF PHILOSOPHY** embodies the work done by her under our supervision.

Supervisor
Dr. Sourav Nandi
Assistant Professor,
BITS-Pilani Hyderabad Campus
Date:

Co-Supervisor
Dr. Parikshit Sahatiya
Assistant Professor,
BITS-Pilani Hyderabad Campus
Date:

Declaration of Authorship

I, **Battina Sindhu**, declare that this Thesis titled, 'Design and Study of Nanomaterial-Based Flexible Antennas for Sensing Applications' and the work presented in it are my own. I confirm that:

- This work was done wholly or mainly while in candidature for a research degree at this University.
- Where any part of this thesis has previously been submitted for a degree or any other qualification at this University or any other institution, this has been clearly stated.
- Where I have consulted the published work of others, this is always clearly attributed.
- Where I have quoted from the work of others, the source is always given. With the exception of such quotations, this thesis is entirely my own work.
- I have acknowledged all main sources of help.
- Where the thesis is based on work done by myself jointly with others, I have made clear exactly what was done by others and what I have contributed myself.

Signed: _____

Date: _____

Acknowledgements

A motivational trigger is always necessary to start any work, and then it goes on. I seek that trigger from my father, who aspires to improve his knowledge regardless of the difficulty involved. At one point or another, we need a hint to crack the puzzles that carry the work forward. With the support of many people, this work reached its current form.

Most importantly, I would like to express sincere gratitude to my supervisor, **Dr. Sourav Nandi**, for his guidance and advice throughout this research. He just believed in me and spared sufficient time to complete every task, resulting in the conclusion of this thesis. He is very patient in clarifying my doubts and making me understand better. I have learned many things professionally and personally through countless discussions. Further, I am also profoundly grateful to my co-supervisor, **Dr. Parikshit Sahatiya**, who has always received my discussions and clarifications with a broad smile while guiding me throughout the research work process. His feedback and suggestions helped me to refine the research outcome.

Besides my supervisor and co-supervisor, I would like to thank my Doctoral Advisory Committee members (DAC), **Prof. Runa Kumari** and **Dr. Sayan Kanungo**, for their productive reviews and suggestions that assisted in progressing my research work. In all my presentations and research, they added extra points and helped mold the work to reach its correct path. I would also like to thank the former and current Doctoral Research Committee (DRC) Conveners **Prof. Prasant Kumar Pattnaik**, **Dr. Prashant Wali**, **Prof. BVVSN Prabhakar Rao**, and **Prof. Sudha Radhika** and DRC members of the department who does the background work for the smooth completion of our research. I am grateful to the former and the current HoDs, **Prof. Sanket Goel**, **Prof. Alivelu Manga Parimi**, and **Prof. Subhendu Kumar Sahoo**, for their continuous commitment while fulfilling our requirements towards research.

I would also like to acknowledge the office & technical staff of the EEE department for their help during my research and lab teaching assistance, especially **Mr. K. Anjan Kumar**, who guided me through my work when needed. Also, thanks to the technical staff of Central Analytical Laboratory, who assisted me in the initial phase of this work.

I would like to thank **Prof. Venkata Vamsi Krishna Venuganti**, Associate Dean, Academic Graduate Studies and Research Division (AGSRD), for all the administrative

support I received throughout my research tenure. I also thank **Mr. Praveen** from the AGSRD office for his consistent help during the doctoral program. I also thank the former EEE staff and current AGSRD member **Mr. Rajesh Kumar K** for his continuous support in the documental work and blissful wishes. I wish to extend my appreciations to all the non-technical departments, especially the gardening and maintenance departments, for maintaining the campus serene by making it a beautiful place to stay.

A special thanks to the director, **Prof. G. Sundar** of BITS Pilani, Hyderabad Campus. I am also grateful to the **Electrical and Electronics Engineering Department** for granting the necessary facilities and aid to accomplish this research work.

I would like to acknowledge my co-scholars, notably **Dr. Arun Mohan**, **Dr. V. Sarath Sankar**, **Mr. B. Dheerendranath**, and **Ms. P. Priyalatha** from Advanced Computing Lab, who guided me in solving problems efficiently through numerous discussions and suggestions. I would also like to thank all my co-scholars who helped me with my initial phase of work while working in the RF & Microwave Lab, MEMS, Microfluidics and Nanoelectronics Lab, and Electronic Materials and Devices Lab.

With cheerful friends, building an enthusiastic environment for dedicated research is easier. The walks and talks around the campus with all my friends from intra and inter-departments make my thoughts lighter when stressed. I feel more lively with these friends who believe in me no matter what I do, always give me a shoulder pat, and go everywhere with me. Collectively, all of us were in the same phase of searching the shore by sailing a boat of research while withstanding high tides and learning to sail smoothly.

A special note of acknowledgment to my family, and I am forever grateful to my dearest Nanna, **Mr. B. Seshu Babu**, who always gave me a positive ray of hope. To my loving Amma, **Mrs. B. Sarada**, for continuously strengthening me to withstand any situation. Because of her, I am so calm and composed. **Dr. B. Anusha**, my little loving sister, always cheers me up while creating a fun-filled environment and also stays as a pillar of strength for our family. Also, my deep gratitude, especially to my maternal grandmother (**Ch. Krishna Kumari Amma**), grandfather (**Ch. Ramadasu Garu**), and all other relatives, whose morals and blessings are always with me, made me reach this phase to create one of the memorable acknowledgments of my life.

Abstract

With the transition to wireless technology, antennas are one of the most availed electronic devices incorporated along with the systems where wireless data transmission is necessary. However, as flexible technology has become more popular, it has led to the development of flexible antennas for sensing purposes. These antennas reduce the number of components while having dual or multi-functional capability and are adaptable to any structural surface. The antenna sensor exhibits both communication and sensing mechanisms using a single device. Initially, the conventional rigid antennas used additional elements for sensing property, which makes the antenna geometry bulky. Also, they could not accommodate the conformability towards any uneven structural surfaces. The antenna as a sensing device requires a sensitive section through which it can sense directly without using additional devices. Hence, the flexible or stretchable dielectric material with conducting metallic or nanomaterial-based materials shows a drastic growth for antennas in sensing purposes.

Mostly, microstrip technology is designed with various combinational soft materials for its dielectric and conducting elements to be effectively used as antenna sensors. These pliable materials are the essential factors that developed the flexible antenna as a sensor instead of a traditional sensor that senses variations in current or voltage. Mainly, the radiating element of the antenna holds a key role in sensing the applied physical measurand by exploiting the electromagnetic performance of the antenna. The antennas with flexible metallic materials (e.g. cu tape, al film) having high electrical conductivity leading to excellent electromagnetic performance were used for sensing, but the metals are not so sensitive towards diverse applications. Fortunately, the utilization of nanomaterials as the conducting element of the antenna extended a wide range of antenna-based sensing applications.

These nanomaterials are very sensitive to any applied external physical parameters. Unlike rigid, flexible metals and nanomaterials have the advantage of flexible morphological structures and different chemical compositions. Hence, any structural or chemical changes in the nanomaterial can directly be sensed through their electrochemical properties. With nanomaterials as an added advantage, the research is expanding towards developing antenna sensors for various applications by creating novel nanomaterials and making the fabrication process less complex, enabling bulk production. Therefore, one of the main

parts of this work is carried out in developing flexible antennas for sensing applications by using nanomaterials as radiating elements.

This work reports on developing the nanomaterials, studying their morphology, chemical composition, fabrication methods, and the sensing analysis of the antenna as a sensor. The materials and their synthesis process used for creating and utilizing them as radiating elements are laser-induced graphene, which is created by engraving polyimide sheet with a laser source, MXene material by minimally intensive layer delamination (MILD) process, and nickel diselenide ($NiSe_2$) through hydrothermal method. The obtained nanomaterials were further analyzed using different characterization techniques to confirm the existence of the produced material. By utilizing the above-described nanomaterials, different facile fabrication techniques were used in manufacturing the antenna for various applications such as laser engraving, laser cutting and drop coating, masking and coating, and PCB printing.

For contact-based sensing applications exclusively, using the antenna for different sensing parameters and its analysis as a sensor is discussed. Here, the antenna as a sensor is used for sensing strain (compressive and tensile), pressure, and level parameters. The sensing analysis is carried out based on the change in the $|S_{11}|$ parameter when an external parameter is applied in contact with the antenna. The antennas were examined for strain sensing under different bending and folding conditions, pressure sensing using various low-pressure loads, and for level sensing, liquids with differently concentrated solutions were used. As a result, these antennas showed a good sensing response towards the applied parameters. As a short-term or a binary sensor, a transient antenna is presented, which melts and dismantles with heat as an external trigger. It could be used as a disappearing antenna for security-related applications.

As a part of sensing, sensing analysis is performed through contactless wireless sensing for motion detection applications. The RF signal between the presented antenna pair is used for smart motion detection. The receiving antenna is made flexible to accommodate conformal applications. Here, the received power level of the RF signal at the receiving antenna is used as a parameter for motion detection sensing. The attenuation in power level varies for different types of obstruction.

A flexible SIW antenna is designed based on the one-sixteenth mode of a circular SIW cavity. SIW antenna, in this instance, is manufactured exclusively with flexible non-textile materials, making it useful for flexible planar antenna applications. Additionally, the

antenna is demonstrated for its flexible performance by straining it to the maximum extent without any structural damage. Consequently, the presented flexible SIW antenna is well suitable towards conformal wireless applications.

Contents

List of Tables

List of Figures

Abbreviations

EM - **E**lectro **M**agnetic

SAR - **S**pecific **A**bsorption **R**ate

FCC - **F**ederal **C**ommunications **C**ommission

RFID - **R**adio **F**requency **ID**entification

DFT - **D**ensity **F**unctional **T**heory

SIW - **S**ubstrate **I**ntegrated **W**aveguide

CMA - **C**onformal **M**icrowave **A**rray

LTCC - **L**ow **T**emperature **C**o-fired **C**eramics

LCP - **L**iquid **C**rystal **P**olymer

EGaIn - **E**utectic **Ga**llium **In**dium

ADC - **A**nalog to **D**igital **C**ircuits

MSA - **M**icro**s**trip **A**ntenna

MSP - **M**icro**s**trip **P**atch

MPA - **M**icrostrip **P**atch **A**ntenna

IoT - **I**nternet **o**f **T**hings

LIG - **L**aser **D**irect **W**riting

PI - **P**olyimide

ISM - **I**ndustrial **S**cientific **M**edical

SEM - **S**canning **E**lectron **M**icroscope

FTIR - **F**ourier **T**ransform **IR**nfrared

XRD - **X**-**R**ay **D**iffraction

XPS - **X**-Ray **P**hotoelectron **S**pectroscopy

VNA - **V**ector **N**etwork **A**nalyzer

RF - **R**adio **F**requency

GO - **G**raphene **O**xide

RGO - **R**educed **G**raphene **O**xide

KBr - **P**otassium **Br**omide

EMI - **E**lectro**M**agnetic **I**nterference

Al - **Al**uminium

MILD - **M**inimally **I**ntensive **L**ayer **D**elamination

LiF - **Li**thium **F**luoride

DI - **D**e-**I**onized

EDX - **E**nergy**D**ispersive **X**-Ray

FBW - **F**ractional **B**and**W**idth

EMI - **E**lectro **M**agnetic **I**nterference

TMD - **T**ransition **M**etal **d**i-chalcogenides

To the surrounding energy in every form ...

Chapter 1

Introduction

The antenna is the crucial interface between electronic devices and the invisible electromagnetic (EM) radiation, enabling wireless communication between devices. The current electronics technology is advancing towards the compactness of devices with a flexible nature in developing cost-effective, lightweight, deformable, and conformal devices by offering novel opportunities in the fields of communication, biomedical and aerospace [1]. The conventional rigid antennas with a fixed geometry restrict their adaptability to accommodate diverse applications that necessitate the ability to conform to curved surfaces. Consequently, flexible antennas have gained enormous interest due to their deformable nature and the conformal ability to irregular surfaces and dynamic structures.

1.1 Flexible Antenna Applications

Flexible antennas with simple structures are becoming prominent in the wireless communication sector by expanding their applications towards various fields as shown in Fig. 1.1. The selection of materials, design considering material characteristics, and fabrication process for the flexible antennas are entirely application-dependent [2]. Now-a-days as a part of smart home, almost many of the indoor devices are having wireless connectivity, which serves a part of continuous monitoring. The internet of things (IoT) concept utilized by communication technology enhances and improves the device connectivity using various antenna designs over different frequency bands. Accordingly, the requirement of a compatible and conformal nature for flexible antennas with ultra-wideband grabs attention towards the selection of easily bendable materials for IoT applications [3], [4].

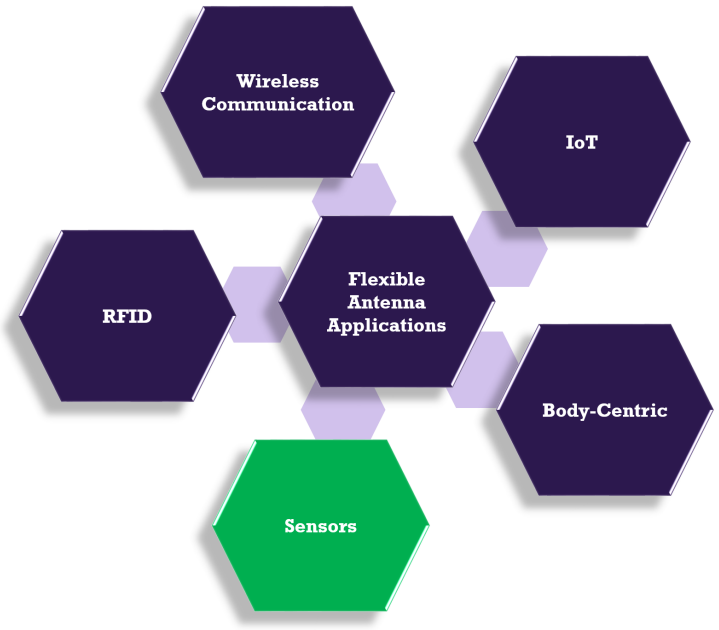

FIGURE 1.1: Applications of flexible antenna in various fields.

Lately, electronics are utilized within (Implantable) and outside (Wearable) the human body as part of body-centric applications when necessary, facilitating diverse wireless connections that provide the benefits of enhanced security and surveillance. When it comes to wearable antennas, the most desirable criterion is their lightweight nature, in this regard textile antennas have gained popularity as they are made from organic textile materials that are easily integrated with clothing [5], [6]. These designed antennas were also tested with specific absorption rate (SAR) due to the effect of human body on the wearable antenna [7]. Whereas, the implantable antennas are designed mainly by considering miniaturization and less power consumption with bio-integrated materials, since they should be radiating from inside the human body, which are open to many biomedical applications [8].

The antennas used for wireless communication applications include single, dual, multiband or ultra-wideband frequency, which is application dependent and is considered according to the Federal Communications Commission (FCC). The swift development of communications along with the increasing demands for flexible, adaptable, and bendable antennas has made printed antennas highly recommendable in the market [9]. The flexible dual or multiband printed antennas were utilized simultaneously for two or more different applications like Bluetooth, WLAN, WiMAX, and 5G, which enhanced the advancement of wireless communications in the market [10]–[12]. The flexible UWB antenna with less power consumption and high data rates makes it attractive for indoor applications [13].

As a part of wireless technology radio frequency identification (RFID) holds a crucial role in remote communication, without the need of external power. In general RFID is designed specifically for identification and tracking applications for short-range communication applications. The RFID tag manufactured with flexible and novel materials extended the RIFD technology to wide range of applicaitons. As for the upcoming 5G systems RFID device has a key role in integrating RFID technology with IoT as I-RFID while making data transfer secure. The flexible RFID tag as a sensor works with the help of additional components such as, logic control and energy harvesting modules to transmit the data through near-field communication [14].

The interest towards flexible antenna-based sensor is driven by several reasons, out of which it is mostly utilized for both wireless communication and sensing purpose with minimal components [15]. The EM characteristics of flexible antennas used exclusively for communication must remain stable in both conformal and non-conformal conditions. Whereas, flexible antennas, whose EM properties change while wrinkling, strain, and bending conditions would be significantly utilized for the advanced modern electronics such as antenna sensors. As a result, the flexible antennas made with textile, paper, or polymer make them highly captivating for the next generation devices. Hence, the utilization of soft materials for the microwave equipments have made a breakthrough towards various wireless sensing applications in expanding the future of flexible antennas as sensors.

1.2 Flexible Antennas for Sensing

The sensors are becoming exceedingly commercial in the wireless world, which converts physical measures into electrical signal for digital data transmission. For more than a decade, antenna-based sensors have grabbed a great attention due to their dual functionality, simple configuration, multimodality sensing with cost-effective methods. These sensors have the advantage of dual functionality, where it acts as a data transmitter and a sensor within single device [16]. The main principle of operation by using an antenna as a sensor is, that it converts various physical attributes like Humidity, pressure, strain, etc. into a measurable parameter that leads to a change in the electromagnetic characteristics of the antenna.

The antenna-based sensor acts as passive sensors, since it requires minimal components on-board for data transmission. It can be fabricated using inexpensive materials with

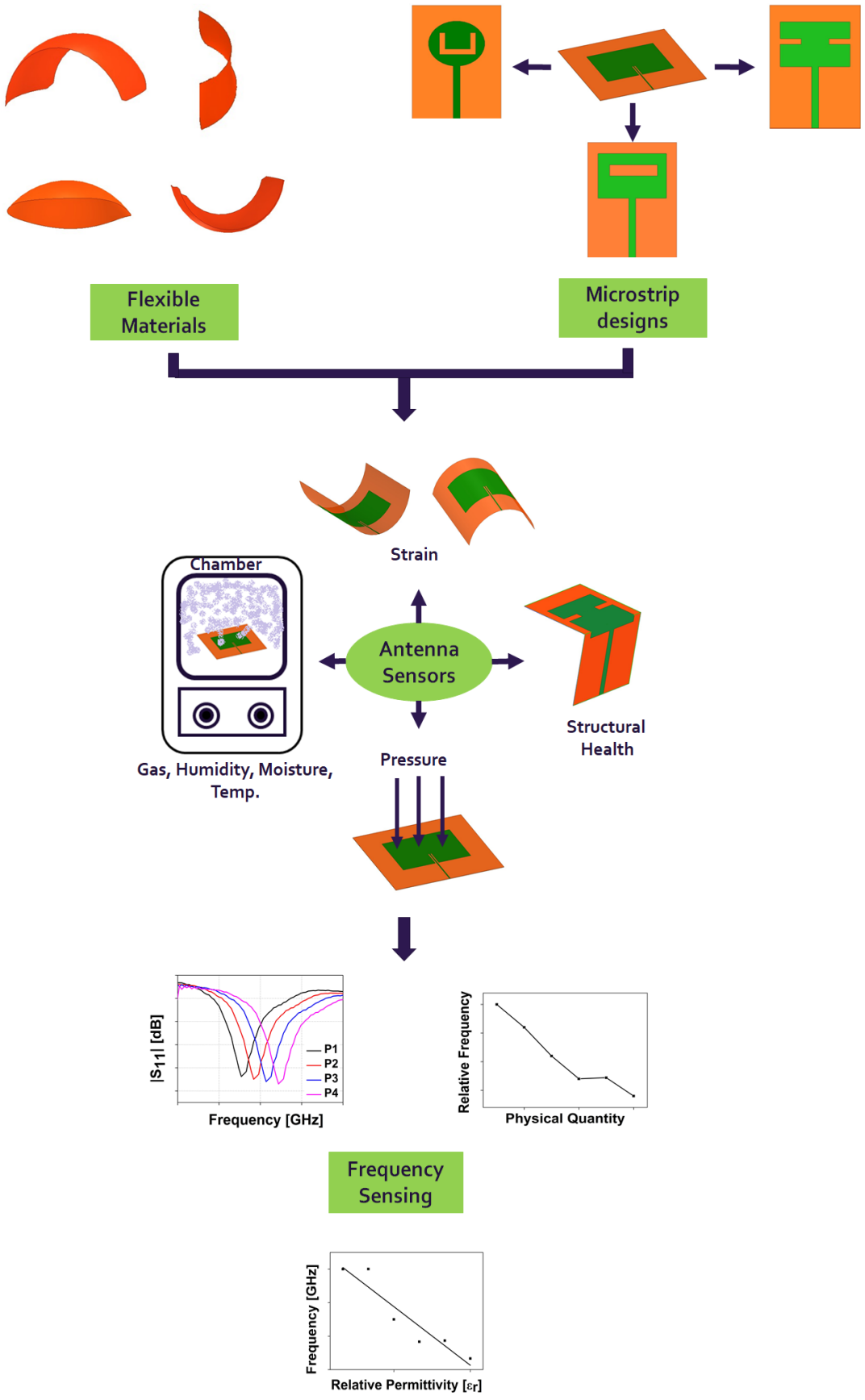

FIGURE 1.2: An overview of the flexible antenna sensors and their sensing parameters.

traditional and novel fabrication techniques. The integration of flexible antenna sensors in accordance with the device orientation to provide the wireless data transmission is necessary for further communication enhancement. Mostly, the first choice in choosing the antenna type for the antenna sensor is microstrip antennas, due to their narrow band nature, which is very convenient for sensing any physical parameter through the frequency variation. Also the simple design of the microstrip patch allows an easy fabrication along with bulk productivity.

For designing a flexible antenna sensor, the selection of material, designing techniques, and fabrication methods are necessary for customized applications as shown in Fig. 1.2. The function of the antenna as a sensor mainly depends on material selection and geometrical changes of the antenna in terms of resonant frequency, which is mostly measured by means of reflection coefficient for various physical parameters. By using the variations in antenna parameters, the measurement of diverse physical parameters is carried out with respect to sensitivity. The sensitivity relays on the resistive property and deformability of selected materials. The high sensing response with respect to frequency by altering the physical and chemical properties of the patch makes it a good candidate towards antenna based sensors for various applications in IoT.

1.3 Nanomaterials for Antenna Sensors

Currently, there is a high demand for developing various novel conducting and non-conducting materials along with the emerging fabrication techniques that can be utilized for manufacturing flexible devices [17]. Generally, the radiating portion of the antenna whether it is rigid or flexible with metal or nanomaterial, it detects and senses the variation in relative permittivity of any physical meausrand that is located in the radiation span of the antenna. Copper is the best-known conducting material used as a radiating element for all the traditional rigid antennas. But as the technology is scaling down to the Nano dimension, the flexible/conformal applications were also expanding by utilizing novel nanomaterials.

For fabricating the flexible antennas mostly copper, aluminium, and silver nanoparticle inks are often used as radiating elements in satellite communication [18], RFID [19], and other wireless communication systems [20]. These antennas normally consist of notable electrical conductivity for transmitting or receiving electromagnetic waves. Besides, resistance to degradation caused by mechanical deformation is also an important factor for

the conductive material. So, the performance of flexible antennas depends significantly on the electrical conductivity of the material and its deformable nature [21]. Flexible antennas manufactured using flexible metals are recommendable for wireless communication and by using extra supporting elements they were also utilized for sensing purpose. But by considering nanomaterial as a radiating element, the antenna itself can act as a device for both communication and sensing purpose.

Compared to flexible metals the nanomaterials are ultra-flexible in terms of their structure, which adds an extra advantage in enhancing the sensitivity of the antenna. The antenna-based sensors utilizing different nanomaterials as the conducting part for sensing various physical measurands can be categorized into two cases. In the first case, since different nanomaterials have different morphological structures, they can sense the deformations easily for the physical quantities like strain, pressure, crack, structural health monitoring, and motion detection. Secondly, the nanomaterial takes a key role in sensing some sensing applications like, gas, pH, temperature, Humidity and moisture by changing its chemical and electrical properties. Hence, the deformations or changes in chemical and electrical characteristics of the nanomaterial tend to enhance the sensitivity of the antenna as a sensor while exploiting its EM properties.

1.4 Motivation

Recently, the usage of flexible and semi-flexible antennas increased drastically over the conventional rigid antennas mainly because of their flexible, conformable and deformable nature. Several wireless applications adopted the flexible antennas due to their structural adaptability towards any uneven surface. Out of which flexible antenna sensors gained more interest because of their dual ability of communication and sensing with a single device. The antennas possessing conformal nature can be attached to any of the structural surfaces without much effect on the antenna's EM performance for flexible related applications. But when it comes to the antenna for sensing purposes, the EM properties were exploited to sense the applied physical parameter. This attention to flexible antennas has extended not only to the flexibility but also to sensing by considering the effect on EM performance as an advantage.

Antennas as a sensor measure the properties of materials based on EM radiation and its interaction with matter. The selection of material is necessary with various physiochemical characterizations for flexible and highly sensible applications. Based on

the properties of the material, the EM characteristics of the antenna changes accordingly. Specifically, the electrical, chemical and mechanical properties of the selected material were considered for the sensor applicative-based utility. Moreover, functional nanomaterials are more sensitive to the physical parameters applied when compared to the conducting metals for sensing applications. These conducting nanomaterials serve as a base for electronic devices in broad range of applications that needs stretching, straining, bending, and folding among other physical attributes that could not be attained by traditional devices. Therefore, the advancement of new methods for flexible microstrip antennas is necessary in selecting the materials and manufacturing the device by maintaining the EM performance of the antenna while enhancing its sensitivity towards various sensing applications.

1.5 Objectives

- By the investigation and characterization of the nanomaterials as the conducting part of an antenna, it is possible to create a less expensive material with a highly flexible nature for real-time wireless sensor, which contributes in enhancing the sensing capability of the antenna.
- To analyse the flexible antennas for various sensing applications while exploiting the essential radiation characteristics of the antenna.
- To design and develop a miniaturized/low-profile planar nanomaterial-based antenna through an effective fabrication process enabling bulk production for short-range wireless communication purposes.

1.6 Thesis Overview

Chapter 1 gives a short introduction about flexible antennas and their applications. The discussion on the antenna as a sensor and the importance of using various flexible materials along with microstrip designs and simple fabrication techniques for expanding sensing applications. Additionally, the analysis of how nanomaterials stand in enhancing the sensitivity parameter of antenna.

Chapter 2 discusses the historical background for the development of flexible antennas based on nanomaterials, which opened the door for expanding the applications involving

various sensing parameters. Surveying diverse nanomaterial-based antennas by understanding the characterization of the materials and their performance towards EM radiation. Studying antenna sensors in response to various applicative physical quantities with their principle of operation and methods for investigating the antenna as a sensor.

Chapter 3 presents a direct laser-induced graphene engraved flexible microstrip antenna for human motion monitoring by giving an insight into the fabrication process. The chemical characteristics of LIG were investigated by various morphological and composition-based characterization techniques, to confirm the formation of graphene. While assessing the strain and its effect on LIG material, the sensitivity of patch antenna is analyzed. In order to explore the feasibility of using the manufactured prototype for real-time applications, the fabricated prototype is attached to a human hand for the purpose of monitoring motion.

Chapter 4 describes the importance of functional nanomaterials over metals as a conducting element of the antenna, particularly in the context of sensing applications. An MXene-based antenna prototype for pressure and level sensing is created and tested under different stability conditions to demonstrate its real-time sensing performance. A comprehensive demonstration of a versatile, affordable MXene-based antenna sensor is carried out. This opens new research directions for 2D materials-based antennas with potential uses in security, healthcare, and other fields.

Chapter 5 proposes a transient/nanomaterial-based antenna using hydrothermally synthesized few-layered $NiSe_2$ as a short-term pressure sensor. One of the main contributions is developing a generic theoretical framework by combining the Density Functional Theory (DFT) calculations with $|S_{11}|$ - Parameter analysis for designing and reliably analyzing the transduction mechanism of such a sensor. The prototype of the designed antenna is extensively tested and analysed for pressure-sensing capability along with the transient behaviour, demonstrating it as a highly promising sensor for transient technology-based wireless sensing applications.

Chapter 6 illustrates a study on contactless flexible antenna-based motion sensor for smart wireless communication. Here, two separate antennas for transmitting and receiving the RF signal were considered at 2.44 GHz resonant frequency for contactless wireless motion detection. The operating principle of the antenna as a motion sensor is explained by detecting the attenuated power of the received RF signal at the receiving antenna in the presence of obstruction. This theory demonstrates in expanding contactless technology-based motion sensing for smart-home and short-range wireless applications.

Chapter 7 introduces a miniaturized sixteenth-mode nanomaterial-based flexible substrate-integrated waveguide (SIW) antenna. The miniaturized geometry of the sixteenth-mode SIW is elaborated from the cavity-backed circular SIW antenna. The advancement of the sixteenth-mode design, along with the step-by-step manufacturing process of the flexible SIW, is detailed. The SIW antenna prototype has undergone flexibility demonstration by straining it to the maximum extent without structural damage, showing its adaptability toward conformal applications.

Chapter 8 concludes the work presented in this thesis by sorting it according to the conceptual analysis, such as antenna for sensing purpose, transient antenna for security-related applications, contactless antenna-based sensing, and flexible SIW antenna. It provides an insight to the future research expansion in nanomaterial-based flexible antennas for wireless sensing applications with miniaturized designs and simple fabrication process.

Chapter 2

Background & Literature

2.1 Historical Background

In the microwave domain, the idea of flexible structures came into existence as smart aperture antennas, to reduce the complexity in structure while achieving directivity variation and increase in ground coverage [22]. They were made of adaptive materials and are utilized for beam scanning and shaping purposes without the need to relocate the antenna [23]. Sequentially, the notion of flexibility, the ability to accommodate structural adjustments while attaining desired radiation characteristics through diverse algorithms has emerged with a flexible space antenna reflector for satellite communication and space observation [24]. As a segment of the space antenna, because of the launcher capability, foldable rigid petals and knit gold-plated molybdenum wire as a reflective mesh were utilized to achieve compact stowage volume with a lightweight structure [25].

As depicted in the timeline Fig. 2.1, an entirely flexible or conformal antennas came into existence with the invention of the strip transmission line technique during the World War II epoch, which later replaced various conventional microwave components like waveguides and coaxial structures using Microstrip technology [26], [27]. Within a short period, the progress of the microstrip microwave antenna [28] made a revolutionary change in antenna technology [29] due to its lightweight, ease of fabrication, and planar geometry with thin structure. Consequently, the idea of conformability, characterized by their ability to wraparound the surface of the respective non-planar applicative devices was developed with a microstrip patch array [30] as a proper conformal antenna for avionic applications to provide omnidirectional coverage [31]. Due to space limitations, the antenna utilized in

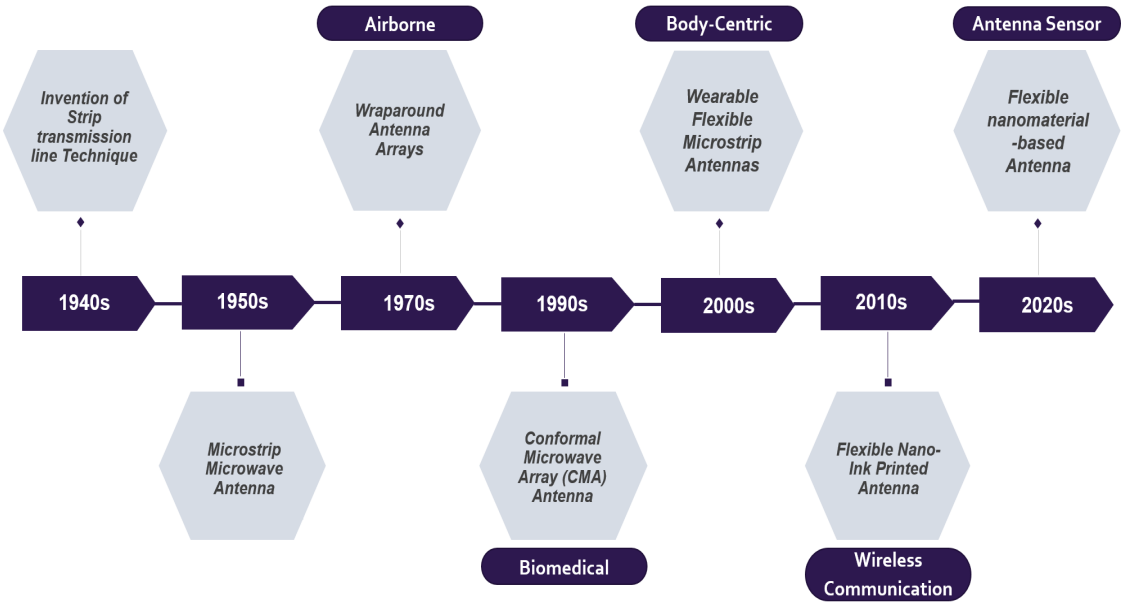

FIGURE 2.1: Timeline for the emergence of flexible antennas along with their applications.

avionics must be extremely thin with multi-functional capability and wraparound ability along with its adaptability to the changes in an open environment [32].

The requirement for small and portable antennas with a conformal nature prompted the research to dig deeper into the domain of microstrip antennas (MSA). Gradually, the simulative study of microstrip patch antenna (MPA) on curved and cylindrical surfaces with respect to planar MSP were initiated by investigating the RF parameters using different methods. Theoretical analysis of a cylindrical-based rectangular patch was presented for the effect of curvature on the resonant frequency [33], radiation pattern, input impedance and Q-factor [34]. By using Dyadic Green's function, the impact of dielectric thickness and dielectric constant on the radiation patterns of a wraparound antenna were obtained [35]. Likewise, the curvilinear FD-TD method was applied for numerically predicting the RF characteristics of MSA when mounted on the non-planar surface [36]. As an initial implementation, a conformal microwave array (CMA) was developed for the purpose of microwave hyperthermia in biomedical applications. To make the patient comfortable and to heat the tissue uniformly beneath each element, a flexible and less bulky CMA applicator was created on a single-layer copper foil [37], [38].

The growth of flexible concept utilizing MSP has enhanced within a short period towards wireless communication. Especially, the research towards flexible wearable antennas with multi-band characteristics has surged because of the invention of personal communication technology [39]. A single compact featherweight FlexPIFA antenna

operating at dual-band frequencies is presented to meet the demands of wearable wireless communication for long and short-range applications [40]. As a part of wearable technology, a patch antenna is entirely fabricated with textile material utilizing fleece fabric as substrate material and knitted copper for conducting part by analyzing the impact of the human body on the performance of the wearable antenna [39], [41]. A wearable antenna is made to test the variation in return loss and gain when bent in both E & H planes where a return loss difference of 25 MHz and 5 MHz respectively and a peak gain of 2.4 dB was shown [42].

The primary benefit of wearable antennas is that they can be easily integrable into clothing, which enabled a wide range of wireless wearable applications. A conformal wideband PIFA antenna is designed to offer reliable communications in the presence of its shape deformation on the space suit of an astronaut while monitoring their health and the ability to perform task in an unpredictable environment [43]. To achieve a better gain, a flexible linearly polarized eight-element array is fabricated with a conductive nora fabric on the felt substrate for use in industrial, scientific, and medical (ISM) band [44]. Another work presented a dual band textile antenna on an electro-magnetic bandgap (EBG) substrate for reducing back radiation when placed against human body [45]. In various studies, the textile-made antennas were performed almost similar to the conventional rigid antennas with an added advantage of flexibility for wearable purpose [46], [47].

For the MSP antenna to be flexible/conformal, various novel dielectric materials were introduced for mechanical flexibility, deformability, easy integration of components with lightweight [48]. Subsequently, the requirements of the flexible antenna were set forth for miniaturization and to provide a multilayer integration approach for system-on-package technology operating in Millimeter-wave frequency range. The usage of low-temperature co-fired ceramics (LTCC) [49] or organic liquid crystal polymer (LCP) [50] as dielectric materials offered a significant advantage in the development of flexible multi-layer technology for RF and microwave devices in easily integrating the circuit components between different layers.

The conducting part of the antenna holds a crucial role in influencing key performance parameters like radiation efficiency, directivity, resonant frequency, etc., Many conducting polymers and conductive materials based on nanomaterials were used to make the antenna flexible and helped in broadening its range of applications. A quantitative theoretical analysis of nanotubes and nanowires along with the exploration of their properties as antennas and their operation at microwave frequencies were studied [51]. Then, the research expanded to fabricate the antenna with conductive polymer inks and carbon

nanotubes (CNT) rather than metal conductors to take a further step toward conformal applications for energy harvesting [52], [53]. Also, the first graphene-based nano-antenna is developed with a thin graphene nano-ribbon for EM nano-communications in the terahertz band [54]. Nanomaterial-based antenna sensors grabbed great attention due to their quick responsiveness with electrochemical properties towards the applicative measurands [55]. By using nanomaterials, it is possible to develop devices ranging from one to few hundred nanometers, which serves as a building block for future nanotechnology based sensors.

2.2 Radiating Elements for Flexible Antennas

For the antenna to be completely flexible, the material selected for the patch as a radiating element should also be flexible, possessing excellent electrical properties. As shown in Fig. 2.2 and Fig. 2.3, various metal-based and nanomaterial-based conductive materials were utilized to make the radiating element of the antenna flexible for diversifying the flexible antenna applications. The materials utilized as radiating elements for the flexible antenna were classified as metal-based and nanomaterial-based materials.

2.2.1 Metal-Based

For metal-based flexible antennas, metals with high conductivity, such as aluminium, silver, and copper, were used for radiating elements in the form of foils and tapes. The conductive copper tape is used on a denim material to manufacture a flexible textile antenna with a simple planar geometry [56], [57]. A flexible antenna sensor with a simple design using aluminium tape is shown for identifying micro-strains, cracks, and folding [58]. A flexible copper wire antenna is made similar to the conductive E-Fiber antenna for the performance comparison [59]. A conformal log-periodic antenna with an aluminium foil on a balloon-shaped polyvinyl chloride is presented for VHF systems [60]. These conductive tape/film-based antennas, when bent, cannot deform back easily. Even though deformed, they will have wrinkles formed on their surfaces.

Various textile-based conducting materials were presented using different fabrication techniques due to a significant outreach towards wearable antennas. The conducting materials used for wearable antennas should withstand the harsh environment and fabric care washing, whereas metals are unsuitable for this application. A flexible conductive E-fiber-based wire antenna embedded into a stretchable polymer is presented for withstanding

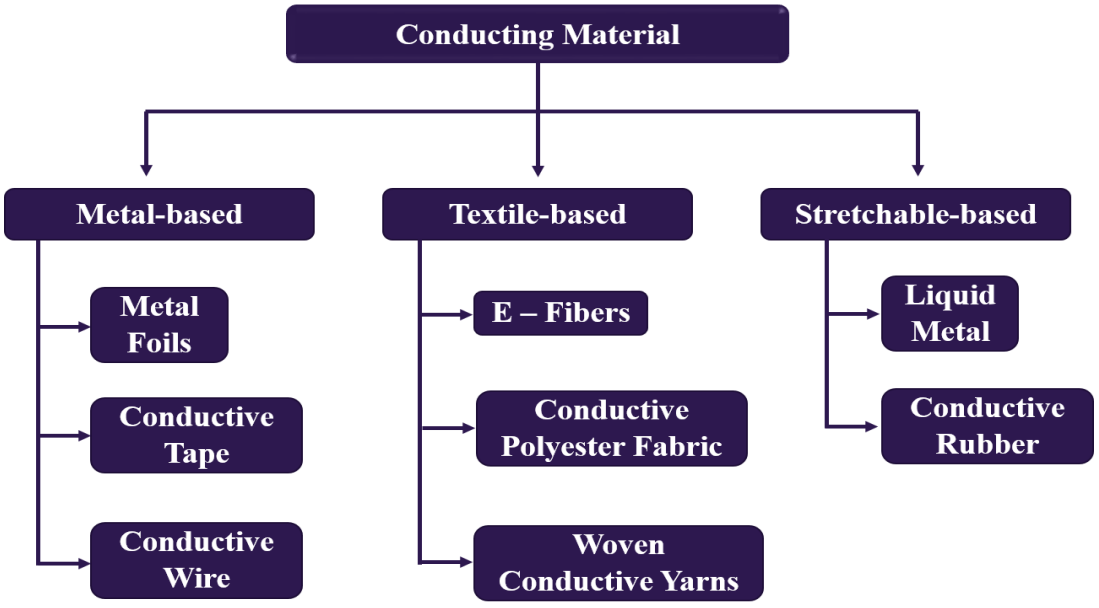

FIGURE 2.2: Metal-based flexible conducting materials utilized for antenna.

hostile environments [59]. The combination of nickel and copper conductive polyester fabric is considered for washable and reusable properties towards rough handling of antenna for daily usage [61]. To observe the weaving effect on the EM performance of the antenna, the copper yarn-weaved radiating element in parallel and perpendicular to the feeding directions is simulated and measured [62]. Nevertheless, these fabric-based antennas need specialized equipment to include the conductive components seamlessly. They also cause difficulties while integrating the connector and feedline.

Different stretchy conductive materials, including conductive rubber, liquid metals in the elastic substrate, and copper traces [63], were created to accommodate the deformability and mechanical strain [64]. A conductive rubber with single or double-layer coated copper is used as a stretchable conductor for reconfigurable antennas [65]. Eutectic gallium indium (EGaIn) is a liquid with less viscosity at the room temperature. The fluid inside the elastomeric channels is mechanically stabilized by its thin oxide coating [66]. However, because of their comparatively poor electrical conductivity, antenna elements still have problems with conductor loss and radiation performance.

Consequently, the exploration of the utilization of nanomaterials in microwave domain is inevitable because of their rapid response towards any applied external changes, which is an added advantage for antenna sensing applications.

2.2.2 Nanomaterial-Based

The name itself hints that nanomaterials consist of particles one billionth of a meter in size or one nanometre. As history says, manipulating matter at its atomic and molecular levels has always inspired scientists, resulting in the discovery of nanomaterials. They exhibit more refined properties than they possess at a bulk level. New techniques for manipulating and synthesizing nanomaterials came into existence and led to the development of nanotubes and quantum dots. Nanomaterials have found their place in a wide range of applications, especially for developing flexible devices in the field of electronics [17]. Upon this success, the concept is further expanded towards the advancement of flexible antennas and their applications. As shown in Fig. 2.3, various nanomaterial-based antennas were designed, developed, and analyzed for wireless communication applications.

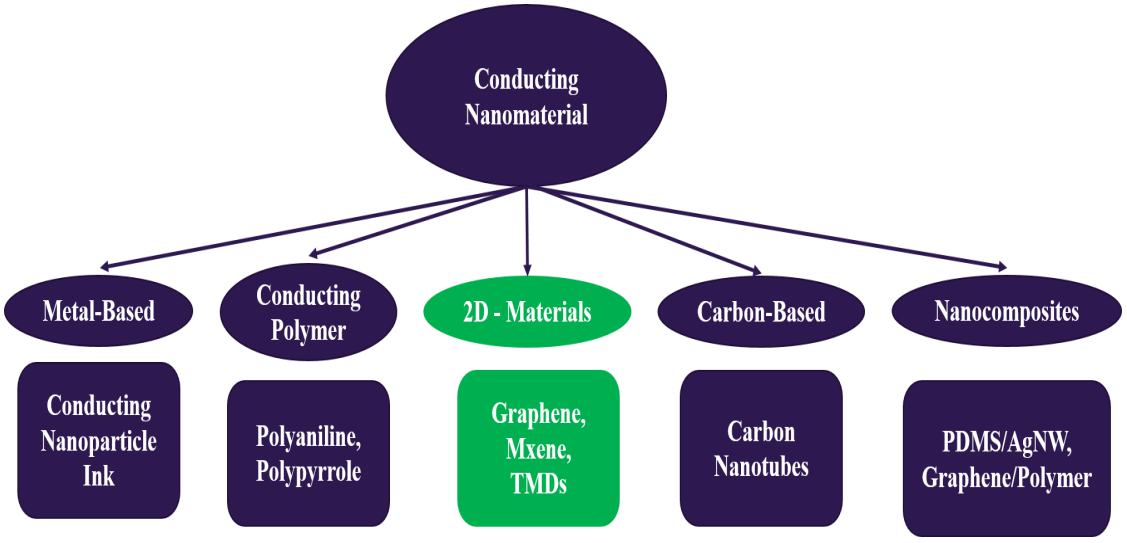

FIGURE 2.3: Material-based classification of nanomaterials utilized as radiating elements of antenna.

When it comes to nanomaterial-based antennas, different types of applicative-specific nanomaterials were used to fabricate the radiating element of antenna. Out of which, nanomaterial-based antennas for sensing applications were highlighted due to their effective performance compared to the conventional one. Since the radiating element of the antenna should possess significant conductivity the metal-based nanomaterials were developed in the form of conductive nanoparticle inks and nanowires. The development of conductive nanoparticle inks using metallic materials has happened rapidly because of their superior electrical conductivity. Printable silver Nano ink-based ultra-wideband antenna is presented for wireless electronics. Even in the bent conditions the EM properties of

the antenna remain unchanged [67]. As a part of reversibly deformable antennas, silver nanowires (AgNWs) were used on the PDMS substrate for strain-sensing applications [64].

Nanomaterials were used in several applications recently due to their adjustable physiochemical properties like transparency, deformability, lightweight, stretchability, and low cost [68]. Conducting polymers, such as polyaniline [69] and polypyrrole [70], are attractive materials for deformable antennas, but their low conductivity illustrates the need of functional nanomaterials in antenna manufacturing.

The conductivity of the materials was effectively increased by the newly developed 2D carbon-based functional nanomaterials, such as graphene [71] and carbon nanotubes [72] metallic submicron and nanoscale layers [73]. A wearable, flexible multi-layer graphene film antenna is studied for strain sensing purposes based on the change in its electrochemical properties [74]. Using nanomaterials such as carbon and graphene paved the way for much lighter, stronger, and cheaper antennas. Also, they modify the structure of the antenna to the nanoscale, which makes it more responsive to any structural changes.

Primarily, graphene and carbon nanotubes are mostly used as radiating elements of antenna because of their high current-carrying capacity and thermal stability [75]. To use graphene in antenna applications, the researchers have explored various modifications of graphene and its forms, which include graphene oxide, reduced graphene oxide, chemically functionalized graphene, and graphene-polymer composites [76]–[78]. Carbon material is also modified in different ways to suit the requirements of applications, specifically for antennas. Carbon is customized based on its structure, such as single-walled carbon nanotubes (SWCNTs) [79] and multi-walled carbon nanotubes (MWCNTs) [80].

Nanocomposites consist of significant electrical conductivity, less weight, improved thermal stability, and tunable electromagnetic properties, which are essential for antenna-based sensing applications. Therefore, recently, nanocomposites were developed based on mixing one or more nanoscale materials with a matrix material at varying mixed ratios to acquire acceptable electrical and electromechanical properties [81]. Two different nanocomposites (PANI/CCo & (PDMS/AgNW)) were used in two separate slots to improve the radiation properties of the antenna, which resulted in the improvement of bandwidth with a good impedance matching [82]. The combination of graphene/polymer-based nanocomposite showed significant electrical properties that are a key factor for high-performance antennas [78].

The metals are highly conductive and provide good EM performance but are significantly less effective towards antenna-based sensing applications, while nanomaterial-based

antennas are highly responsive toward any applied changes through external parameters. Therefore, synthesizing and investigating various nanomaterials for improving the sensitivity of the antenna is necessary.

2.3 Antenna Sensors

Recently, researchers have focused on electromagnetic wave sensing using flexible microstrip antenna technology. These microstrip antennas act as sensors that can detect the changes in the applied physical input through scattering parameters and transmit the data. The EM wave interactions of reflection and transmission coefficients with the respective applied physical parameters onto the antenna sensor allow to sense and analyze the variations in physical quantities. Some physical quantities like crack, pH, glucose, gas and, structural health monitoring, etc., are assessed by the antenna-based sensor using the sensing function for various applications, as depicted in Fig. 2.4.

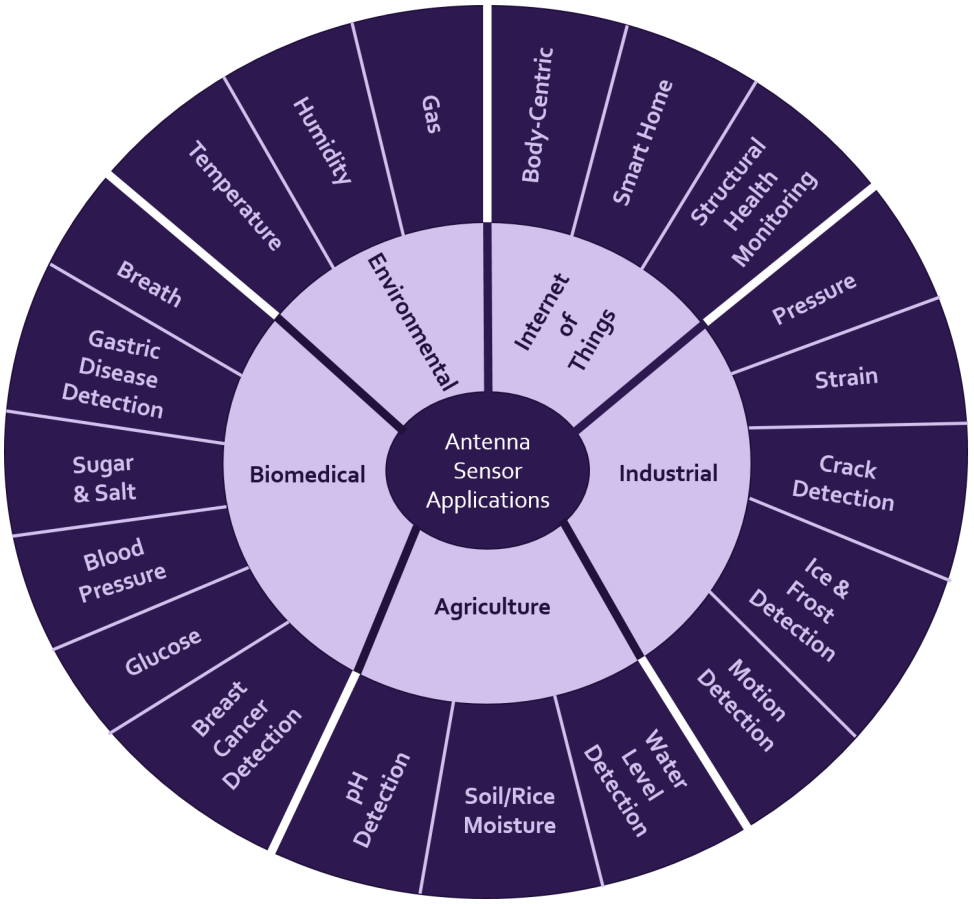

FIGURE 2.4: Applications of flexible antenna sensors in various fields.

2.3.1 Biomedical

Respiration is a physiological task that is to be monitored for the detection of abnormalities in the breath rate. The presented antennas are made of textile that can be seamlessly integrated into the clothing, which can directly detect the breath rate wirelessly [83]. The antenna as a breath sensor operates with a shift in resonant frequency or variation in RSSI range based on the chest expansion, air volume displacement in the lungs, and different breathing patterns, including eupnea, apnea, hypopnea, and hyperpnea [84], [85].
A rapid variation of blood pressure is seen in hypertensive patients, which is a high-risk factor that leads to various health problems, including heart failure and aneurysm. By placing a pair of antennas on the human arm, the blood pressure (BP) is measured based on the pulse transit time of a pulse wave, which refers to the time difference between the changes in distal and proximal transmission coefficient waveforms to varying artery coefficients [86]. Here, the EM transmission propagation characteristics of the antenna as the sensing element were used to measure and monitor the BP non-invasively [87].

A continuous screening of glucose levels is essential for diabetic patients, where several research works were demonstrated showing implantable and non-implantable antenna sensors for glucose detection through in vivo and in vitro analysis [88]. The implantable antenna-based biosensors were proposed to detect and monitor the glucose levels invasively through the shift in resonant frequency [89]. Several works proved to sense the glucose also through non-invasive analysis using the dielectric properties of the sensing region of a microstrip antenna [90]–[92].
Intake of sugar and salt percentage in food and beverages is also equally important to cut the disease at its root. An MSA sensor is proposed to detect the contents of sugar and salt on the basis of reflection coefficient with respect to the variation in dielectric properties of the substance [93]–[96].

In women, the commonly detected disease is breast cancer, which needs regular check-ups by continuous monitoring and early detection. The dielectric medium with similar properties to the breast tissue is used for the antenna only to detect breast cancer and its tumor depth through electromagnetic (EM) waves [97], [98]. Recently, a flexible antenna sensor is developed to detect and monitor breast cancer in the microwave band. The electromagnetic microwave is utilized to detect the changes in electrical properties by analysing the S-Parameters in the presence and absence of tumor-affected tissue. Here, two procedures are used to metallize the flexible antennas, such as the first employs Roger, and the second utilizes conductive textile on a cotton substrate. Both the reflection and

transmission coefficients were measured using single-antenna and dual-antenna sensing tests [99].
Wireless capsule endoscopy is a painless and non-invasive technique for diagnosing gastrointestinal disease. As a part of the capsule, the antenna detects the difference in permittivity of the gastric based on the resonant frequency [100]. According to the capsule size and instability, the antenna is miniaturized by making a layered structure with less power consumption and dual polarization ability [101].

2.3.2 Environmental

The patch antenna for temperature sensing was analysed with the relationship between frequency shift and temperature variation. To reduce the difference between predicted and measured sensitivities, a strain constant is introduced to balance the strain effect on the dielectric constant of the substrate [102]. The temperature also influences the conducting elements (Patch and ground) along with the dielectric materials due to their dependency on temperature. The temperature variation influences the electrical and chemical properties of the materials used for the antenna fabrication. Using conditioning monitoring (CM) specific parameters can be tracked continuously to identify quantitative measurement changes [103]. A dual-function flexible loop antenna is presented with a conducting polymer poly (3,4-ethylenedioxythiophene): polystyrene (PEDOT: PSS) printed on a PVC substrate specifically for temperature sensing. Here, due to the temperature variation, the resistance of the (PEDOT: PSS) has a drastic change, which also tends to vary the resonant frequency of the antenna [104].

The antenna-based sensor is utilized to sense the humidity level in the environment by detecting the changes in terms of the reflection coefficient with respect to humidity. As the relative humidity in the climate changes, so does the resonant frequency as a sensing element [105]. The humidity performance is also validated by introducing different organic compounds that can affect the environment and humans, including acetone, ethanol, methanol, etc., into an antenna sensing test chamber. Here, the MXene & graphene oxide-modified polyimide materials were used as conducting material, which acts as a sensing part while changing the EM properties of the antenna when exposed to humidity [55], [106].

To sense some physical parameters like gas, the antenna sensor uses separate conducting materials like, semiconductor metal oxides or carbon nanotubes [107]. By changing

their electrical properties in response to physical quantities, these materials aid in enhancing the sensitivity of the antenna as a sensor through EM properties. A sensitive silver porous film is loaded on the patch for sensing the oxygen gas, which detects the variation in concentration of O2 by analyzing the reflection parameter [108]. A Microstrip patch along with a circular waveguide is proposed to sense different gases as they flow through the pipe [109].

2.3.3 Internet of Things

The body-centric communication refers to the in-body, on-body and off-body network by using implantable and wearable devices. The antenna sensors were in both implantable and wearable applications for biomedical and security purposes [110], [111]. For the implantable purpose the antennas were miniaturized with low power consuming capacity for sensing and monitoring the human internal related issues [112]. By detecting the salt concentrations in sweat, a disposable antenna sensor is presented for monitoring sweat non-invasively [113].

Continuously monitoring the data and transmitting it wirelessly is necessary for human health monitoring or surveilling the structure of a machine. A flexible biodegradable paper antenna with aluminium tape is presented for monitoring and detection of human motion under compressive and tensile bent strain. The evaluation of strain sensing performance is made with respect to the normalized resonant frequency for different compressive and tensile bending angles [58]. In smart home sensing applications, it is crucial to detect all the essential physical factors in order to ensure the comfort of the occupants[114].

2.3.4 Industrial

Several methods were presented in the literature to sense the pressure, and most of them use frequency shift for detecting pressure [115], [116]. Here, the pressure detection is made with an extra element placed as a metal reflection plate or a flexible fabric spacer over the microstrip antenna with some measured distance. So, when the pressure is applied to the device, the distance between the antenna and the reflection plate or spacer varies with respect to the shift in resonant frequency [117], [118]. Other ways to monitor the pressure changes are using deformable and stretchable sponge antenna and reconfigurable dipole antenna. The first antenna consists of polydimethylsiloxane (PDMS) with gold nanowire

and the second with a microfluidic channelled substrate material as PDMS, which is filled with a liquid metal (eutectic gallium–indium alloy) [119], [120].

Under the applied strain on sensor, the influence of strain variation ratio is observed by using the strain sensitivity. Related to mechanical properties, strain sensing is one of the direct measurements from the deformation of a material. By using the change in resonant frequency of the antenna the applied strain is measured [121], [122]. The coplanar waveguide monopole antenna as a strain sensor gave a linear resonant frequency shift [81]. To sense the strain with respect to resonant frequency, three different versions of textile antennas, such as meshed patch over solid ground, meshed patch over meshed ground, and gold meshed patch over solid ground were fabricated and analysed for better strain sensitivity [123].

The occurrence of a crack in the ground plane of the crack-sensing field tends to a change in the current flow. The current flows around the crack formed instead of a straight direction, which causes the shift in the frequency of the antenna. Where, the effect of the crack orientation is directly proportional to the resonant frequency [124]. When a sub-patch is partially constructed over a rectangular radiation patch, the width of the crack is represented by the resonate frequency shift that results from their overlapped length. A cavity model theory is used as a proof of concept to demonstrate the resonant frequencies of the crack sensor with respect to the length between the overlapped patch and the sub-patch [125]. By using resonant frequency offset, a dual-band antenna is presented for detecting multiple cracks in metals and their length, width, and depth, which can also be extended to a multiband sensor [126].

For security-related applications, detecting motion and continuous monitoring became an important parameter, which can be implemented contactless through frequency sensing [127]. A wearable coplanar keyhole antenna is presented for on-body motion detection by analysing the motion of various humans in response to reflection and transmission coefficients [128].

In the industrial sector, it is crucial to identify ice formations in order to prevent any potential harm or malfunction of equipment. Patch antennas are proposed to detect the presence of ice along with its size, thickness, and weather conditions [129]. Here, the antenna as a sensor is used for detecting water and ice, which is analyzed in terms of the transmission coefficient. The freezing rate is also extracted through exponential data [130].

2.3.5 Agriculture

For water level detection, simple microstrip patch antennas are utilized as sensors while analysing the effect of changing dielectric constant on the resonant frequency [131], [132]. Another antenna sensor is utilized to detect the oil-water mixture, which is made with two substrate layers to achieve a better sensitivity by avoiding copper contact with oil [133]. For the offset measurement of soil moisture, the antenna sensors were used in sensing and detecting the moisture content wirelessly by burying the antenna in soil [134]. Also, the soil samples with different pH values were considered to detect the moisture content using S-parameter [135], [136]. The other patch antennas were proposed to sense the moisture content in the rice grain with a dual frequency analysis [137], [138].

The potential of the hydrogen (pH) factor of liquid is sensed using a metamaterial antenna, which is designed by using a hexagonal split-ring resonator. Based on the dielectric distraction phenomena, the metamaterial-based sensor is used to measure the transmission coefficient of the antenna with various concentrated solutions. The dielectric constant varies depending on the presence of positive and negative ions in the solution. The higher retardation force tends to increase the resistance, which shows a parallel effect on the dielectric value of the material [139]. Therefore, the amplitude of the S-parameter varies along with a certain change in pH level. The frequency of a slot antenna here is regulated by a back-metal coating applied to a pH-sensitive hydrogel designed in a specific pattern on a glass substrate. The variation in resonant frequency is directly proportional to the variation in pH value between a particular provided pH range [140]. The pH liquid dropped on the slotted rectangular region causes a change in the dielectric constant, resulting in a shift in radio frequency (RF) signals [141].

2.4 Summary

In literature, the microstrip patch antenna with extended techniques is widely used because of its compactness and adaptable size with easy integration in electronics using flexible materials. Most antennas used for sensing were rigid and not adaptable to the applicative surface. The work presented on the nanomaterial-based antennas was scant. Because of their feasible electrochemical properties, the analysis of antennas as sensors while using nanomaterials as a radiating element is necessary. This promising detailed study could further expand the nanomaterial-based flexible antenna towards a wide variety of sensing applications.

Chapter 3

Laser-Induced Graphene Printed Flexible Antenna for Strain Monitoring

3.1 Introduction

The requirement for wireless data transmission using flexible antennas is becoming one of the main focuses for the IoT driven sensing applications. With graphene as an active material, the antenna-based strain sensors are drawing significant attention for continuous motion detection and structural health monitoring in biomedical and industrial areas [142]. The performance of the antenna mainly depends on the geometry of the radiating surface, and structural property of the selected materials. The deformation of the antenna structure by applying external forces leads to an instant variation in the frequency response [64]. The utilization of the antenna as a sensing element simplifies the sensor design by enabling the wireless read-out of analog information without the use of on-board analog to digital circuits (ADC) circuits, inductive loops, and battery for power supply. Hence, a compact and highly sensitive flexible microstrip antenna act as a good candidate for antenna-based IoT enabled strain sensing applications.

In addition to the wireless sensor nodes used to obtain strain signals, the MPA is shown to be a feasible sensor for wireless strain sensing [143]. Conventional MSA with rigid structures have constrains for conformal demands. The progress of antenna-based sensors using soft materials has led to advancements in a broad range of communication applications [57]. Furthermore, the sensors for wearable [144], and body-centric [145] applications are fabricated using various materials for effective sensitivity and radiation

characteristics. Such possibilities become limited while enhancing the sensitivity by modifying the geometrical structures only [146]. However, material selection with flexibility and better physical and chemical properties is one of the highly challenging aspects of antenna-based sensors.

There were several reports of antennas fabricated using different conductive inks and printing methods utilizing various flexible dielectric substrates [12], [147]. The properties like stability, mechanical strength, electrical sensitivity, and stiffness that porous graphene can tolerate under extreme strain have drawn much interest [148]. To produce graphene, various techniques have been utilized with high proportions of strong acids, and oxidants [149]. A graphene-based flexible film fabricated using a three-step process involving thermal annealing and roll compressing, has reported high stability and less weight [150], [151]. Nevertheless, these techniques have lower control over a 3D structure, requiring a lengthy process with high temperature for graphene synthesis.

As an alternative, laser-induced graphene (LIG) is becoming popular for diverse flexible and wearable electronic applications [152], [153]. LIG is produced by direct scribing infrared CO_2 laser on carbonated polymers without requiring any additive chemical and high-temperature treatments [154]. The production of few-layer graphene using laser direct writing (LDW) is a simple, relatively inexpensive, and rapid process with high precision and throughput [155]. Unlike other existing multistep synthesis methods, LDW is a straightforward single-step process that allows engraving complex designs directly by generating few graphene layers onto the polymer films [156]. The direct CO_2 lasing on polymers offers an efficient substitute as a conductive material with patterns of few-layer graphene on its surface in a fully controlled manner [157]

Here, a flexible and compact LIG-based antenna sensor with a high compressive and tensile strain sensitivity of 14.08 and 11.34, respectively is presented. The device is utilized for wireless strain sensing purposes using a single-step fabrication process. Besides, various LIG printing technology prospects were also studied while designing the flexible antenna. A 26.22×27.58×0.12 mm^3 sized rectangular patch antenna using LIG and copper tape on each broadside of the polyimide (PI) sheet was created as an alternative to existing multistep fabrication techniques using the synthesized conductive inks. The surface composition of the engraved LIG material has been reviewed using various structural and morphological characterization methods. The effect of bending on operating frequency was examined to measure sensor sensitivity. The device can convey data through microwave transmission of WLAN frequency at 5.8 GHz with remarkable

sensing capability and can be utilized in IoT sensor applications, such as biomedical and industrial purpose.

3.2 Experimental Section

3.2.1 Design & Methodology

A simple MPA for sensing applications operating in the industrial, scientific, and medical (ISM) band has been designed using an infrared CO_2. Firstly, an appropriate low thickness substrate material for the laser ablation process is selected as it provides the desired mechanical stability for the microstrip antenna during the straining process. A deformable PI sheet of thickness 0.127 mm, having a dielectric constant (ε_r) of 3.5 and a loss tangent of 0.0026, was chosen as the substrate [158]. The top and bottom conductive parts of the substrate, such as ground and patch, are given copper attachment (5.96×10^7 S/m) and LIG imprinted (7.18×10^2 S/m), respectively. Dimensions of the designed antenna with an inset feed are obtained from the standard microstrip rectangular patch antenna design equations [159].

3.2.2 Materials & Methods

The LIG film obtained by inscribing CO_2 laser on the PI sheet is studied further using different characterization techniques. Chemical characterization includes scanning electron microscope (SEM) from field electron and ion (FEI-Apreo LoVac) was used to determine the surface and structural morphology. Furthermore, confocal Raman Microscopy (Witec Alpha 500) and fourier transform infrared spectrometer (FTIR-4200 from Jasco) were used to observe the chemical compositions of LIG. X-Ray diffraction (XRD) method (ULTIMA-IV by Rigaku) was used for phase identification of LIG. A vector network analyzer (VNA-ZVL by Rohde and Schwarz) was used for measuring the radio frequency (RF) characterization while examining the sensing performance of the device. To observe the conductivity of induced graphene with lasing parameters, a four-probe conductive meter (by Ossila) was utilized.

MPA as a sensor was developed using CO_2 laser fabrication process (VLS 3.75 from Universal Laser Systems). Below a certain threshold power of the laser, the PI sheet acts as an insulator with a relatively higher sheet resistance. The gradual increase in power

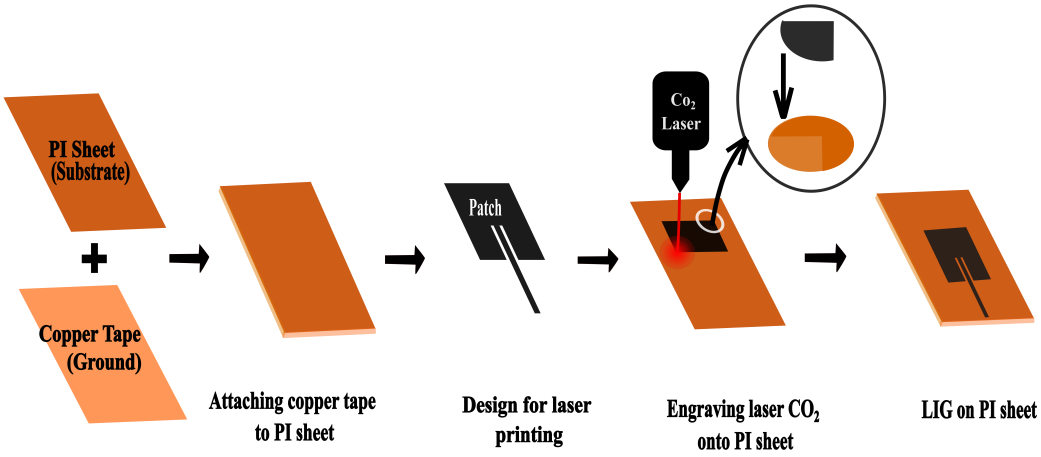

FIGURE 3.1: A detailed illustration of the fabrication procedure of LIG antenna-based sensor.

tends to reduce its sheet resistance and increases the conductivity of engraved porous graphene. The laser spot allows elevated local heating to carbonize the PI sheet at certain ambient conditions [160]. By irradiating laser onto the PI, sheet forms a highly flexible porous material that can be used for strain sensing [161]. Fig. 3.1 depicts the fabrication procedure of the LIG antenna-based sensor using CO_2 laser at an optimal power of 3 W. One side of the PI sheet is attached to a single-sided adhesive copper tape before realizing the LIG. The CO_2 laser with required power and speed, as shown in Fig. 3.1, induces graphene by engraving on the PI sheet. Finally, the CO_2 laser directly cuts an outline as per the specified antenna dimensions. The major microfabrication issues can be overcome by maintaining consistency in dimensions, enabling bulk fabrication within less time. For example, the duration required to engrave a PI sheet of $5 \times 5\ mm^2$ takes less than 60 s.

3.3 Results and Discussion

3.3.1 Chemical Characterization

The SEM images are used to depict the morphological evaluation of the plain PI sheet and the LIG engraved PI sheet. Fig. 3.2a shows the plane surface of the PI sheet without LIG. Fig. 3.2b and 3.2c depicts the lengthwise images of PI sheets engraved with LIG having rough 3D porous graphene structure with cross interlinks at high magnifications. Most of the pores possess circular or oval-shaped geometries with random distributions. These pores of LIG are versatile and can be controlled by altering the laser power [162].

As depicted in Fig. 3.2d, by using the cross-sectional SEM imaging, the depth of the engraved LIG observed was measured to be approximately 60 μm. The transition of a plane surface of the PI sheet to few layers of porous graphene exhibits a clear structural morphology of LIG.

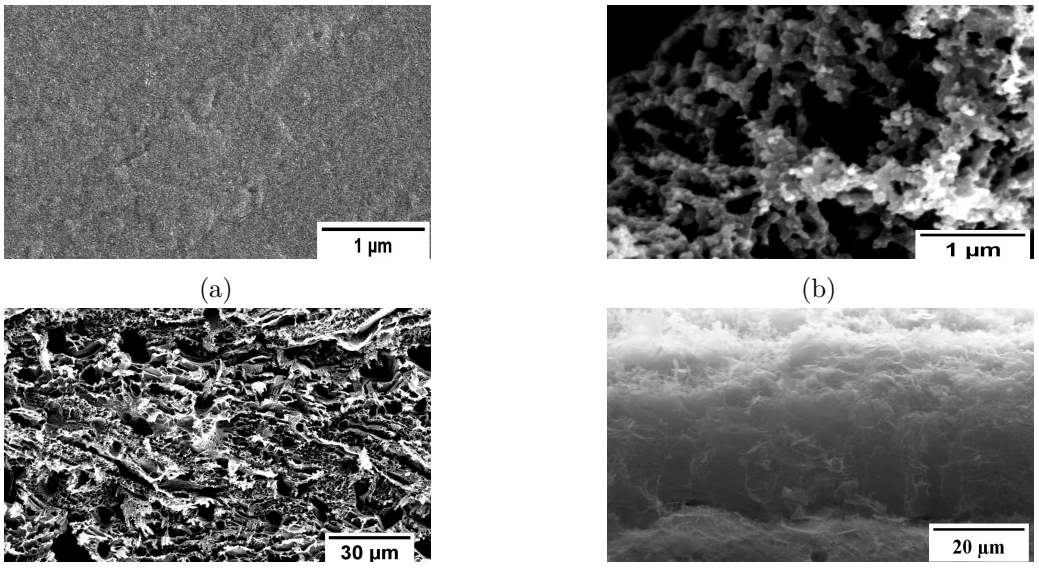

(a) (b) (c) (d)

FIGURE 3.2: (a) SEM image of a plane PI sheet, (b) & (c) Lengthwise images of LIG (d) Cross-sectional image of LIG.

The developed LIG on the PI sheet was examined to understand the structural information of the material. The sample was characterized using Raman Spectroscopy, and the peaks are demonstrated in Fig. 3.3a. The intensity peaks of D, G, and 2-D bands observed are 1330.039 cm^{-1}, 1557.686 cm^{-1}, and 727.80 cm^{-1}. The carbon structure can be explained using the intensity ratios of D band and G band (I_D/I_G) [163]. The obtained (I_D/I_G) and (I_{2-D}/I_G) values for the LIG sample are 0.853 and 0.467, respectively. These results indicate the formation of graphene oxide (GO). Since the device was fabricated in ambient environmental conditions, the presence of oxygen was also observed.

XRD spectra play a key role in characterizing the crystalline structure of a material. Fig. 3.3b illustrates the XRD spectrum of LIG material carried out with a scanning range of 10^0 – 80^0. A broad diffraction peak from 15^0 – 30^0 proves the existence of amorphous carbon structures having various peaks with different intensities due to the appearance of oxygen functional groups along with water molecules. The same is also evident from FTIR spectra as shown in Fig. 3.3c. The strong intensity peak at $2\theta = 26.12^0$ indicates the presence of graphite (JCPDS card no. 75-2078), and by using Bragg's law, the calculated d spacing is around 3.4Å, which is between (002) planes. The peak centered at $2\theta = 21.7^0$

corresponds to reduced graphene oxide (RGO), and the abrupt peak appeared at $2\theta = 14.5^0$ is referred to as GO having some random structures with low peak intensity.

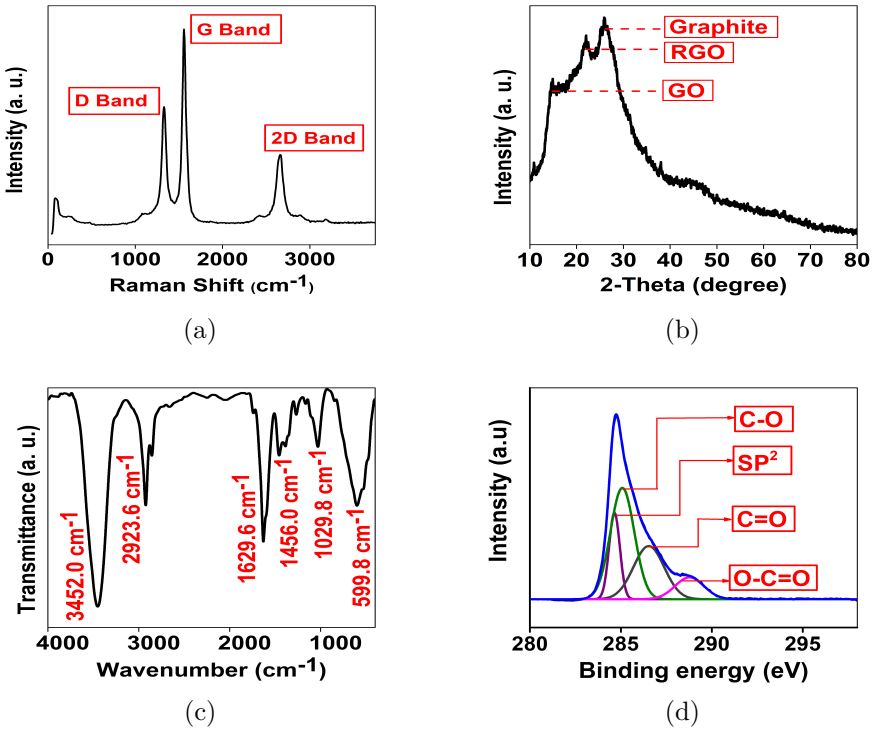

FIGURE 3.3: (a) Raman spectra of LIG (b) XRD pattern of LIG (c) FTIR spectrum of LIG (d) XPS spectrum of LIG.

Fig. 3.3c exhibits the FTIR Spectrum for observing the characteristic chemical composition of LIG powder produced from CO_2 laser. The extracted powder is mixed with Potassium Bromide (KBr) in the ratio of 1:100 to turn it into a transparent palette by applying appropriate pressure. The FTIR spectrum obtained from the palette measurement has a vibrational peak at 3452.0 cm^{-1}, indicating the presence of hydroxyl group (O-H) with strong intensity and a broad peak. The region between 3000 cm^{-1} and 2800 cm^{-1} is analogous to the stretching vibration of the methyl group (C-H bond). The peak at 1456.0 cm^{-1} corresponds to the methylene region. From the plot, remaining vibrations at 1629.6 cm^{-1}, 1029.8 cm^{-1}, and 599.8 cm^{-1} exhibits aromatics (C=C) with strong intensity, an alkoxy group, and some halo compound [164]. The above vibrational peaks show the presence of carbon materials like graphene and GO by the interaction of oxygen along with some impurities.

For the elemental characterization of LIG material, XPS analysis was performed. From the observation shown in Fig. 3.3d, the de-convoluted peak values were at 284.5 eV, 285.1 eV, 286.5 eV, and 288.6 eV, which represents the sp^2, C-O, C=O, and O-C=O

functional groups, respectively. The functional groups indicate that the formed LIG sample consists of GO. The XPS spectrum confirms the presence of C and O groups with the absence of impurities.

3.3.2 RF Characterization

The LIG antenna has been simulated in ANSYS HFSS V.15.0. As proof of concept, a prototype antenna was fabricated, and the return loss measurements were compared using a vector network analyzer (VNA). The radiation characteristics such as return loss, E-Plane and H-plane patterns for polarization, and a realized gain over the operating frequency band were analyzed. Fig. 3.4 depicts the fabricated LIG antenna.

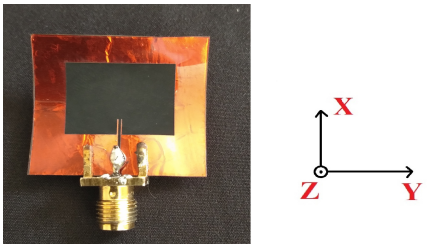

FIGURE 3.4: Fabricated LIG antenna.

The $|S_{11}|$ parameter is plotted in Fig. 3.5a. The measured and simulated results have a centre frequency at 5.8 GHz with a return loss less than -10 dB. Fig. 3.5b shows the plot of gain and efficiency over the operating frequency of the antenna. A maximum gain of 4.24 dBi was observed at the centre frequency of 5.8 GHz. The Efficiency greater than 50% was observed at the required bandwidth for ISM band 5.725 – 5.875 GHz. Since the antenna is compact in size and is designed on a very thin substrate, the efficiency is comparatively low but is sufficient for the target application.

Fig. 3.6 depicts the simulated and measured radiation patterns of co-polarization and cross-polarization at 5.8 GHz as the center frequency. Both the XZ and YZ planes have comparable gain at 0^0 around 4.24 dBi for simulated and 1.82 dBi for measured with stable unidirectional radiation patterns. The cross-polarization radiation levels of both the planes are also better than -30 dB at the operating frequency.

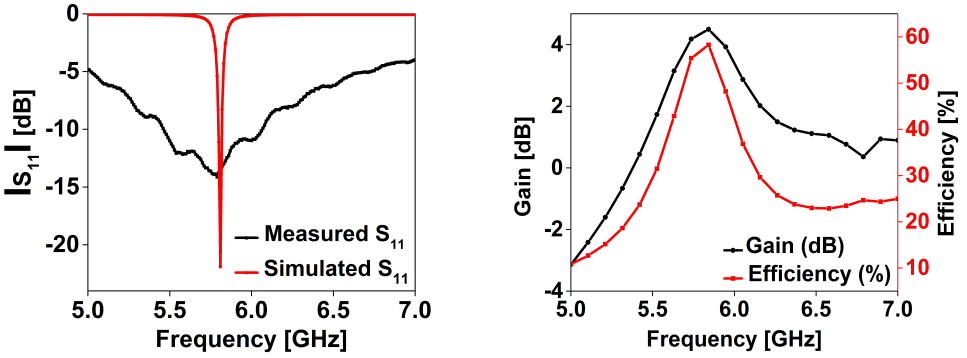

FIGURE 3.5: (a) Simulated and measured $|S_{11}|$ parameters at 5.8 GHz (b) The frequency with gain & efficiency plot.

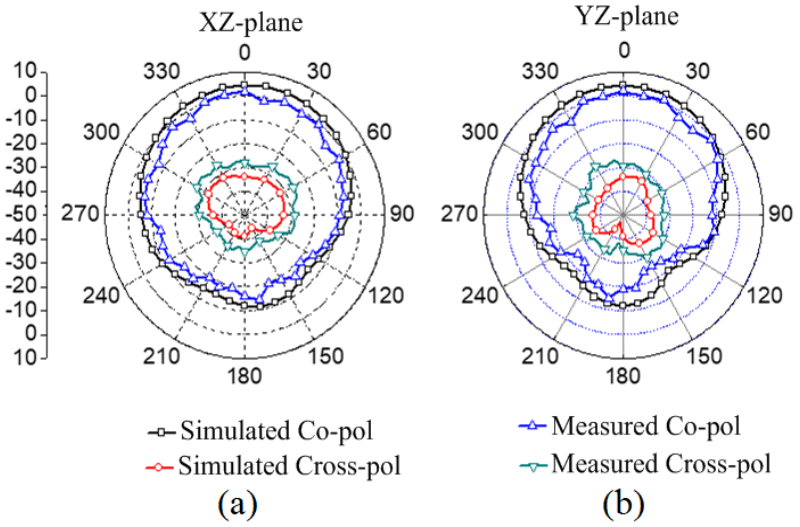

FIGURE 3.6: Simulated and measured 2-D radiation patterns at 5.8 GHz (a) XZ-plane (b) YZ-plane.

3.3.3 Strain Analysis

The LIG printed antenna was subjected to different tensile and compressive strain, while the resulting frequency shift was analyzed for strain sensing performance. The frequency change of the LIG antenna is mainly due to the applied external strain. As the LIG has a porous structure, the pore dimension changes with the applied strain. For compressive strain, the pores of the LIG material become more compact resulting in enhanced conductivity and possibly an increase in the frequency. When it comes to tensile strain, the pores of the LIG material gets enlarged which leads to reduced conductivity and possibly a decrease in frequency.The physical property of the conducting part varies along its length that tends to change with the frequency of operation. The resonant

frequency of an MPA with length L is given by (3.1),(3.2) & (3.3) [159]

$$f_r = \frac{c}{2L_{eff}\sqrt{\varepsilon_{reff}}} \tag{3.1}$$

$$\Delta L = 0.412h\frac{(\varepsilon_{reff}+0.3)(\frac{W}{h}+0.264)}{(\varepsilon_{reff}-0.258)(\frac{W}{h}+0.8)} \tag{3.2}$$

$$\varepsilon_{reff} = \frac{\varepsilon_r+1}{2} + \frac{\varepsilon_r-1}{2}\left[1+12\frac{h}{W}\right]^{-\frac{1}{2}} \tag{3.3}$$

where, $L_{eff} = (L + 2\Delta L)$ is the effective length of the patch, which is slightly more than the actual patch length L due to the presence of fringing field at both the ends of the patch. ε_{reff} is the effective dielectric constant of the dielectric substrate. Hence, L_{eff} and ε_{reff} are two factors, which play a key role to determine the resonant frequency of the antenna.

As shown in Fig. 3.7a, when the antenna is bent inward (compressive strain), the effective length of the patch reduces resulting in an increase in the resonant frequency. Similarly, from the Fig. 3.7b, during the tensile strain, the antenna is bent outward and the relative length of the patch increases. Hence the resonant frequency decreases. Another dominant factor, which plays a significant role in finding resonant frequency of the antenna is the changing dielectric constant due to the bending of the substrate. A flexible substrate, having less thickness with more variation in dielectric constant while bending, can provide a better bending performance and stability. It is experimentally found for a wide variety of dielectric substrate materials that the dielectric constant decreases with increasing compressive strain and enhances with increasing tensile strain [165], [166]. From Fig. 3.7c and 3.7d plots, because of the wideband, there is an overlap between each band for each applied input parameter. However, for sensing purposes here, the main focus is on the change in resonant frequency for different inputs applied, which could be distinctly identified.

A decreasing dielectric constant results in higher resonant frequencies, which we have observed for our proposed antenna under the compressive strain. On the other hand, we have obtained a lower value of resonant frequency with increasing tensile strain thereby indicating that the dielectric constant is increasing with tensile strain. Hence we can well anticipate that the dielectric substrate used in designing the proposed antenna comes under this category.

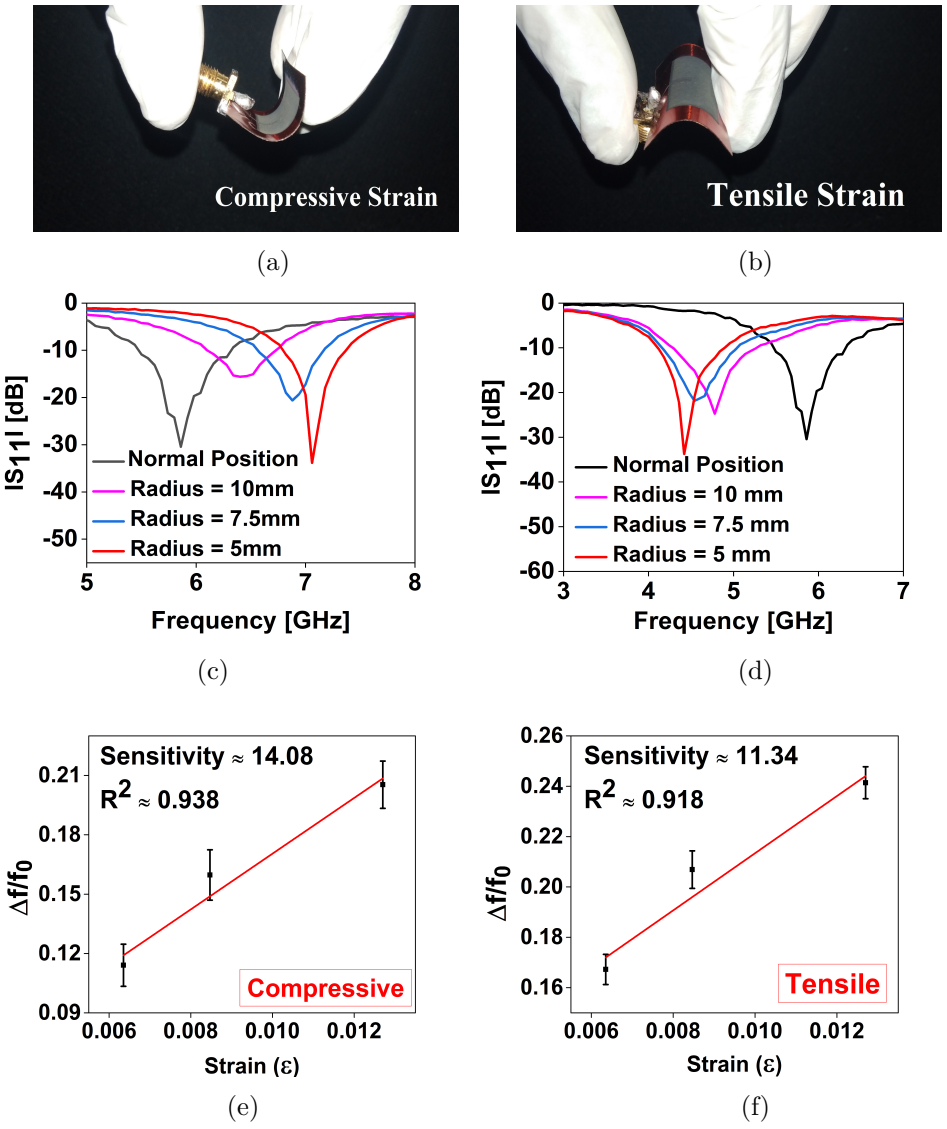

FIGURE 3.7: (a) and (b) Images for compressive and tensile bending of LIG antenna, respectively (c) and (d) Frequency versus S-Parameter variation plot for compressive & tensile strain, respectively (e) and (f) Sensitivity plot with the applied compressive & tensile strains for N=2 devices.

From Fig. 3.7c and 3.7d plots, it is clear that as the radius of the radiating element decreases, the frequency shifts towards right for compressive strain and shifts left for tensile strain. The sensitivity is calculated as $\varepsilon = \pm h/2r$ and $S = (\triangle f/f_o)/\triangle\varepsilon$ [58]

where ε is the amount of strain applied, h is the height of the antenna (0.127mm), r is the bending radius, S is the sensitivity and $\triangle$f is the frequency difference between bent (f) and flat states (f_o) of the antenna. Fig. 3.7e and 3.7f shows an approximately linear change in normalized frequency with applied strain. Using two fabricated devices, the sensitivity values observed for the compressive strain are 14.08 with $R^2 = 0.938$ and tensile strain is 11.34 with $R^2 = 0.918$, approximately.

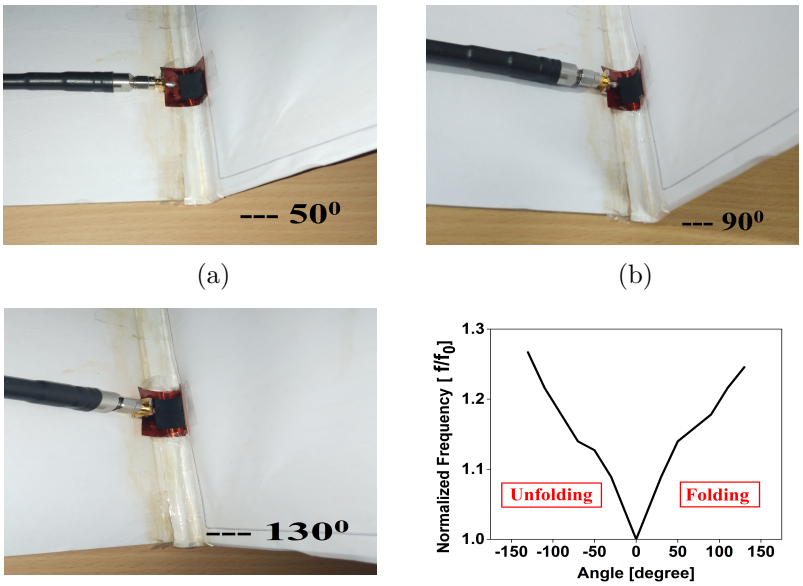

FIGURE 3.8: (a) - (c) Images of LIG antenna at various folding & unfolding angles (d) Angle with respect to normalized frequency plot.

To observe the sensing performance of the LIG antenna sensor, angle measurement by folding and unfolding movement using compressive strain is carried out. As depicted in Fig. 3.8a - 3.8c, the antenna sensor was bent in different angles between 0-150^0 while folding and unfolding. From Fig. 3.8d, an increase in normalized frequency while folding the antenna and a decrease in frequency when unfolding is shown.

The fabricated sensor is utilized in real-time applications to evaluate the repeatability performance using two different cases. In the first case [Fig. 3.9a & Fig. 3.9b], the antenna as a sensor is subjected to a motion detection test while placing the antenna ground on the palm for compressive bending analysis Fig. 3.9c depicts the compressive bending and stretching plot of antenna based sensor. In the second case [Fig. 3.9d & Fig. 3.9e], the LIG antenna ground is placed on the backhand for tensile bending analysis. Fig. 3.9f depicts the tensile bending and stretching plot of antenna-based sensor.

By alternating between bent and stretched hand positions as shown in the figure Fig. 3.9c & Fig. 3.9f, uniform change in normalized frequency under repeatable strain positions is noted. The hand positions 1, 3, 5, 7, 9 are considered for bending, and 0, 2, 4, 6, 8, 10 are for stretching to observe the consistency in frequency. In stretched position, for both cases the normalized reference frequencies($f/f_0 = 1$) are same. Whereas in bent positions, the frequency is increasing from the reference frequency (stretched position) for compressive strain, and is decreasing for tensile strain. A consistent restoration to the original frequency from bent position for each and every individual bending cycle is noted.

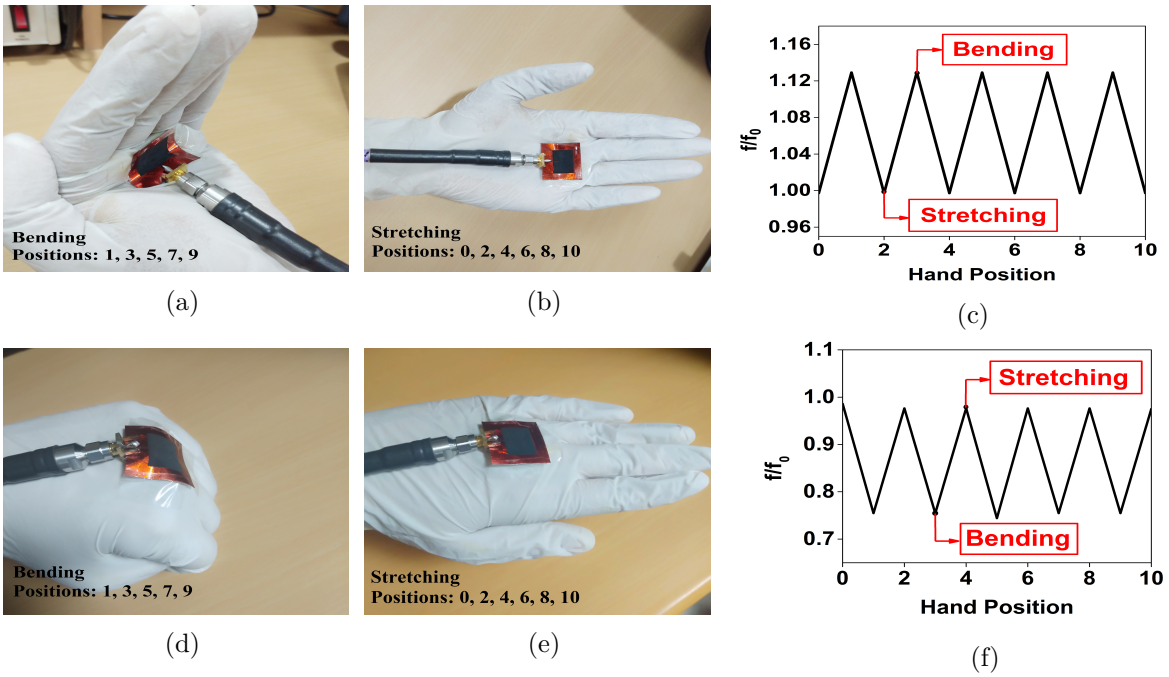

FIGURE 3.9: (a) & (b) Images of LIG antenna at compressive bend and stretch positions (c) & (d) Images of LIG antenna at tensile bend and stretch positions (e) & (f) Hand position with respect to normalized frequency plot for compressive & tensile strain.

This indicates the repeatability and suitability of the LIG antenna as a sensor for motion detection and health monitoring applications.

TABLE 3.1: Comparison table for sensitivity & compactness of LIG antenna-based sensor with previous works

Material (Substrate/Radiating Patch)	**Electrical Size**	**Dimensions (mm)**	**Sensitivity**	**Reference**
Cellulose filter paper/Aluminium	$0.23\lambda_0 \times 0.3\lambda_0 \times 0.002\lambda_0$	29.5 × 37.7 × 0.3	3.34	[58]
Silicone elastomer/Copper	$0.35\lambda_0 \times 0.35\lambda_0 \times 0.017\lambda_0$	30 × 30 × 1.5	3.35	[167]
Cellulose paper/Copper	$0.64\lambda_0 \times 0.38\lambda_0 \times 0.002\lambda_0$	119.4 × 70 × 0.46	5.39	[74]
Cellulose paper/Graphene	$0.64\lambda_0 \times 0.38\lambda_0 \times 0.002\lambda_0$	119.4 × 70 × 0.46	9.8	[74]
polydimethylsiloxane (PDMS)/Copper	$1.21\lambda_0 \times 1.21\lambda_0 \times 0.12\lambda_0$	50 × 50 × 5	-	[168]
Jean cotton/Copper	$0.52\lambda_0 \times 0.58\lambda_0 \times 0.024\lambda_0$	64 × 71 × 3	-	[169]
Rubber/Copper	$0.49\lambda_0 \times 0.44\lambda_0 \times 0.015\lambda_0$	60 × 55 × 1.88	-	[170]
Polyimide Sheet/LIG	$0.50\lambda_0 \times 0.53\lambda_0 \times 0.002\lambda_0$	26.22 × 27.58 × 0.12	14.08	This Paper

Table 3.1 shows the comparative analysis of sensitivity and physical dimensions of the fabricated prototype antenna with state-of-the-art. This study shows that the proposed design offers better sensitivity compared to the previously reported works while retaining comparable dimensions. The λ_0 in the Table 3.1 is the free space wavelength.

3.4 Summary

This work demonstrates a flexible rectangular LIG patch antenna with an inset feed at the 5.8 GHz ISM band. The performance of the antenna with LIG is examined using various characterization techniques. The chemical characterization of the LIG addresses the formation and composition of the graphene onto the PI sheet. From the measured RF characteristics, the antenna provides a gain of 1.82 dBi in the operating band. The strain sensing analysis of the fabricated prototype antenna was used for examining the sensitivity. The significant sensitivity of the antenna-based sensor enables its usage in real-time IoT strain sensing applications, such as human motion detection and structural health monitoring. Finally, more rigorous optimization of laser parameters can provide even better sensitivity and stability for enhancing the performance of the antenna.

Chapter 4

MXene-Based Flexible Patch for Pressure and Level Sensing

4.1 Introduction

Flexible antennas with simple structures are becoming prominent in the communication sector, majorly for sensing applications. Generally, for fabricating the patch antennas mostly copper, aluminium, and silver nanoparticle inks are often used as radiating elements in satellite communication [18], radio frequency identification (RFID) [19], and other wireless communication systems [20]. These antennas normally consist of high electrical conductivity for transmitting or receiving electromagnetic waves. Besides, resistance to degradation caused by mechanical deformation is also an important factor for the conductive material. So, the performance of flexible antennas depends significantly on the electrical conductivity of the material and its deformable nature [21]. Moreover, metals are not excellent candidates for sensing applications when compared to functional nanomaterials.

In general, devices with high sensitivity and flexibility were developed by synthesizing novel nanomaterials to analyse physical parameters [171], [172]. However, microwave sensing has become one of the diversifying technologies for various wireless sensor applications. By using the microwave sensors, continuous sensing of two different physical sensing parameters such as pressure and level can be monitored in a simplified manner. With the progress of the IoT, there is a need for the compact integration of radio communication devices without sacrificing portability, flexibility, and lightweight properties [173]. MPA's

are the most conventional planar antenna type, especially those used in the sub - 6 GHz frequency range [174]. Recently, the usage of nanomaterials for the conducting part and high dielectric constant thin materials as a substrate have made patch antennas more effective for wireless applications. Therefore, the advancement of new methods for flexible patch antennas is necessary for selecting the materials and fabricating the device.

Lately, a new material MXene was introduced to compensate for the mentioned issues with an excellent electromagnetic interference (EMI) shielding performance [175], [176]. MXenes belong to the family of 2D materials and are represented by $M_{n+1}X_nT_X$, where M denotes the early transition metals (Ti, Zr, V, Nb, or Mo) and X represent carbon and/or nitrogen. Here the T_X symbolizes the terminating groups (–OH, –F, or =O), which are mechanically durable, metallic with good conductivity [177]. The MXene films allow simple, eco-friendly, and scalable manufacturing from aqueous solutions with no surfactant or binder [178]. The MXenes were developed in several ways using a variety of patterning and coating processes, including spray coating, dip coating, inkjet printing, and 3D printing [179], [180], [181]. A few applications like RFID tags and dipole antennas were demonstrated using MXene as a promising material for wireless communication [182]. In addition, the rapid research is expanding in utilizing MXene as an advanced nanomaterial for supercapacitors [183], electromagnetic wave absorption [184], [185], energy harvesting [186] and wearable technologies [187]. Hence, flexible antennas utilizing MXenes are assuring due to their decent electrical conductivity and better mechanical deformability.

The work proposes for the first time the fabrication of MXene on a paper-based flexible rectangular MPA with a target resonant frequency of 5.8 GHz for pressure and level sensing applications. The chemical properties of MXenes were experimentally investigated in demonstrating their potential for usage in MPA's. The proposed rectangular patch antenna has a narrow single band with a reasonable gain and stable radiation patterns having the electrical dimensions of 0.49 λ_0 × 0.47 λ_0 × 0.002 λ_0. The key idea of this research is to use the single antenna-based sensor for multiple applications as presented for both pressure and level sensing. In both the cases, the shift in the resonant frequency is observed due to the variation in the effective physical parameters of the MXene and the polyimide caused by the variation in the sensing parameters.

4.2 Experimental Section

4.2.1 Synthesis of MXene

The synthesis of multilayer $Ti_3C_2T_X$ MXene solution was produced by selective etching of Aluminium (Al) layers from Ti_3AlC_2. Fig. 4.1a elaborates the detailed illustration of the MXene synthesis using the minimally intensive layer delamination (MILD) process. Firstly, 0.8 g of Lithium Fluoride (LiF) was dissolved in 10 ml (6M) hydrochloric acid (HCl) under continuous stirring for 5 minutes. After the complete dissolution of LiF in HCL, 0.5 g of Ti_3AlC_2 powder was added to it. The then blended solution was again stirred constantly with 700 rpm speed and was upheld for 36 hrs at 35^0 C. The resultant solution was diluted with approximately 150 mL of De-Ionized (DI) water, then followed with multiple wash cycles by centrifugation until the pH of the solution is higher or equal to 6. Once the solution becomes neutral, it is ultra-sonicated in an ice bath for 60 min, which finally results in the MXene colloidal solution with a multi-layered structure.

4.2.2 Fabrication of Mxene Based Antenna

Fig. 4.1b depicts the detailed fabrication process of the MXene coated paper-based antenna. The resultant Mxene solution was utilized in producing thin MXene film on cellulose paper by vacuum filtration technique. The Mxene coated cellulose paper film was then cut with a laser according to the specified patch dimensions (13.3×17.23 mm^2). Here, the laser-cut MXene coated film works as a patch with the measured conductivity of 2.89×10^5 S/m (using four-probe), which is affixed to the substrate material polyimide sheet. The copper tape as a ground plane with the conductivity of 5.96×10^7 S/m is attached to the other side of the polyimide sheet having a thickness (h) = 0.127 mm, relative permittivity (ε_r) = 3.5, and loss tangent (δ) = 0.0026 [158]. This work is proposed to design a conventional MPA adhering to ISM standards, which is operating at 5.8 GHz resonant frequency for sensing applications. A microstrip antenna was designed by using the standard microstrip antenna design equations [159], to resonate at 5.8 GHz. Fig. 4.1c shows the geometry of the MXene coated cellulose paper-based patch antenna along with the fabricated prototype.

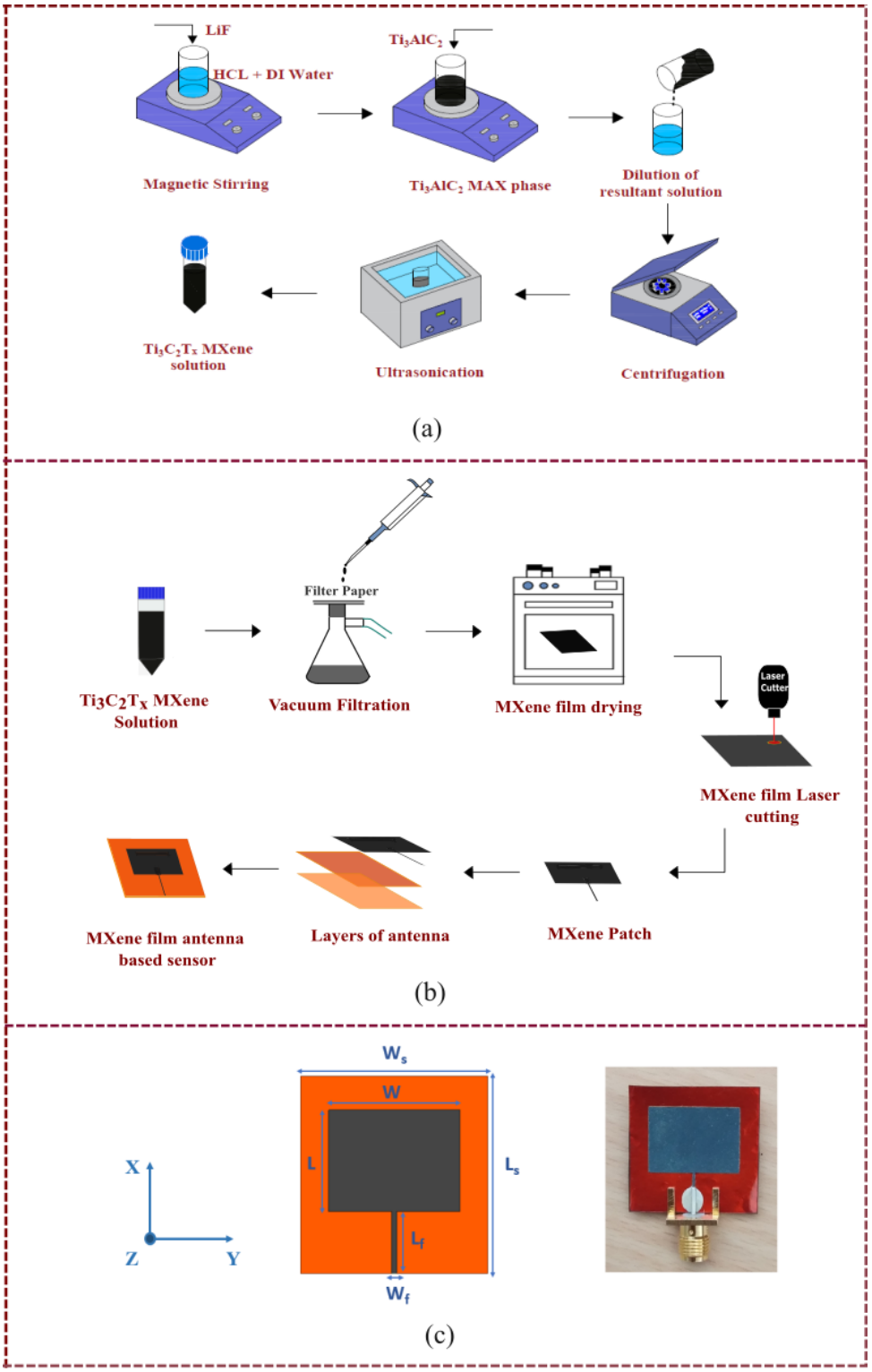

FIGURE 4.1: a) Process for the synthesis of MXene solution b) Fabrication procedure of MXene film antenna based sensor c) Geometry of the rectangular patch antenna with dimensions resonating at 5.8 GHz [L_s = 25.8, W_s = 24.584, L = 13.3, W = 17.23, L_f = 12.303, W_f = 0.618 (all the dimensions are in mm)] along with its fabricated prototype.

4.3 Results and Discussion

4.3.1 Chemical Characterization

The XRD patterns of both Ti_3AlC_2 and fully exfoliated $Ti_3C_2T_X$ are recorded to investigate the material structure, as shown in Fig. 4.2a. The attained diffraction peaks of the Ti_3AlC_2 pattern were analogous with the JCPDS card number 52-0875. The resultant $Ti_3C_2T_X$ pattern depicts the elimination of crystal plane (1 0 4) at $2\theta = 38.79^0$, and the characteristic peak (0 0 2) has shifted from $2\theta = 9.47^0$ to 6.9^0, which indicates the exfoliation of Al layers from Ti_3AlC_2 pattern. It also shows the presence of –F, –OH, –O terminal groups formed in the $Ti_3C_2T_X$ after the eradication of Al atoms from the original Ti_3AlC_2 [188].

The functional groups formed on the surface of the $Ti_3C_2T_X$ were examined using FTIR spectra, as shown in Fig. 4.2b. The band observed at 3468.4 cm^{-1} is the stretching vibration of –OH, and the peaks at 1601.5 cm^{-1} and 1035.2 cm^{-1} confirm the existence of C=O and C–O, respectively. The two typical peaks at 1337.8 cm^{-1} and 568.5 cm^{-1} correspond to the surface terminal group of C-F and bending vibration of –OH [189], [190].

Fig. 4.2c shows the XPS survey spectra of the $Ti_3C_2T_X$ material that is coated on the cellulose paper. The peaks at various binding energies 35.0, 60.0, 285.0, 456.0, 531.0, 563.0, and 686.0 eV were attributed to Ti 3p, Ti 3s, C 1s, Ti 2p, O 1s, Ti 2s and F 1s respectively. The detailed information of Ti 2p, C 1s, O 1s, and F 1s XPS spectra is depicted in Fig. 4.2d – 4.2g. As shown in Fig. 4.2d, two doublet peaks located at 461.6 and 455.5 eV in Ti 2p de-convoluted XPS spectra are allocated to Ti–C bonds indicate the existence of $Ti_3C_2T_X$ structure after the electrochemical exfoliation procedure [191]. The binding energies at 455.3, 456.4, 457.5, and 459.4 eV were assigned to Ti–C, Ti–X, which relates to sub-stoichiometric titanium oxycarbides or titanium carbides, Ti_XO_Y and TiO_2 [192]. Fig. 4.2e shows the C 1s spectra that can be fitted to five components centered at 281.9, 284.3, 285.2, 286.5, and 289.0 eV, which are attributed to the bonds of Ti–C, C–C, –CH2 & –CH3, C–O, and –COO respectively. The O 1s spectra in Fig. 4.2f shows three components at 529.8, 530.8, and 532.7 eV, allocated to O–Ti species, related to amorphous or crystalline TiO_2, C=O, and C–O bonds, respectively. The XPS spectra of F 1s depicted in Fig. 4.2g illustrates two peaks at 684.8 and 686.8 eV, which were assigned to F–Ti and F–M bonds (i.e. M is an unknown metal), respectively. The appearance of F–M might be from the minimal residual amounts of MF_3. The de-convoluted core-level fitted XPS spectra were in correspondence with the reported literature [193], [194].

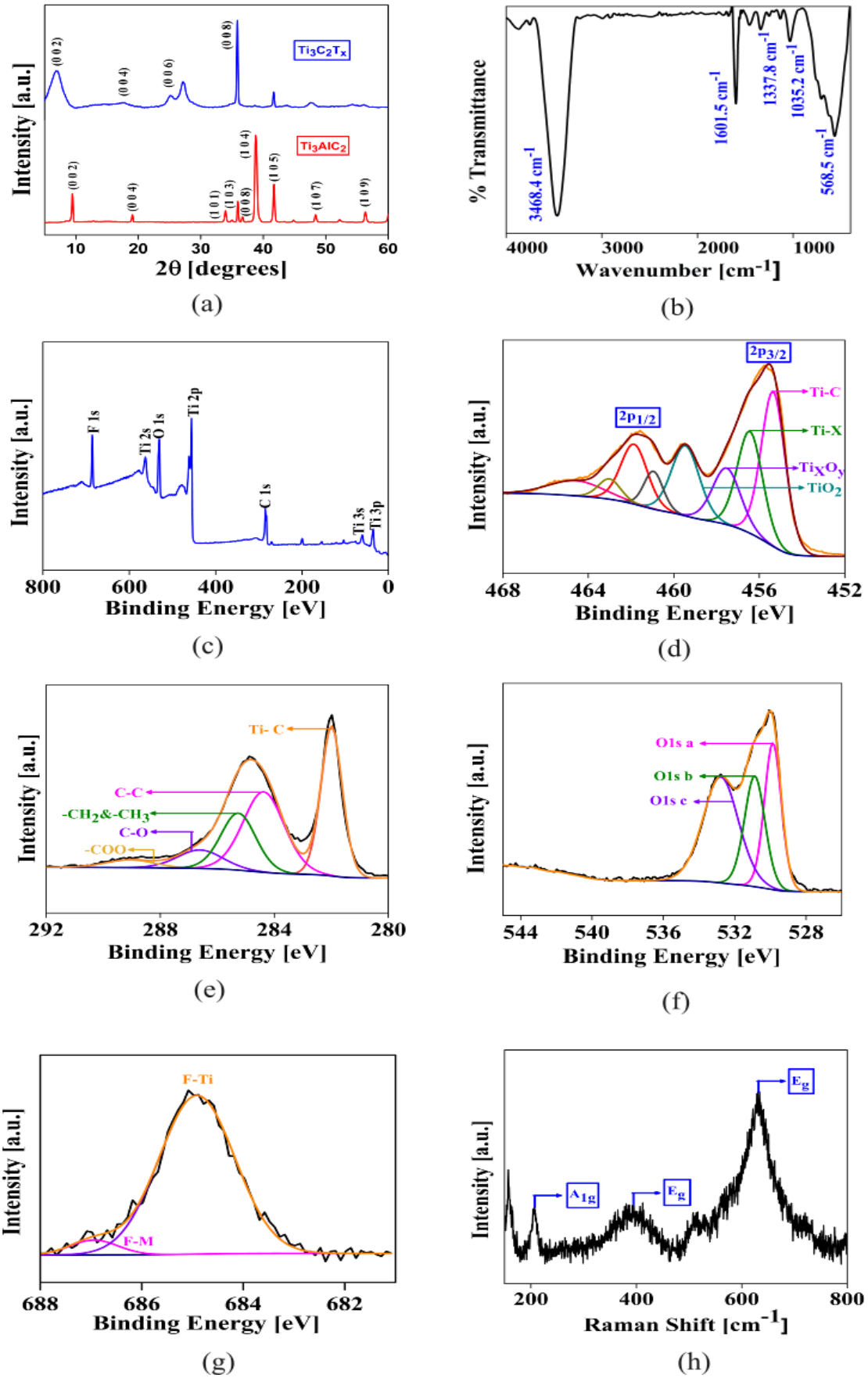

FIGURE 4.2: a) XRD patterns of MAX (Ti_3AlC_2) and MXene ($Ti_3C_2T_X$) b) FTIR spectra of $Ti_3C_2T_X$ film, c), d), e), f) and g) are the XPS survey spectra of $Ti3C2T_X$ and the patterns of Ti2p, C 1s, O 1s and F 1s respectively, h) Raman spectra of $Ti_3C_2T_X$

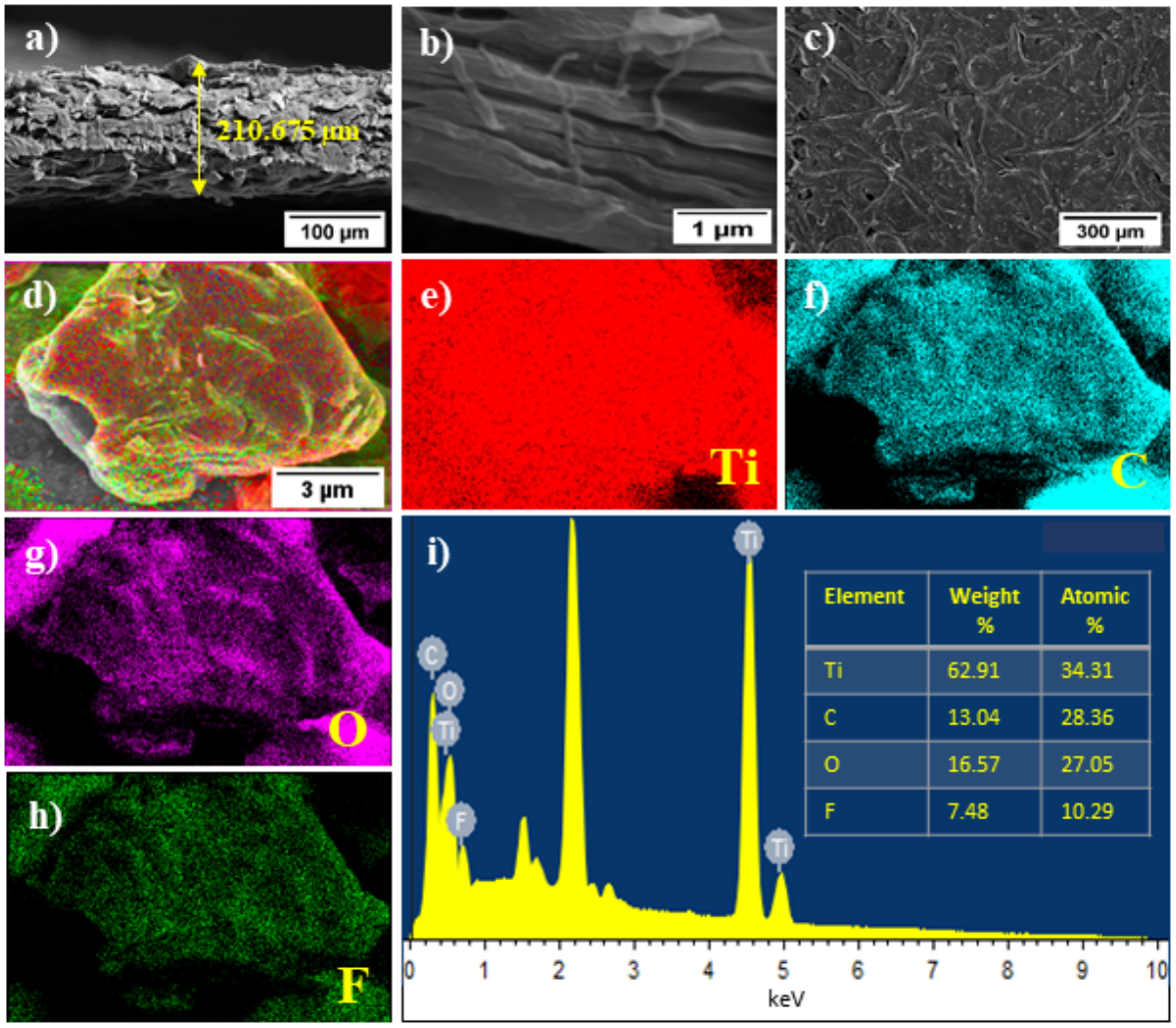

FIGURE 4.3: SEM images of $Ti_3C_2T_X$ film-coated cellulose paper a), b) Cross-sectional view c) Top view d), e), f), g), h) Elemental mapping images of Ti, C, O and F at 3 μm resolution i) energy dispersive X-ray (EDX) spectrum with weight and atomic percentage of elements for $Ti_3C_2T_X$

Furthermore, the synthesized $Ti_3C_2T_X$ material was analysed for molecular interactions by Raman spectroscopy, as depicted in Fig. 4.2h. The Raman shift at 205 cm^{-1} is assigned to the first order out-of-plane vibrations corresponding to Ti and C elements [195]. The Raman bands appeared at 420 cm^{-1} and 633 cm^{-1} representing the vibrational band of E_g and A_{1g} and were allocated to the in-plane modes of Ti and C, which belong to the surface functional groups of $Ti_3C_2T_X$ [196], [197].

The SEM images shown in Fig. 4.3a, 4.3b portrays the cross-sectional view, and Fig. 4.3c, 4.3d shows the top view at magnification levels (100 μm, 1 μm) and Fig. 4.3c, 4.3d shows the top view of MXene coated cellulose paper with magnifications (300 μm, 3 μm). The thickness of the Mxene coated cellulose paper is analyzed form cross-sectional

view, which is ∼210.675 μm. The high-resolution cross-sectional SEM image shown in Fig.4.3b depicts the layered structure of $Ti_3C_2T_X$ with visible Interlayer spacing between the layers. Also, from Fig. 4.3c, it is evident that $Ti_3C_2T_X$ is uniformly deposited on the cellulose paper. Further, the elemental distribution of $Ti_3C_2T_X$ is confirmed with the elemental mapping images as depicted in Fig. 4.3d - 4.3h. The EDX spectrum shown in Fig. 4.3i and elemental mapping images revealed the existence of Ti, C, O, F, elements indicating the presence of $Ti_3C_2T_X$ on cellulose paper.

4.3.2 RF Characterization of MXene-Based Antenna

The presented rectangular MPA was designed, optimized, and simulated using the HFSS V.15.0. The fabricated prototype was interfaced with a VNA to measure the $|S_{11}|$ parameter. Fig. 4.4 exhibits the simulated and the measured $|S_{11}|$ parameters. The simulated antenna resonates at 5.8 GHz with a fractional bandwidth (FBW) of 3.96 %, whereas the measured one resonates at 5.84 GHz having an FBW of 1.72 %.

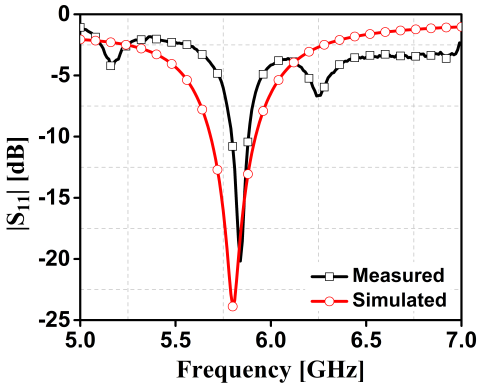

FIGURE 4.4: Simulated and measured plots of $|S_{11}|$

Fig. 4.5 depicts the simulated radiation patterns in the XZ and YZ planes of the designed patch antenna. The antenna has a unidirectional pattern with the simulated and measured gain of -4.941 dBi and - 6.1413 dBi respectively in both the planes at 5.8 GHz resonant frequency. The designed antenna also offers a difference of 40 dB between co-polarization and cross-polarization levels in both the planes. The observed reduced gain for the MXene based antenna is primarily due to its lower conductivity of the patch and is comparable with the other flexible antennas in the literature. Therefore, the proposed MXene based antenna can be used for IoT-based sensing applications.

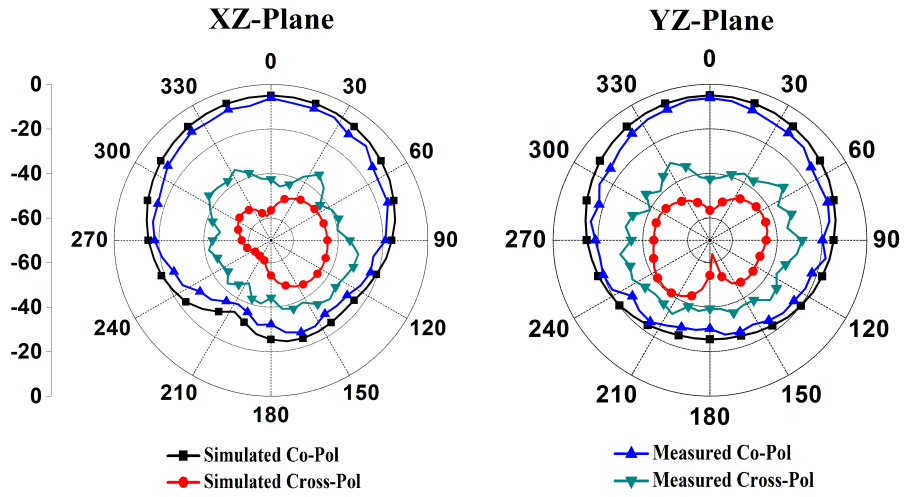

FIGURE 4.5: Simulated & measured radiation patterns of XZ & YZ planes at 5.8 GHz

4.3.3 MXene Based Antenna for Pressure Sensing

The pressure in this context refers to the loading pressure. Different loads are considered to apply the pressure on the rectangular patch antenna for analysing the effect on the antenna parameters. Fig. 4.6a presents the applied pressure with a load on the antenna. Three discrete loads of different weights were placed one after the other on the MXene patch which is connected to VNA via an SMA connecter to observe the frequency variations. Fig. 4.6b depicts the comprehensive plot for change in resonant frequency while applying different loading pressure, varying from 2.169 kPa to 3.429 kPa. From Fig. 4.6c, it is clear that as the loading pressure on the antenna increases, the resonant frequency of the pressure sensor reduces significantly. By varying pressure with different loads, an approximately linear variation in the resonant frequency was observed. Hence, the pressure sensor at this range between 2.169 kPa to 3.429 kPa can be used in solid-state pressure switches which are available in different pressure ranges from 0-1 bar.

In order to observe the restoration of the frequency with and without pressure, a continuous repeatability analysis was performed. For each increment of pressure, the normalized resonant frequency is observed to decrease by approximately 20 MHz. When the pressure is applied as presented in position 1 (Fig. 4.7a), the resonant frequency decreases, and while no pressure is applied as shown in position 0 (Fig. 4.7b), the frequency returns to its original state, indicating the deformable nature of the antenna. As depicted in Fig. 4.7c, the resonant frequency of the antenna-based sensor is stable during the continuous measurements and is easily restored after the removal of external pressure.

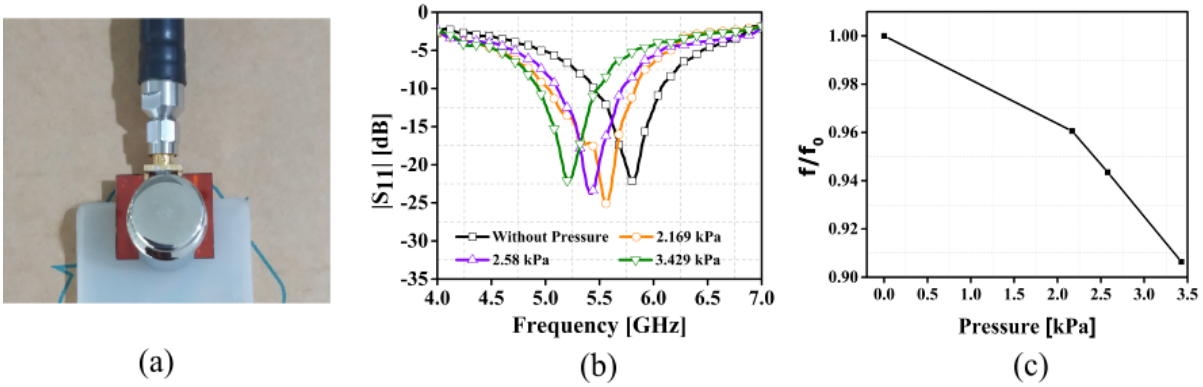

FIGURE 4.6: a) Pressure sensing with a load on the antenna, b) Frequency variation plot with and without applied pressure, c) Pressure versus normalized frequency plot

This is possible due to the thin layers of the antenna while applying a relatively lower amount of pressure.

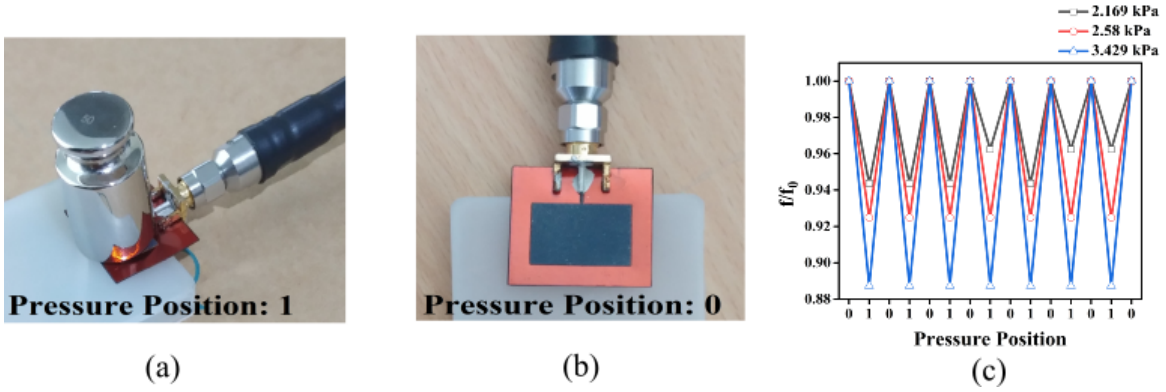

FIGURE 4.7: Repeatability analysis by applying continuous loading pressure a) With different pressure loads, b) Without pressure loads, c) Plot for continuous measurements with different pressure loads

The enhancement in the sensitivity of MXene based antenna with external stimuli (i.e., pressure) as a force transport layer was well attained owing to a significant enhancement in the contact area even at applied minimal external pressure. The external pressure transmits the load onto the conductive layered $Ti_3C_2T_X$ thin-film, decreasing the interlayer spacing between the layers depicted in the SEM image above in Fig. 4.3b, leading to a reduction in interlayer resistance, consequently increasing the probability of electron hopping in between the layers. However, upon the external load, the interlayer resistances from R_1 to R_n are decreased to RL_1 to RL_n, and the equivalent circuit diagram can be deemed akin to resistors in parallel, as displayed in Fig. 4.8. In brief, when external pressure was applied onto the MXene based antenna, the distance between two parallel sheets of $Ti_3C_2T_X$ was reduced. It became more petite than the tunneling distance owing to which there is a reduction in the tunneling resistance. Hence, the increased

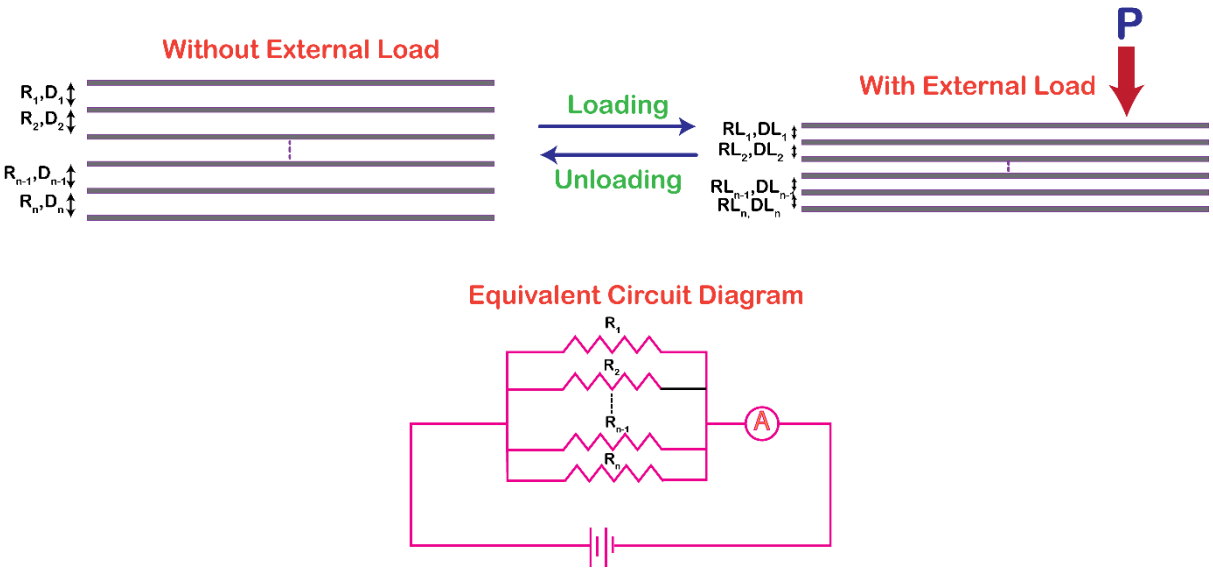

FIGURE 4.8: Illustration of conventional underlying transduction mechanism for MXene antenna based pressure sensor schematic

electron hopping upsurges the fabricated device current, which in turn helps to decrease the resonant frequency of the antenna at applied external load. The tunneling resistance can be theoretically determined using Eqn. (4.1) [198].

$$R_{tunnel} = \frac{V}{aJ} = \frac{2}{3}\frac{h^2 t}{ae^2\sqrt{2m\Phi}} exp\left(\frac{4\pi}{h}\sqrt{2m\Phi t}\right) \tag{4.1}$$

Where V, J, a, e, and m denote the potential difference applied, tunneling current density, the cross-sectional area of the tunnel, charge, and mass of the electron. Also, h, ϕ, and t indicate Planck's constant, height of the potential barrier, and thickness of insulating material (in this case, air) between the conductive flakes/ layers of $Ti_3C_2T_X$, respectively. As mentioned, the R_{tunnel} is directly proportional to $te^{\sqrt{t}}$, Which indicates that with the application of external pressure, the void space (i.e., insulating medium) between the layers reduces, decreasing the tunneling resistance steeply. However, quantification of tunneling resistance will require integration of the parameters over a 3D coordinate system along with a sophisticated in-situ TEM technique to quantify the change in interlayer distance ($t_f - t_o$) under applied pressure which is well studied in the literature [199]. The schematic conventional underlying transduction mechanism for the MXene antenna-based pressure sensor is illustrated in Fig. 4.8.

Further, the linearity in the sensitivity signifies the tunneling resistance that has been responsible for the increment in current when external pressure is applied. Thus, the

enhancement of current flow in the radiating element creates the change in the magnetic field as shown in Eqn. (4.2),[200] which in turn increases the electric field (E-field) strength.

$$\hat{n} \times \bar{H} = \bar{J}_s \tag{4.2}$$

The increment of E-field strength within the antenna is due to the application of external pressure. Fig. 4.9a – 4.9d depicts the electric field distribution of the antenna with and without loads. At the maximum pressure load, the E-field strength is higher when compared to that in case of the antenna without pressure.

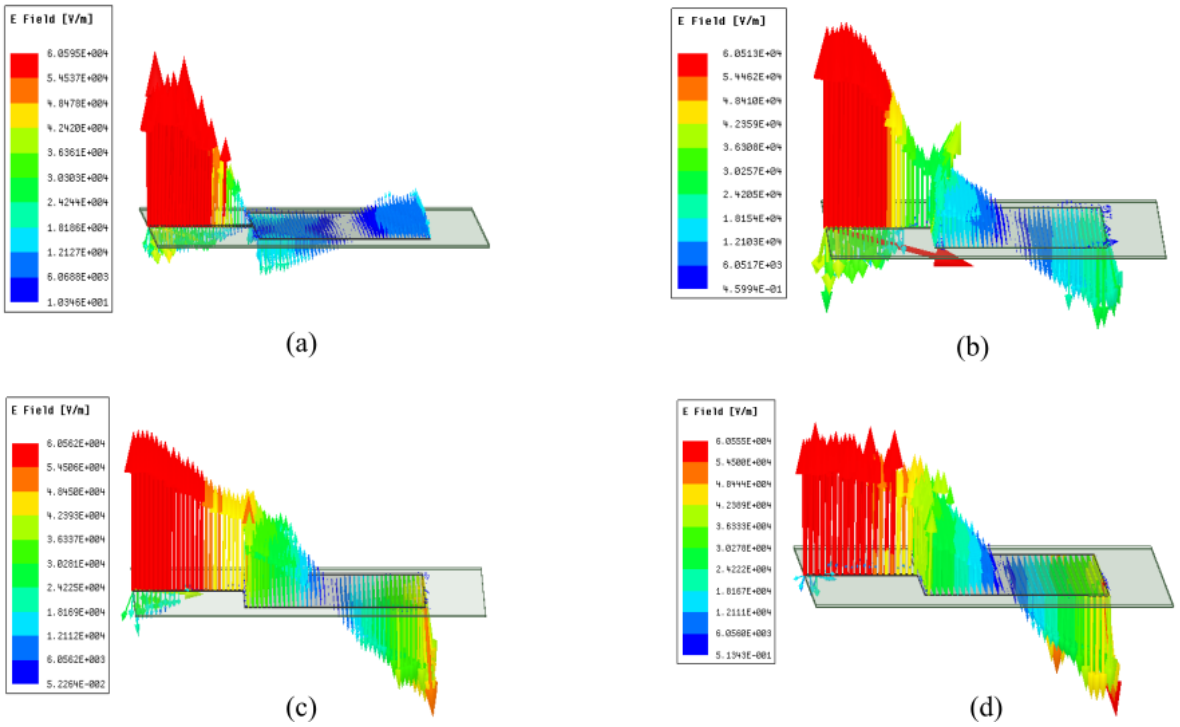

FIGURE 4.9: Electric field distribution within the substrate at the resonant frequency in case of a) Without pressure b) With 2.169 kPa (50 g) applied pressure c) With 2.58 kPa (100 g) applied pressure d) With 3.429 kPa (200 g) applied pressure

The pressure-sensing operation has also an effect on the dielectric constant, which is related to the piezo-dielectric and piezo-resistivity properties. Here the dielectric constant changes according to the pressure applied as shown in Eqn. (4.3) [201].

$$\frac{\partial ln\alpha}{\partial p} = \frac{3}{\varepsilon}\frac{\partial ln\varepsilon}{\partial p} \tag{4.3}$$

Where α is the polarizability, ε is the dielectric constant, and p is the applied pressure onto the material. From Eqn. (4.3), the increase in applied pressure leads to an increase

in the dielectric constant of the polyimide material which in turn reduces the resonant frequency of the antenna. The resonant frequency (f_r) is inversely related to the effective dielectric constant (ε_{reff}), when the effective length of the patch (L_{eff}) is constant. So, as the dielectric constant increases with applied pressure, the resonant frequency decreases accordingly as shown in Eqn. (4.4) [159].

$$f_r = \frac{c}{2L_{eff}\sqrt{\varepsilon_{reff}}} \tag{4.4}$$

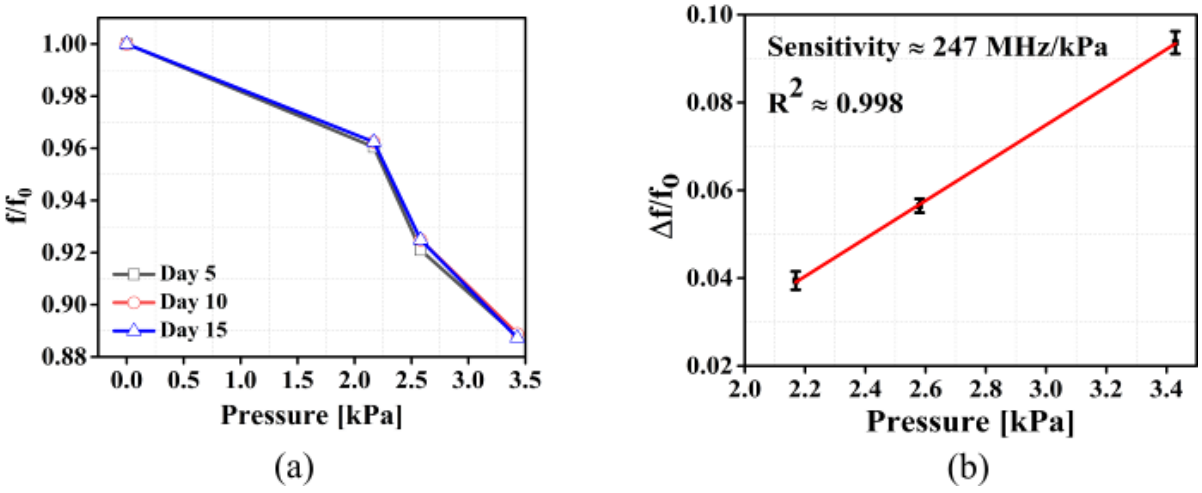

FIGURE 4.10: a) Stability analysis with discontinuous measurements, b) Experimental relationship between frequency and pressure

Thus, the pressure sensing operation is based on the resonant frequency shift due to the pressure applied on an MXene based patch antenna.

Figure 4.10a shows the plot of stability performance with respect to the different loading pressure. The measurements were taken discontinuously over a period of fifteen days with a five-days of an inherent gap. The same loading pressures were applied on the antenna-based sensor for several days and observed the frequency shift with the function of pressure. As per the results, approximately the normalized frequency variations are the same for various pressure loads on different days. As shown in Fig. 4.10b, a linear relationship exists between normalized frequency and applied pressure. The sensitivity of the antenna for pressure sensing is approximately 247 MHz/kPa, which can be used for low-pressure sensing applications. The sensitivity of pressure is calculated using the following Eqn. (4.5) [159], where $f_{reference}$ is the initial resonant frequency, f_{shift} is the shifted frequency after applying the pressure.

$$\frac{\Delta f}{f} = \frac{|f_{reference} - f_{shift}|}{f_{reference}} \tag{4.5}$$

4.3.4 MXene Based Antenna for Level Sensing

This work mainly focuses on the effect of the interaction between the liquid level and the dielectric property of the antenna. The change in liquid level exactly at the radiating element of the antenna tends to shift the resonant frequency due to the variation in dielectric constant from air to liquids. There is a scope to exploit this property to design a level sensor for different liquids. To test the level sensing mechanism, various liquids with differently concentrated solutions were used. Formic acid with molecular weight 46.03 g/mol, 11 mmol glucose, de-ionized (DI) water, and saline water were considered to observe the change in frequency for differently concentrated solutions. Figure 4.11a & 4.11b shows the antenna, which is kept at room temperature is attached to the beaker with half-filled and completely filled levels. As depicted in Fig. 4.11c, all the four variants are having the shift of frequency with respect to the change in the liquid level. The minute difference in resonant frequency shift between the examined liquids could be attributed to the variation in the dielectric constants of the liquids. Here, since the antenna-based sensor is attached to the beaker, the frequency change is nearly same for all the considered aqueous solutions and the frequency shift does not depend on the pH level of the liquids. This experiment proves, regardless of the concentrations of the liquid, that the frequency shift is mostly similar depending on the occupancy of the liquid level.

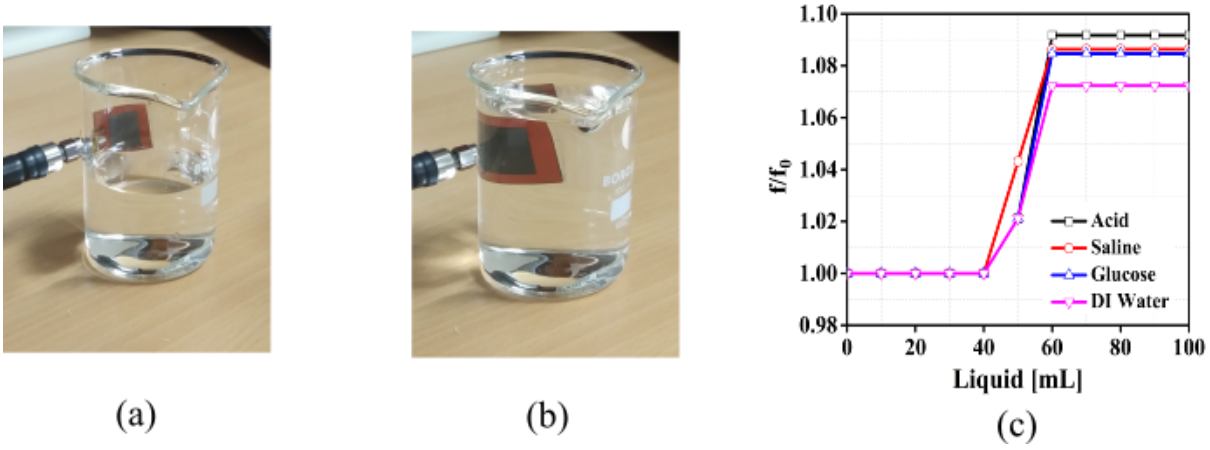

FIGURE 4.11: a) & b) Antenna attached to the beaker with a half-filled and filled liquid solution, c) Level versus normalized frequency plot for differently concentrated solutions

The level sensing performance of the antenna-based sensor was measured at different temperatures varying from 25^0 C (room temperature) to 150^0 C with various concentrated

liquids as shown in Fig. 4.12a & 4.12b. The antenna is heated using the magnetic stirrer hot plate at temperatures 80^0 C and 150^0 C, which is then mounted on the empty beaker at a medium height at each temperature. By filling the water in the beaker, it is observed that the level sensor exhibits almost the same frequency shift starting from medium level at each temperature. This results in the device can be used at high temperatures until 150^0 C, which has a stable effect on frequency variation.

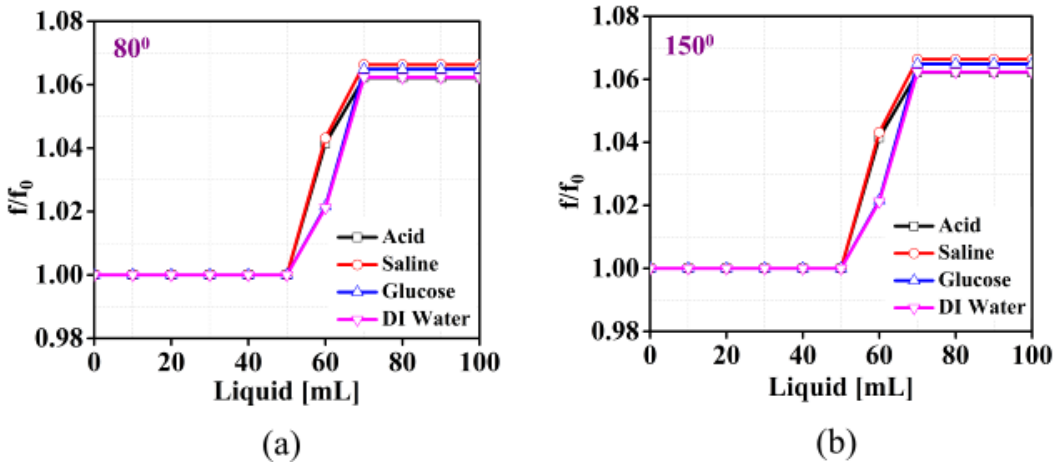

FIGURE 4.12: a) & b) Measurement of the frequency with respect to level by temperature variations of antenna at 80^0 and b) 150^0

The basic principle of the antenna-based level sensor presented depends on the dielectric perturbation phenomenon. It does not require a direct interface in monitoring the liquid level, thus offering a simple mechanism as compared to traditional sensors. Here, the antenna-based sensor-enabled beaker is presented with two different cases. In the first case, the beaker is empty Hence, the air is acting as an effective dielectric constant to the antenna and thus no variation in resonant frequency is observed. In the second case, when the beaker is getting filled with liquids such as, acidic or neutral solutions the effective dielectric constant changes to the dielectric constant of solutions, which tends to vary the resonant frequency by sensing the liquid level variation. Once the level crosses the radiating element of the antenna, the frequency becomes constant. Thus, the resonant frequency depends on the effective dielectric constant as shown in Eqn. (4.4) [159].

The placement of the antenna on the beaker makes it to be used as a discrete level sensor, i.e., either as a high-level detector or a low-level detector sensor. The frequency shift is the same regardless of the location of the antenna with respect to the beaker. As shown in Fig. 4.13a & 4.13b, when the antenna is placed on the lower side portion of the beaker the frequency shift was observed from 20 mL to 40 mL approximately. While in Fig. 4.13c & 4.13d the antenna is placed on the top side portion of the beaker, the

frequency shift was noted from 60 mL to 80 mL approximately. This experiment shows the placement of the antenna holds a dominant role in using it either as a high-level or low-level sensor for continuous observations for various IoT applications.

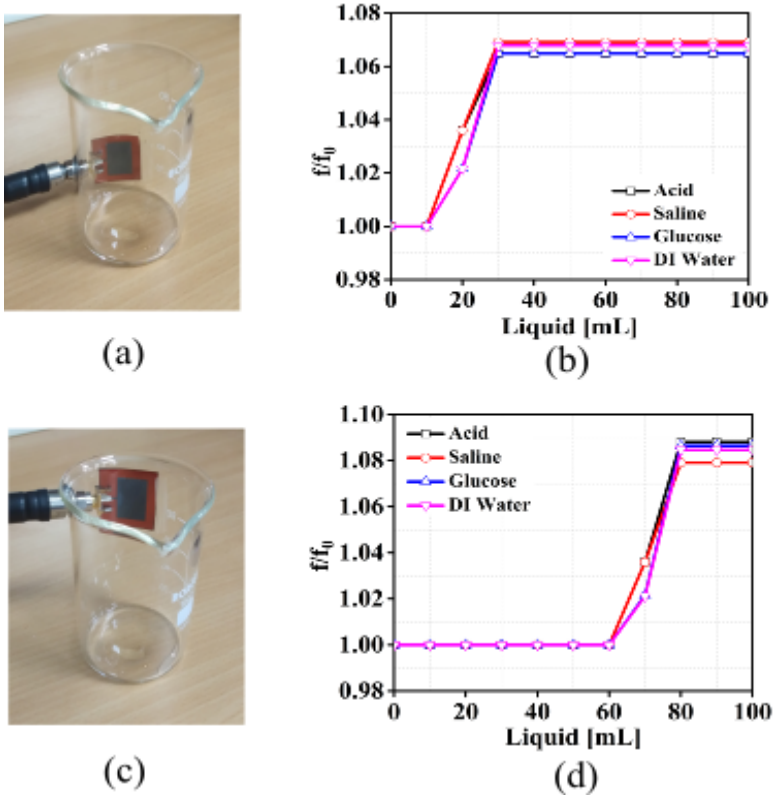

FIGURE 4.13: a) & b) Low-Level sensing c) & d) High-level sensing

4.4 Discussions

Table 4.1 presents the comparison of different features of the flexible antennas with the proposed work in this literature. Most of the reported works developed novel conductive materials/inks for usage in flexible wireless applications. Based on the conductivity of the conductive material the characteristic parameters like gain and efficiency of the antenna vary. The geometry of the antenna reduces with an increase in flexibility depending upon the design and the thickness of the materials utilized in device fabrication. In addition to the flexible nature of the antenna, the change in antenna parameters with respect to physical parameters like strain, pressure, temperature, and level makes it suitable for flexible antenna-based wireless sensing applications.

TABLE 4.1: Parameter comparison table for flexible antennas

Conducting Material	**Conductivity [S/m]**	**Electrical Dimensions**	**Gain [dBi]**	**Sensing Parameter**	**Reference**
Conductive polymer	1.5×10^4	$(0.16 \times 0.10)\ \lambda_0$	- 8.6	Wireless sensor applications	[202]
Silver Nanoparticle	3.53×10^7	$\pi\ (0.04 \times 0.04)\ \lambda_0$	- 5.6	-	[203]
flexible multi-layer graphene film	$\sim 10^6$	$(0.64 \times 0.38)\ \lambda_0$	-	Strain	[74]
Liquid metal (eutectic gallium–indium alloy)	3.4×10^6	$(0.40 \times 0.24)\ \lambda_0$	-	Pressure	[120]
Silver flakes, TEA, 4-methyl-2-pentanone, Fluorine rubber ink	8.49×10^4	$(0.66 \times 0.58)\ \lambda_0$ (Approx.)	-	-	[204]
Nanocomposite	7.5×10^3	$(0.34 \times 0.24)\ \lambda_0$	1.22	-	[205]
Silver Nanowires	8.1×10^5	$(0.43 \times 0.38)\ \lambda_0$	0.37	Strain	[64]
MXene	$\mathbf{2.89 \times 10^5}$	$\mathbf{(0.49 \times 0.47)}\ \lambda_0$	**- 6.14**	**Pressure/Level**	**This Paper**

4.5 Summary

The MXene based flexible and conformal antennas for pressure and level sensing are one of the promising candidates for wireless sensor applications. The synthesized MXene has a favorable chemical characteristics that can be utilized as a low-cost flexible radiating material. The antenna is designed at the operating frequency of 5.8 GHz having a gain of around - 6.14 dBi with unidirectional radiation patterns. This gain is suitable for flexible wireless sensing applications and is in line with the literature. To analyse the pressure and level sensing performance, the antenna has undergone testing with repeatability, stability, and temperature parameters. The antenna parameters are exploited to sense the applied pressure and level of the liquid. The calculated sensitivity of the pressure sensing is approximately 247 MHz/kPa. In level sensing, there is an ample amount of frequency shift with respect to the change in liquid solution levels. As a result, the proposed MXene based antenna is suitable for both IoT-based wireless pressure and level sensing applications.

Chapter 5

Heat Triggered Transient Microstrip Antenna for Pressure Sensing Applications

5.1 Introduction

The evolution of wireless communication devices has become an active area of research with the rapid development of novel materials [206]. Antennas have multiple parameters, e.g., S-parameters, radiated power, etc., which are very sensitive to external physical quantities such as temperature [207], strain [74], and pressure[120]. Hence, those antenna parameters are recently being studied and exploited as well-behaving sensing parameters. Moreover, currently, there is a requirement for one-time usage devices while ensuring biodegradability in several wireless communications-dependent security applications[208]. The transient antenna-based sensor is one pathway that opens up new methods for building such devices. Besides its self-destructive nature, the transient technology opens a wide range of security applications while securing confidential data [209]. Even though transient electronics field has evolved over the past decade, reports on the fabrication and study of transient antennas for sensing applications remain scant. Consequently, there is a scope for utilizing transient electronics in developing transient antennas for wireless communication and IoT applications.

The transient devices require materials that get degraded with an external trigger in a controlled environment. As the dielectric material, various water-soluble and acid-soluble polymers and green materials [210], [211], which will degrade through fungal biodegradation, were studied [212], [213], . But the degradation of material through biodegradation will take a longer period when compared to the external stimuli. Lately, some water-soluble polymers like Polyvinyl Alcohol (PVA), Polyvinylpyrrolidone (PVP), polycaprolactone (PCL), and other materials were considered in manufacturing transient devices [214], [215]. While degradation in wet transience, the materials exhibit swelling or a long time solubility. Hence, transient devices with other triggers, such as heat, light and temperature, are needed. Wax-based dielectric heat-triggered devices can be one of the possible solutions to resolve the issue.

Transitory technology is advancing its research across multiple domains because of its momentary nature which is helpful for a range of short-term applications. Some of the previously presented transient electronic applications include RF power harvesting systems [216], the transient electronic antenna [214], electrochemical sensors [217], wearable pressure sensors [218], and thin film transistors [219], and their disappearing nature is wet transience. Sensors with conformal and flexible nature are one of the diversifying fields in healthcare, robotics, security, etc., by making them wireless, low-cost, and precise [220], [221]. The sensor-based applications require effective nanomaterial to sense any physical parameter. The complex and miniaturized antenna designs are essential for various communication application purposes [222], [223]. The simple patch antenna with nanomaterial makes the device more sensitive towards sensing applications.

The utilization of functional nanomaterial is necessary to make the antennas sensitive-friendly and short-term usage devices. Existing research shows the development of transition metal di-chalcogenides (TMD) based antennas with LIG-MoS_2 [224] and silver nanoparticle ink [225] in enhancing RF performance. Specifically, in the two-dimensional (2D)-TMD family, the Nickle di-chalcogenides (NiS_2) have gained significant attention due to their distinct optoelectronic properties, environmental stability, and compatibility with low-cost synthesis process. The researchers developed non-metal-doped transition metal-based materials to enhance the inherent activity and charge-transfer rate of the Ni-based di-chalcogenides [226], [227]. The sixth group elements, such as O, S, and Se are utilized to incorporate into transition metal Ni, out of which the metallic nature of Se is higher when compared to S and O [228]. In a recent report from our group, a detailed experimental and theoretical investigation was performed for different TMDs for physical sensing, where the performance of $NiSe_2$ was found to be the best because of its lower

density of states and bandgap [229]. Thus, it is noteworthy to carry forward the research on $NiSe_2$ as a conducting material for antenna-based physical sensing parameters.

The work presents a timely and original contribution by developing a Wax/$NiSe_2$ transient antenna for low-pressure sensing applications, emphasizing the detailed analysis of the transduction mechanism through a complementary approach, including experimental characterization and first principle calculation. In our work, the S-parameter of the proposed antenna is exploited as a sensing parameter. The wax is utilized as a substrate that shows instant transience upon application of an external heat trigger, and $NiSe_2$ is a conducting material to the patch for efficient sensing. The synthesis of $NiSe_2$ and its material and electrical characterizations were studied to confirm the material characteristics and its suitability for antenna application. Using the acquired parametric values of the chosen materials, the antenna is designed in HFSS software and also is analysed for pressure sensing. Then, the fabricated Wax/$NiSe_2$ antenna is analysed for low-pressure sensing analysis using different pressure loads in terms of the resonant frequency. Then, the repeatability and transience behaviour of the Wax/$NiSe_2$ antenna is analysed to observe its performance. As per the study, this Wax/$NiSe_2$ antenna is suitable for short-term industrial low-pressure sensing applications.

5.2 Materials & Methods

5.2.1 Synthesis of $NiSe_2$

The widely used hydrothermal method is considered for the synthesis of $NiSe_2$. Initially, 213 mg of Se and 113 mg of $NaBH_4$ were added to the 30 mL of water, where $NaBH_4$ helps to disperse the Se powder in Deionized (DI) water. After that, the solution is placed in a sonicator for 15 minutes. Later, 570 mg of $NiCl_2$ is added to the solution. Then, magnetic stirring is employed for 1 hour at 750 rpm until the dispersed solution is obtained. The thoroughly stirred solution was transferred to Teflon and placed in the hydrothermal reactor at 200 ^{0}C for 20 hrs. Finally, the synthesized solution is transferred to the centrifuge tube and kept in the centrifuge at 3000 rpm for 30 minutes. The centrifuge process is repeated three times to remove any residues in the solution. Later, the DI water is carefully separated from the centrifuge and added to 5 ml of acetone. The reason for adding the acetone is that while coating $NiSe_2$ on the wax surface, the acetone quickly evaporates and keeps the $NiSe_2$ on the surface of the wax. The complete synthesis of the $NiSe_2$ procedure schematic is shown in Fig. 5.1

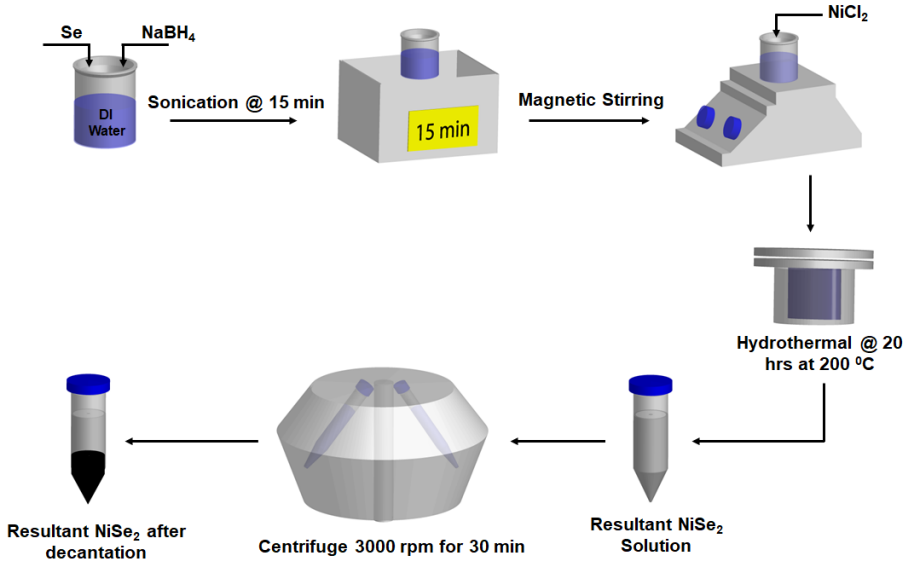

FIGURE 5.1: Complete synthesis procedure of $NiSe_2$.

5.2.2 Characterization of $NiSe_2$

The morphology of the coated $NiSe_2$ on the engraved surface of wax was analysed using scanning electron microscopy. Fig. 5.2a depicts the SEM image of $NiSe_2$ on the wax surface. It illustrates that $NiSe_2$ got distributed on the wax surface as nanocrystals and are chained with each other. The chemical composition, binding energies, and surface states of $NiSe_2$, X-ray photoelectron spectroscopy, were performed. Fig. Fig. 5.2b illustrates the broad range spectra of $NiSe_2$. The survey spectra depict the binding energy peaks of Ni 2p, Se 3d, C1s, and O1s, confirming the presence of $NiSe_2$. Fig. Fig. 5.2c illustrates the Ni 2p de-convoluted spectra. Two spin-orbit doublets and two shake-up satellites of Ni 2p spectra, with peaks for Ni $2p_{3/2}$ and Ni $2p_{1/2}$ at 855.87 eV and 873.83 eV, respectively, were obtained with a binding energy split of ∼18.20 eV. The obtained peaks matched with Ni2+, which confirms the Ni in divalent states of $NiSe_2$. From Fig. Fig. 5.2d, the Se de-convoluted spectra peaks at 59.21 and 54.20 eV for Se $3d_{3/2}$ and Se $3d_{5/2}$, respectively, states that the $NiSe_2$ has metal selenium bonds [230]. The high-resolution XRD spectra of $NiSe_2$ is reported in our recent works [229].

5.2.3 Antenna Design

For transient antenna-based sensing, a conventional microstrip antenna is designed using microstrip patch design equations [159] by selecting materials before calculating dimensions. For the transient nature of the antenna, a dielectric material like wax is chosen that

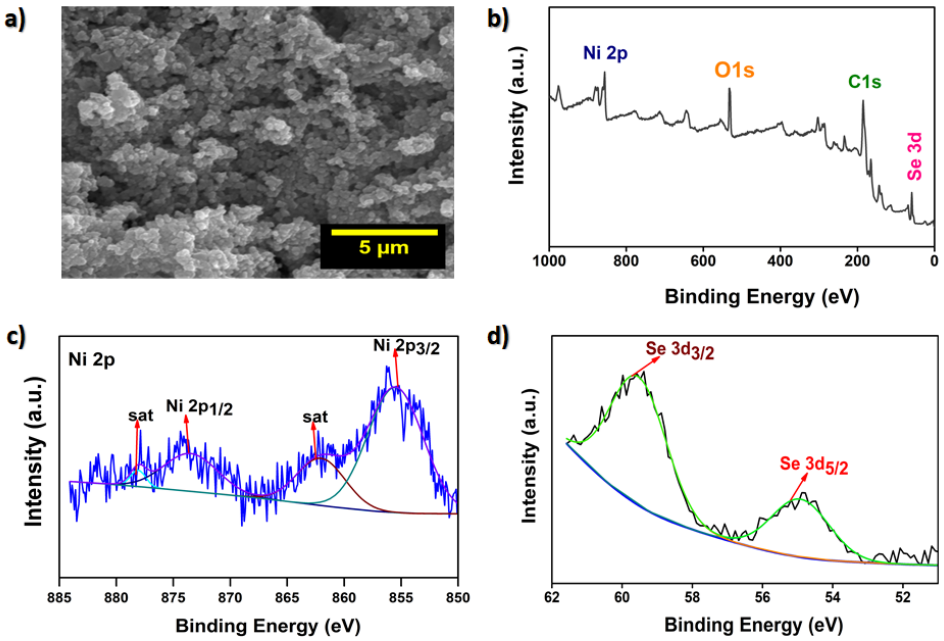

FIGURE 5.2: Characterization of $NiSe_2$. a) SEM morphology of $NiSe_2$ on wax surface, b) Survey spectra, Ni 2p, c) De-convoluted spectra of Ni 2p, d) De-convoluted spectra of Se 3d.

disappears while heat is given as an external trigger. Materials sensitive to the applied and derived physical qualities are a requirement for the antennas for sensing operation. Utilizing nanomaterial like $NiSe_2$ as a conducting patch for the antenna gives an efficient sensitivity when applied pressure. The variation in resonant frequency with respect to effective dielectric constant when pressure is applied on the antenna is analysed from the following patch design Equations (5.1) & (5.2). Where, f_0 is the operating frequency of the antenna, C is the speed of the light (3×10^8 m/s), L is the physical length of the patch, ΔL is the extended length due to the fringing field effect and ε_{reff} is the effective dielectric constant of the dielectric material.

$$L = \frac{c}{2 \times f_0 \sqrt{\varepsilon_{reff}}} - 2\Delta L \tag{5.1}$$

$$f_0 = \frac{c}{2\,(L + \Delta L)\,\sqrt{\varepsilon_{reff}}} \tag{5.2}$$

5.2.4 Device Fabrication

The fabrication of the Wax/$NiSe_2$ antenna starts by melting Candelilla wax pellets (dielectric constant = 2.4 and loss tangent = 0.0093) [231] at 80 ^{0}C using a hotplate. The

melted wax solution is then poured into a pre-prepared rectangular acrylic sheet template with dimensions of 26.9 × 24.93 mm^2. The negative template of the acrylic sheet with the patch structure is prepared to provide an outline of the patch on the wax substrate. Then the patch template is used on the wax surface to manually engrave the marked pattern because $NiSe_2$ liquid cannot get appropriately coated on the plane wax surface. Finally, the $NiSe_2$ liquid is coated on the wax surface as a conductive material. The conductivity of $NiSe_2$ is around 4.52 × 10^5 S/m, which is measured using a four-probe device. Compared to the other transition metal-based composites, Ni-based composites, specifically, $NiSe_2$ is highly considered due to its effective electron transfer efficiency. Fig. 5.3a shows the preparation of the wax substrate and coating of $NiSe_2$ as a patch on the front side of the wax substrate. The actual digital images of the wax substrate with copper tape attached to the back side of the wax substrate are depicted in Fig. 5.3b. Using silver paste, the SMA connector is attached to the $NiSe_2$ and copper tape of the wax substrate. Finally, the Wax/$NiSe_2$ antenna was kept in a hot air oven at 50 ^{0}C for one hour to solidify the silver paste. The fabricated prototype of the Wax/$NiSe_2$ antenna is shown in Fig. 5.3c. The dimensions of the presented antenna are illustrated in Fig. 5.3d.

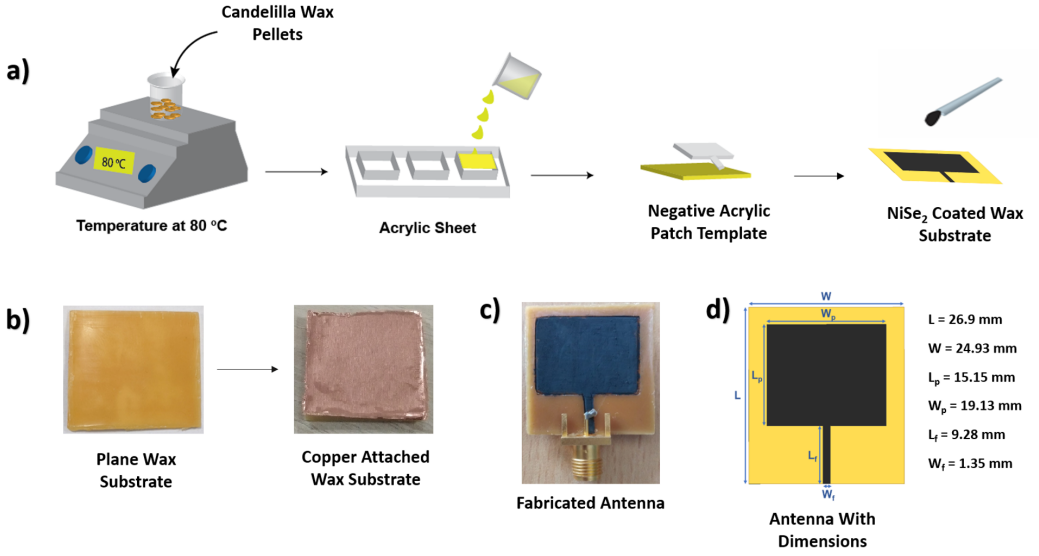

FIGURE 5.3: Fabrication procedure of Wax/$NiSe_2$ antenna. a) Fabrication of wax substrate and coating of $NiSe_2$ liquid on the wax surface, b) Real image of the wax substrate and copper tape attached to the wax substrate, c) Fabricated Wax/$NiSe_2$ antenna prototype, d) Dimensions of presented antenna.

5.3 Results and Discussions

The Wax/$NiSe_2$ antenna is attached to the measurement setup with a vector network analyzer (VNA, R&S ZVL Series) for the analysis of the S-Parameter, as shown in Fig. 5.4a. In Fig. 5.4b, the $|S_{11}|$ parameter is simulated, and measured results of Wax/$NiSe_2$ antenna at 5.8 GHz is presented. Both the simulated and measured results have a resonant frequency of around 5.8 GHz, which are in accordance with each other. A bandwidth of 25 MHz is observed in the simulation, while the bandwidth is approximately 285 MHz in the measured result. The cause of difference in bandwidth might be due to the facile fabrication effects that are not considered in simulations which include, the surface roughness of the dielectric material, complex nanomaterial properties and connector loss. The intrinsic low conductivity of $NiSe_2$ and the defect in synthesis of $NiSe_2$ during hydrothermal process leads to effect the overall conductivity of $NiSe_2$, which also plays a major role in bandwidth variation.

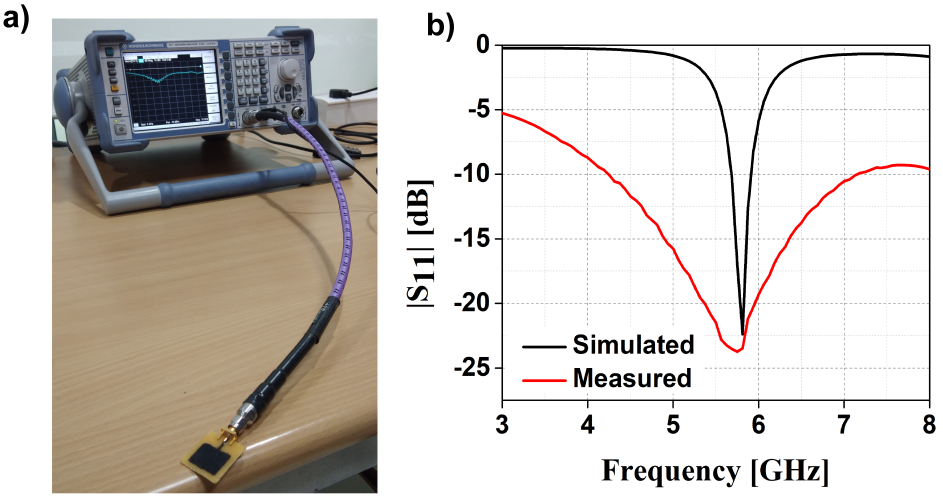

FIGURE 5.4: a) Wax/$NiSe_2$ antenna connected to the VNA, b) Simulated and measured $|S_{11}|$-Parameters of the presented Wax/$NiSe_2$ antenna.

Fig. 5.5 presents the simulated radiation patterns of XZ and YZ planes, respectively, at 5.8 GHz resonant frequency. The maximum gain obtained is around 6.12 dBi with minimum cross-polarization for both planes.

5.3.1 Pressure Sensing

The fabricated Wax/$NiSe_2$ antenna is subjected to pressure sensing analysis with respect to the resonant frequency. Since the NiSe2 patch on wax has nanocrystal morphology,

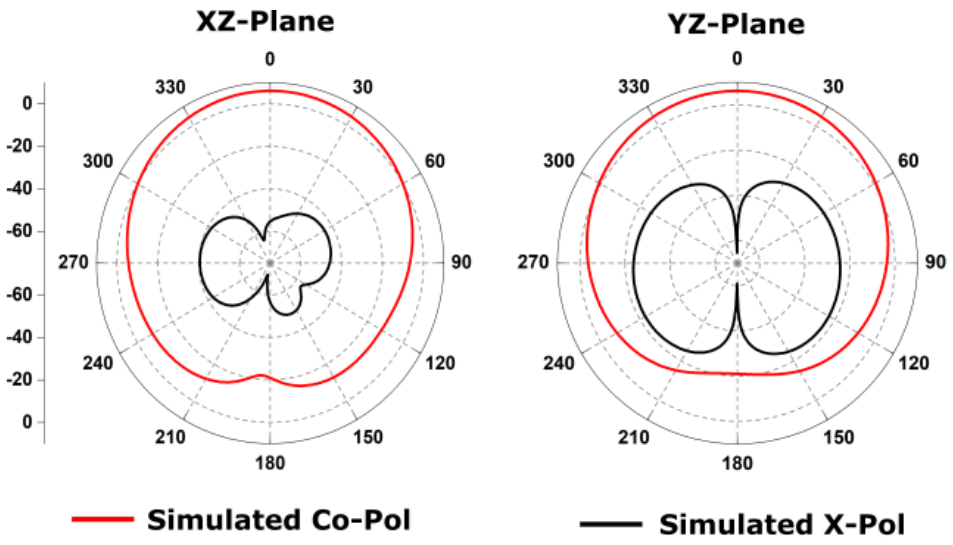

FIGURE 5.5: Simulated Wax/$NiSe_2$ antenna radiation patterns at 5.8 GHz.

the resonant frequency varies while applying pressure onto the patch. As the physical structure of the nanocrystal expands while applying pressure loads, the gaps between the crystals reduce by increasing the patch length. Due to this, the conductivity varies and probably leads to the reduction in frequency. Hence, as the applied pressure increases, the reduction in resonant frequency is noticed. The relation between operating frequency and length is analysed using the microstrip patch antenna Equations (5.1) & (5.2).

For the pressure sensing analysis, different pressure loads are considered from 1.48 kPa to 3.42 kPa. These pressure loads are utilized separately, one after the other, to apply pressure on the Wax-based $NiSe_2$ patch and analyse the change in antenna parameters. Fig. 5.6a depicts the applied pressure load onto the $NiSe_2$ patch while connected to the VNA. The variation in frequency is observed while applying the pressure on the $NiSe_2$ patch using different loads. It is observed in Fig. 5.6b that both in simulated and measured results, there is a drastic reduction in the normalized frequency as the applied pressure is increasing. This observation shows the sensitivity of the device towards applied pressure.

The repeatability analysis depicted in Fig. 5.7a is considered for around 50 cycles (Trail Number) with different pressure loads to observe the repeatable nature of the fabricated device. When no pressure is applied, the normalized frequency reaches its maximum initial resonant frequency. In contrast, when a pressure load is applied on the Wax/$NiSe_2$ antenna, as shown in Fig. 5.7a, there is a reduction in frequency according to the applied amount of pressure using different pressure loads. To conclude, while the amount of pressure applied increases, the frequency reduces linearly with a minute change in resonant frequency for each span of the trail. A linear variation in normalized frequency

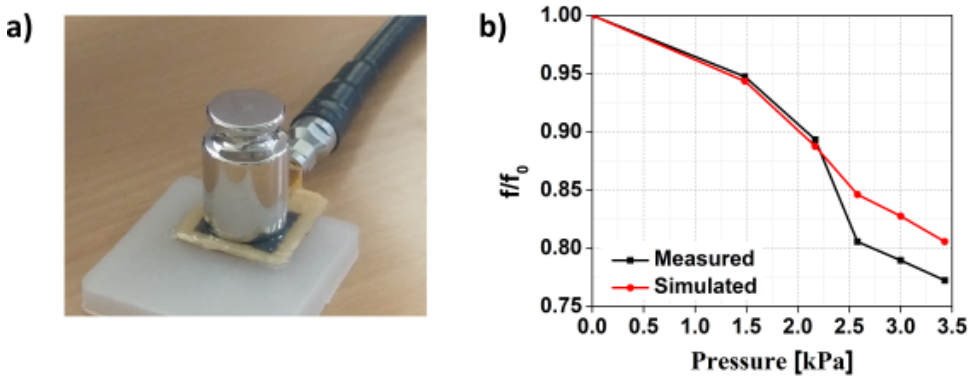

FIGURE 5.6: a) Wax/$NiSe_2$ antenna with an applied pressure load, b) Variation of normalized resonant frequency with pressure.

is observed with respect to the applied pressure loads. From Fig. 5.7b, the sensitivity for the proposed antenna is approximately 0.0683 kPa^{-1}, which is significant for sensing purposes. Therefore, this Wax/$NiSe_2$ antenna has potential in transient low-pressure sensing applications.

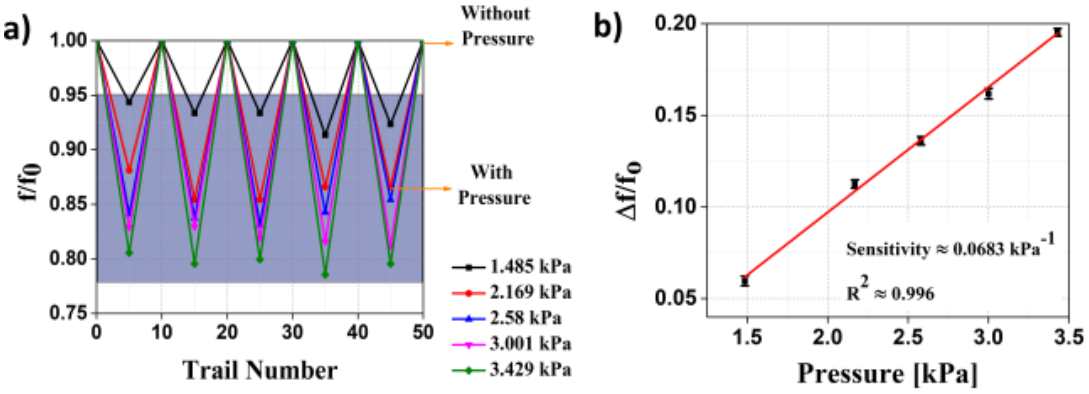

FIGURE 5.7: a) Repeatability plot of Wax/$NiSe_2$ antenna with and without pressure loads, b) Sensitivity analysis for the pressure sensing.

5.3.2 Theoretical Methods & Analysis

To interpret the variation in resonant frequency with respect to the dielectric constant when pressure is applied on the antenna, density functional theory (DFT) based ab initio calculations were performed. In this work, the tri-layer (3L) Nickel Selenide ($NiSe_2$) was considered for representing the experimentally synthesized $NiSe_2$ Nano-flakes. The $NiSe_2$ is a Group-X Transition Metal Di-Chalcogenides (TMDs) considered in hexagonal 1T-phase, where one nickel (Ni) atom is covalently sandwiched between two selenium (Se) atoms in individual sites of a hexagonal honeycomb lattice structure and forming a single atomic

layer [229]. As shown in Fig. 5.8a the $NiSe_2$ transform from semiconducting to metallic phase from monolayer to multi-layer configuration and exhibits AAA interlayer stacking orientation, where the adjacent atomic layers are identical to each other. Moreover, under applied normal pressure, the interlayers distances of 3L-$NiSe_2$ are reduced, which leads to a normal compressive (S_{normal}) [232] strain that can be calculated as follows

$$S_{normal} = \frac{d_{strained} - d_{relaxed}}{d_{relaxed}} \tag{5.3}$$

In Equation (5.3), $d_{strained}$ and $d_{relaxed}$ represent the interlayer distance of the strained and relaxed 3L-$NiSe_2$, respectively. In this case, S<0 indicates the presence of normal compressive stress in the lattice.

Here, the DFT-based ab initio calculations are performed by using the Atomistix Tool Kit (ATK) and Virtual Nano Lab (VNL) simulation packages which are commercially available from Synopsys Quantum Wise [233]. The 3L-$NiSe_2$ are considered in their unit-cell (1×1×1) configuration, with a vacuum of 40Å in the out-of-plane directions to eliminate artificial interactions from periodic images in that direction. Here, the ab initio calculations are performed using the Linear Combination of Atomic Orbitals (LCAO) double zeta-Polarized basis set with a 10×10×1 Monkhorst-Pack grid for sampling the k-points in Brillouin zone with a density mesh cut-off energy of 125 Hartree.

In order to minimize the system's overall energy, the unit cell is first relaxed. Additionally, the forces acting on each individual atom are reduced using the Limited-memory Broyden Fletcher Goldfarb Shanno (LBFGS) algorithm, which has force and stress error tolerances of 0.01 eV/Å and 0.0001 eV/$Å^3$ respectively. For geometry optimization, the Local Density Approximation (LDA) Density Functional Theory (DFT) method is used along with Perdew Zunger (PZ) exchange-correlation functional [233]. The electronic and optical properties are calculated using the Generalized Gradient Approximation (GGA) method with the Perdew-Burke-Ernzerhof (PBE) exchange-correlation functional [233]. Furthermore, the Grimme DFT-D3 empirical correction is incorporated with GGA-PBE to account for the weak van der Waals forces acting between the layers [233]. It should be noted that under applied normal compressive strain, the Brillouin zone of 3L-$NiSe_2$ preserves its hexagonal symmetry, and correspondingly, the energy band structure of both relaxed and strained 3L-$NiSe_2$ is analysed by considering by high symmetry route (G-M-K-G) of Brillouin zone with fifty points per segment as shown in Fig. 5.8b. Moreover, in this work, the optical spectrum calculations are performed using 15×15×1 k-points

sampling while keeping ten bands below above and twenty bands above the Fermi level [233].

Initially, the 3L-$NiSe_2$ is geometry optimized, and its electronic (band structure) and optical properties (k vs. freq.) are explicitly calculated following the procedure mentioned above. Next, the 3L-$NiSe_2$ is subjected to different normal compressive strains by varying the interatomic distances and is geometry optimized for individual strain values. Consequently, the energy band structures of strained and relaxed 3L-$NiSe_2$ are compared and are depicted in Fig. 5.8b.

Fig. 5.8b clearly indicates that both relaxed and strained 3L-$NiSe_2$ are metallic in nature, which agrees with the experimentally measured conductivities in this work. It is worth mentioning that the fabricated device contains a percolating network on few-layer $NiSe_2$ nano-sheets, where both the intra-flake as well as inter-flake electronic conductivities are expected to influence the overall conductivity of the percolating network. Moreover, the results clearly demonstrate that the application of a smaller compressive strain does not significantly influence the overall energy band structure, whereas the band structure is notably modulated for a larger compressive strain. Next, the relative changes in the out-of-plane dielectric constant with frequency are considered for relaxed and different strained configurations of 3L-$NiSe_2$ and are illustrated in Fig. 5.8c. In this context, it should be noted that for the theoretical study, the frequency range is considered from 0 to 10 GHz, which covers the experimentally realized resonant frequency of the antenna (5.8 GHz). The results indicate that the dielectric constant remains independent of applied frequency within the studied frequency range. To further elaborate on the strain dependence on the dielectric constant, the zero frequency dielectric constant of relaxed and strained 3L-$NiSe_2$ are exclusively analysed and are presented in Fig. 5.8d.

Fig. 5.8c & 5.8d exhibit that the dielectric constant increases with the applied compressive strain, and the rate of change also increases with the applied strain. Such observation can be attributed to the notably higher modulations in energy band structure at a larger applied strain, as shown in Fig. 5.8b. Such an increase in dielectric constant with increasing compressive pressure leads to the experimentally observed reduction in the resonant frequency following Equation (5.2), as demonstrated in Fig. 5.6b. Usually, in conventional antennas ε_{reff} is derived solely from the dielectric material sandwiched between the metal. Since $NiSe_2$ has some dielectric nature as per the DFT theoretical analysis, here the ε_{reff} is having the combined dielectric values of both wax and $NiSe_2$.Consequently, the theoretical analysis satisfactorily explains the observed experimental trends of this work. In this context, it is worth mentioning that an ideal condition is considered for the

theoretical analysis considering strain response on the dielectric constant of individual pristine 3L-$NiSe_2$. At the same time, under experimental conditions, the effective dielectric constant can be influenced by other factors, including the effect of pressure on wax, wax/nanomaterial interface, inter-flake interface, and the impact of defects like Se or Ni vacancies in the Nano-flakes. However, the qualitative trend observed in experimental results and theoretical analysis are in good agreement, wherein the theoretically observed increase in the dielectric constant of $NiSe_2$ with increasing pressure appears to dominate the overall qualitative trend observed in experimental results.

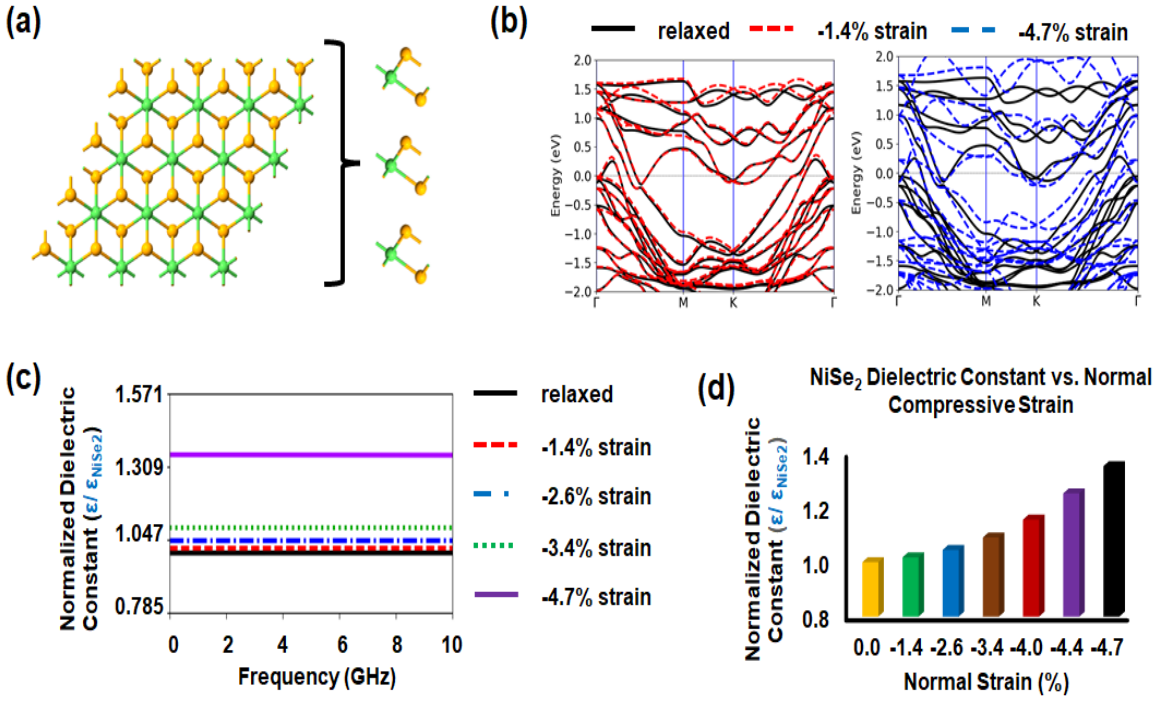

FIGURE 5.8: (a) Schematic representation of 3L-$NiSe_2$ lattice in supercell (4×4×1) configuration from top-view and unit cell configuration (1×1×1) from side-view, (b) plots of comparative energy band (E-k) structures of relaxed and normal compressive strained 3L-$NiSe_2$ for low and high strain conditions, (c) plots of out-of-plane dielectric constant vs. frequency response of 3L-$NiSe_2$ for different applied normal compressive strain, (d) plots of zero frequency dielectric constant vs. applied normal compressive strain in 3L-$NiSe_2$.

5.3.3 Transient Behaviour

To verify the transient nature, the dismantling process of the Wax/$NiSe_2$ antenna with heat as a trigger is depicted in Fig. 5.9. Candelilla wax has a hydrocarbon content of 42 % [234], When triggered with heat, the hydrocarbon molecular bonds break, and the wax

vaporizes while turning into liquid form. Due to the heat trigger, initiating the reaction between oxygen and hydrocarbons tends to produce water and carbon dioxide, as shown in equation $4C_31H_64 + 95O_2 \longleftrightarrow 62C_2O + 128H_2O$. In this procedure, due to heat, the solid Wax/$NiSe_2$ antenna dismantles by transforming the wax substrate from solid-state to liquid form.

Fig. 5.9a depicts the initial phase of the antenna at the room temperature of 26 ^{0}C before initiating the heat trigger. From the captures, as shown in Fig. 5.9b - 5.9d, the Wax/$NiSe_2$ antenna started melting at around 45 ^{0}C to 50 ^{0}C leaving partial remains. By the 150th second, the complete device got dismantled, which is instantaneous compared to the wet transience (i. e., dismantling using a liquid substance). Modulation of transient time is also an important factor when it comes to the transient behaviour of a device. Here, the modulation of transient time is not possible with respect to the variation in thickness of the substrate that leads to a change in the centre operating frequency. But by instant temperature trigger, the variation in modulation time is possible. As shown in Figure 9e as the trigger temperature increases there is a drastic reduction in transient time. Consequently, this transient Wax/$NiSe_2$ antenna can be used in a wide range of short-term security-based low-pressure sensing applications.

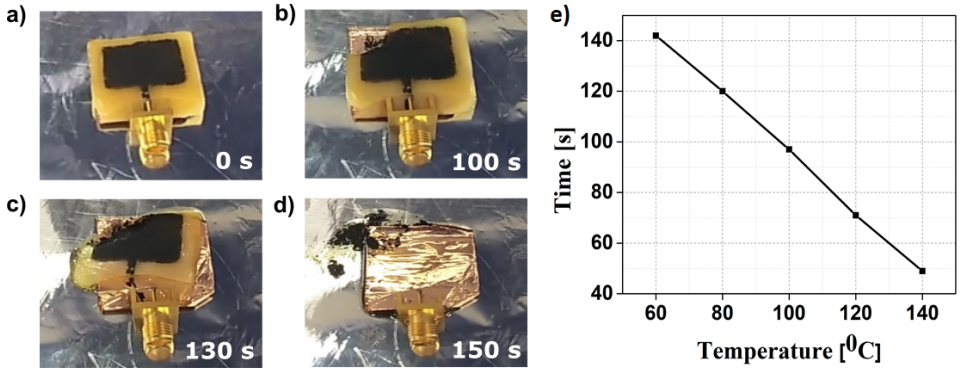

FIGURE 5.9: Illustration of the transient behaviour of Wax/$NiSe_2$ antenna at various time intervals. a) Initial phase, b) 100 s after the initiation of heat trigger, c) Partially dismantled device at 130 s, d) completely dismantled after 150 s, e) Modulation of transience time by varying temperature.

5.4 State of the Art

In below Table 5.1, the comparison between various flexible antennas along with their dielectric and conductive materials are considered. From the study, the nanomaterials

and conductive polymers [146], [235] provides better-sensing property when compared to metals due to their material morphology. The combination of flexible and rigid materials, as shown in [236], [237] also improves the sensitivity of the device. Only using rigid materials like [101], [116] requires external support for the sensor to analyze sensing parameters. For transient applications, the materials must disappear when triggered with an external stimulus like, PVA/TiO_2 film gets dissolved in water [214]. As far as the authors' knowledge go, there are no reports on transient technology-based antenna for sensing purposes. Here, the prototype of a transient technology-based antenna and the sensing application is proposed, which dismantles within seconds when triggered with heat after its usage.

TABLE 5.1: Material comparison table for different sensing applications.

Dielectric Material	**Conducting Material (Patch)**	**Electrical Dimensions**	**Gain (dBi)**	**Sensing Application**	**Transient Nature**	**Reference**
PET	Graphene-assembled film (GAF)	$(0.60\times0.60\times0.001)\lambda_0$	-	Strain	-	[146]
T-Shirt	Conductive polymer	$(0.39\times0.03\times0.003)\lambda_0$ [Approx.]	2.14	Strain	-	[235]
FR4/PDMS	Copper	$(0.36\times0.36\times0.015)\lambda_0$	-	Moisture	-	[236]
Cotton	Copper Tape	$(0.57\times0.52\times0.02)\lambda_0$	3.81	Temperature	-	[237]
RT6010	PEC	$(0.021\times0.024\times0.0031)\lambda_0$	-9.7	Wireless Capsule endoscopy	-	[101]
RO3003	Copper	-	-	Pressure	-	[116]
PVA/TiO_2	Silver	-	0.5	-	Yes	[214]
Candelilla Wax	$NiSe_2$	$(0.52\times0.48\times0.03)\lambda_0$	6.12	Pressure	Yes	**This Paper**

5.5 Summary

A transient technology-based antenna with heat as an external stimulus is developed to extend the antenna performance for wireless sensing applications like, environment sensors and security based applications. Here, Candelilla wax is used as a substrate which is a quick degradable material upon heat trigger. A few layers of nickel di-chalcogenides shows metallic property and hence is very lucrative for use as a conductive patch for microstrip antennas, which can also withstand the mechanical strain. The simulations and measured results depicts the variation in frequency response with respect to the pressure applied. Additionally, theoretical analysis is performed to prove the effect of effective dielectric constant on the resonant frequency with the application of pressure on the antenna. Further, the antenna is verified for its transient behaviour, which gets dismantled within 150 seconds from the initial room temperature. In essence, the research is expected to offer theoretical understanding-driven design insight, which is expected to be instrumental for the application of such nanomaterial/transient-based sensors for emerging application areas like IoT-enabled data security and biomedical applications. The superior mechanical

stability and transient behaviour observed in the design prototype can also be considered promising for systematic design and performance optimization of such sensors in future with other emerging nanomaterials. Furthermore, the theoretical framework developed in this work for analysing the transduction mechanism can be further extended in future to develop a robust predictive model for estimating the performance of antenna-based sensors using the class of hydrothermally synthesized nanomaterials.

Chapter 6

A Study on Flexible Antenna-Based Contactless Motion Sensor

6.1 Introduction

Recently, flexible antenna-based sensors are in high demand, specifically in the microwave domain. Due to their wireless communication ability, non-contact sensing capacity, simple structural design and integrity, they are the excellent choices in wireless sensing applications. Furthermore, as compared to conventional sensors, there is a possibility of reducing the size and complexity of the design and improving the accuracy of the sensor by modifying the antenna characteristics, which makes them versatile [15]. The antenna-based sensors have emerged as another approach for measuring diverse physical sensing parameters and transmitting the data wirelessly.

Up till now, antenna-based sensors were applied for various sensing applications such as humidity [238], gas [239], ice [130], and strain [235], which is mainly based on contact sensing mechanism. Indoor and outdoor modern systems are equipped with intelligent sensors based on various physical parameters. Out of which motion sensor plays a key role in detecting the motion and presence. There is an increase in security issues at various commercial places [240], and observing the elderly people having health issues at home is necessary. Continuous monitoring of human activity using simple and compact technology is emerging as a significant area of research and development [241]. So, it is necessary to develop a conformal smart contactless low-power motion sensor for short-range health, industry and security-based applications.

Several operating principles have evolved to investigate the sensing parameter of the motion sensor according to its applicative usage. Microwave technology is increasingly used in motion detection sensing for security-related applications [242]. For motion sensing purposes, microwave sensors mostly made use of Doppler radar principle which is based on the reflected microwave frequency [243]. The existing contactless motion sensors were used for long-range applications with heavy post-processing [244], and for human motion monitoring [245], the available sensors are in contact with humans. Consequently, the necessity of contactless antenna-based sensors is rising progressively for wireless low-power smart sensing applications.

In this work, two separate antennas for transmitting and receiving the RF signal were considered at 2.44 GHz resonant frequency in the presence of the obstruction for contactless wireless motion detection. Here, the operating principle lies in detecting the attenuated power of the received RF signal at the receiving antenna in the presence of obstruction. The attenuation of the received power varies according to the size and structural area of the object, material of the object and the amount of the emitted energy from the object. The threshold limit is experimentally recorded for various materials, including metals, dielectrics, and humans of variable height and structural area. The observed threshold for various obstructions can be directly utilized in detecting the motion according to the received attenuated power for smart sensing. Hence, this work proposes a simple operating principle in smart wireless motion detection for short-range IoT applications.

6.2 ANTENNA DESIGN

6.2.1 Transmitting Antenna

A Microstrip monopole-like antenna with a partial ground is designed as a non-flexible transmitting (TX) antenna. Fig. 6.1a and 6.1b depicts the fabricated prototype of the TX antenna. The combination of a circular patch and the rectangular slot within it results in a broadband antenna. The operating band of the transmitting antenna covers the frequency range from 1.57 GHz – 3.48 GHz. The antenna is fabricated on the FR-4 substrate (ε_r = 4.4, δ = 0.02, h = 1.6 mm) with the dimensional values presented in Table 6.1, were calculated using circular patch equations [159].

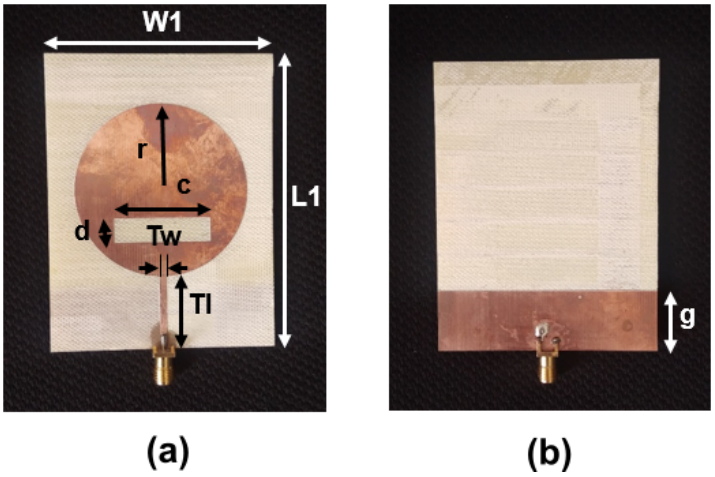

FIGURE 6.1: a) Front view b) Back view of the transmitting antenna.

TABLE 6.1: Geometrical values of the transmitting antenna.

Parameters	W1	L1	r	c	d	Tl	Tw	g
Dimensions (mm)	65	85	25	28	7	30	2	18

6.2.2 Receiving Antenna

As the receiving (RX) antenna, a simple circular microstrip patch is designed and fabricated by using deformable material, as shown in Fig. 6.2a. Unlike rigid antennas with considerable parametric values, the characteristics of the conducting and non-conducting parts are crucial in the case of flexible antennas. Here polyimide sheet ($\varepsilon_r = 3.5$, $\delta = 0.0026$ [158], h = 0.254 mm) as a substrate is sandwiched between copper tape on both sides. The usage of the above materials makes the antenna more flexible, portable, inexpensive, and low profile for various conformal wireless applications. The resonant frequency of the receiving antenna is 2.44 GHz, which is suitably designed for the above-mentioned broadband antenna. As depicted in Fig. 6.2b, the antenna possesses bending feasibility, which makes it appropriate for conformal applications. The dimensional values of the RX antenna presented in Table 6.2 were calculated from the microstrip antenna design equations [159].

TABLE 6.2: Dimensions for the receiving antenna.

Parameters	W	L	a	b	Rl	Rw
Dimensions (mm)	48	60	19.7	10.46	26.33	0.7

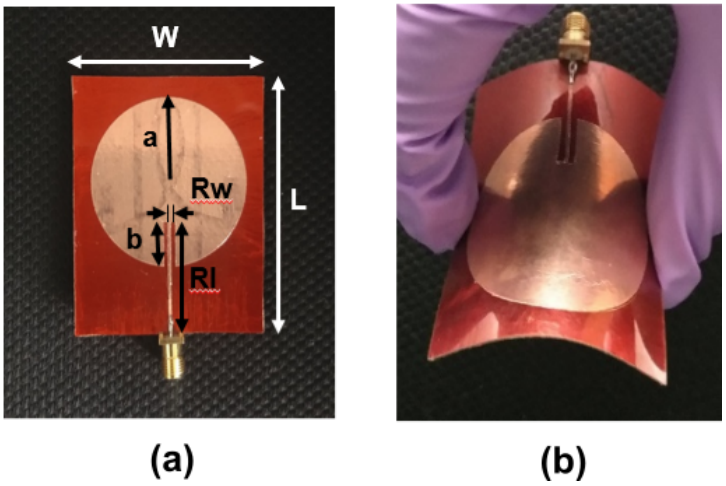

FIGURE 6.2: Fabricated prototype of the flexible receiving antenna. a) Flat view b) Bent view.

6.3 Results and Discussion

To examine the simulated results, the TX and the RX antennas designed in HFSS V.15.0 were fabricated using a PCB prototyping machine. Then, both prototypes are measured using a VNA (VNA-ZVL by Rohde and Schwarz). As shown in Fig. 6.3a the simulated TX antenna is operating at a frequency span of 1.54 GHz to 3.46 GHz, and the measured prototype is from 1.54 GHz to 3.55 GHz. The fractional bandwidth observed for the simulated and measured is 71.6% and 80.07%, respectively. The minor variations between measured and simulated return loss can be due to the open environment measurement. The simulated maximum gain of the TX antenna is plotted in Fig. 6.3b, where the gain is linearly increasing from 2.10 to 3.25 dBi in the operating frequency band. The simulated efficiency is found to vary from 92% to 97% as shown in Fig. 6.3b. Fig. 6.4 depicts the radiation patterns of transmitting antenna both in XZ and YZ planes. At 2.4 GHz the antenna is radiating omnidirectional radiation patterns with minimum cross-polarization.

From Fig. 6.5a, the simulated and measured results show that the receiving antenna is resonating at 2.44 GHz with a narrowband. At the resonant frequency, a maximum gain of 1.10 dBi with an efficiency of 29.1% is observed from the simulated plot in Fig. 6.5b. Fig. 6.6 depicts that the simulated 2-D radiation patterns are unidirectional at 2. 44 GHz.

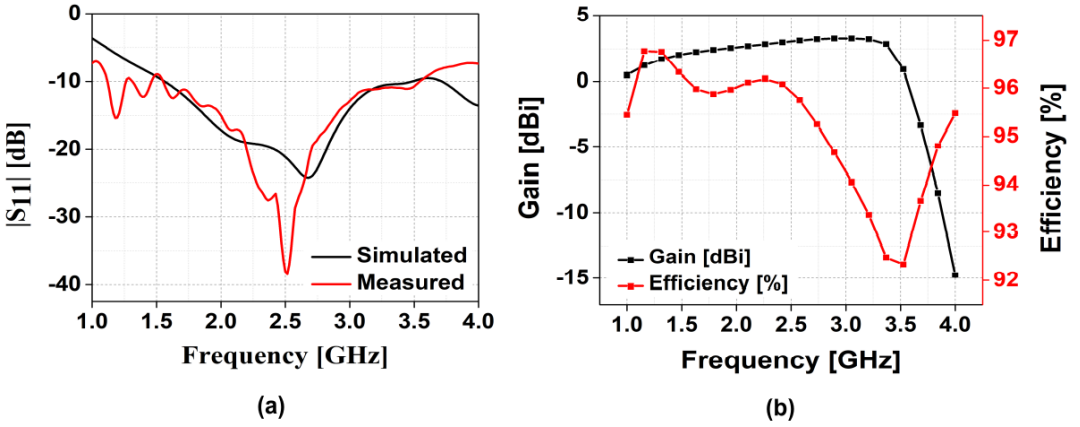

FIGURE 6.3: a) Simulated and measured $|S_{11}|$ parameter b) Simulated gain and efficiency of the transmitting antenna.

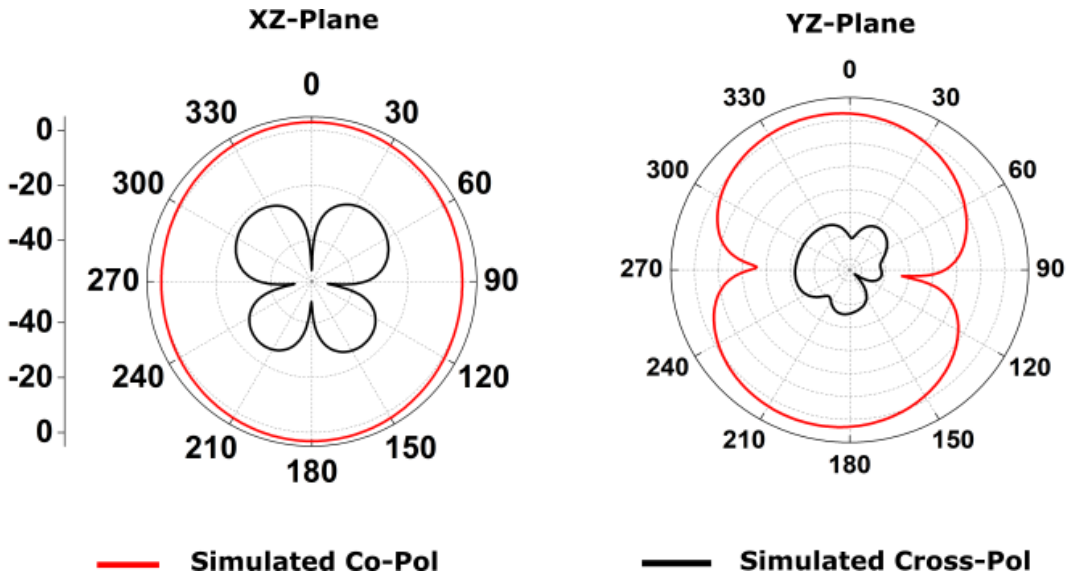

FIGURE 6.4: 2-D Radiation patterns of the transmitting antenna.

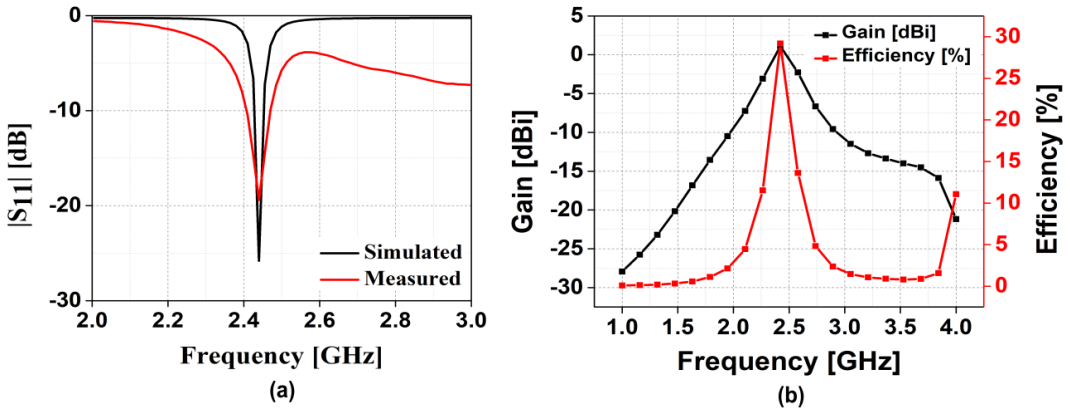

FIGURE 6.5: a) Simulated and measured $|S_{11}|$ parameter b) Simulated gain and efficiency of the receiving antenna.

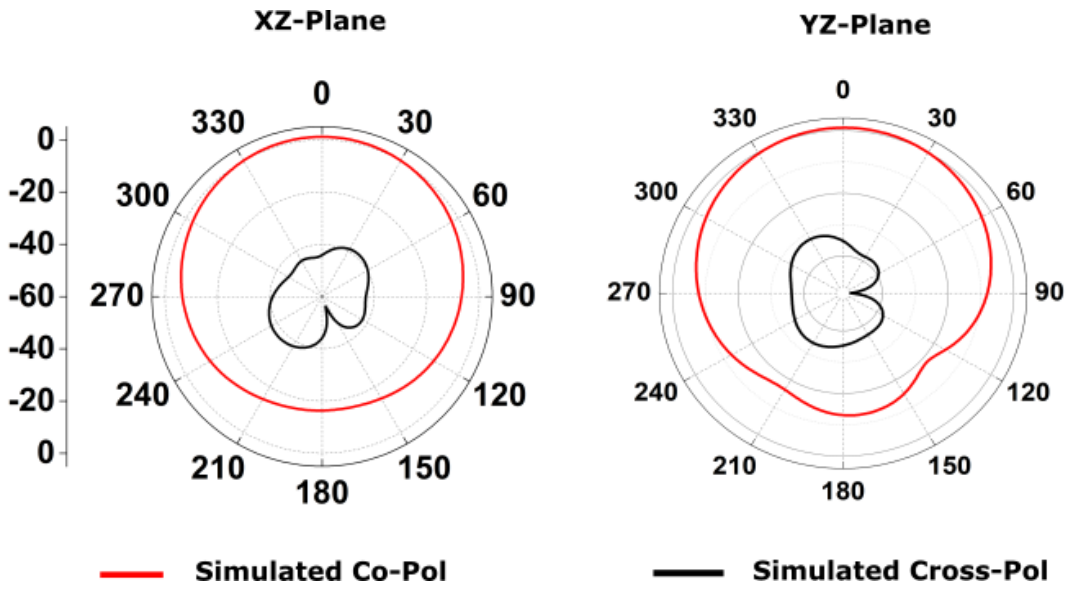

FIGURE 6.6: 2-D Radiation patterns of the receiving antenna.

6.3.1 Proposed Sensing Mechanism

The sensing mechanism becomes contactless to the physical parameter under applicative consideration by utilizing the antenna pair as a sensing device. As a microwave sensor, the antenna has various parameters to exploit and sense particular physical quantity. Currently, the antenna is used for sensing the motion of the target or its presence based on the received power of the RX antenna. In this case, the electromagnetic (EM) radiation between the TX and RX antenna is proposed as an operating principle for sensing the movement or presence of the obstruction. Any obstruction between the TX and the RX antenna causes a direct impact on the radiation parameters, includes frequency of the radiated signal, radiation pattern, efficiency, and received power. Here, the attenuated received power is utilized to sense the presence of an object in between the antennas.

A setup is arranged as depicted in Fig. 6.7, a broadband transmitting antenna and a narrowband receiving antenna were designed and then analyzed for communication and sensing purposes in an open environment. Here, the transmitting antenna is made as a conventional non-flexible antenna for generating better radiation so as to support the receiving antenna. Whereas the receiving antenna is flexible, which is appropriate for conformal applications and is suitable on any structural surface. An RF source generating a 2.44 GHz frequency is connected to the TX antenna while a spectrum analyzer is linked to the RX antenna to check the variation in received power. When the obstruction is present or passing in between the antennas the variation in received power is captured as a sensing parameter.

FIGURE 6.7: Communication and sensing mechanism in terms of radiated power between transmitting and receiving antennas.

From the radar range equation (6.1) [159], the power received is measured with respect to the input transmitted power from the antenna when scattered by the obstruction with a radar cross-section. The received power varies depending on the characteristic behaviour of the material, size, and structure of the obstruction. Accordingly, Fig. 6.8 depicts the analysis of the received power by using different materials as obstructions and Fig. 6.9 shows the experiment performed with different humans having variation in height and structural area. Hence, the received power varies in the presence of an obstruction with respect to the input power, which is also theoretically given in the equation (6.1). Where, P_r is the received power, P_t is the transmitted power, σ is the radar cross-section, G_{0t} and G_{0r} are the maximum gain of the TX and the RX antenna respectively, λ is the wavelength, and R_1 R_2 are distance from transmitter to obstruction and obstruction to receiver respectively.

$$\frac{P_r}{P_t} = \sigma \frac{G_{0t} G_{0r}}{4\pi} \left[\frac{\lambda}{4\pi R_1 R_2} \right]^2 \tag{6.1}$$

A controlled EM radiation continuously radiates from the TX to the RX antenna with a constant receiving power. The distance between the transmitting and the receiving patch is around 1.432 m, which is investigated for short range applications. When an object is placed in between or passing through the antenna pair, an abrupt power level reduction is observed at the receiving antenna. From Fig. 6.8, the attenuated power is studied for different obstructions, when they are stable and in movement. The effect of EM radiation varies depending on the material of the object under consideration. Accordingly,

three different characteristic obstructions such as dielectrics, conductors and human were investigated to observe the pattern of attenuated power.

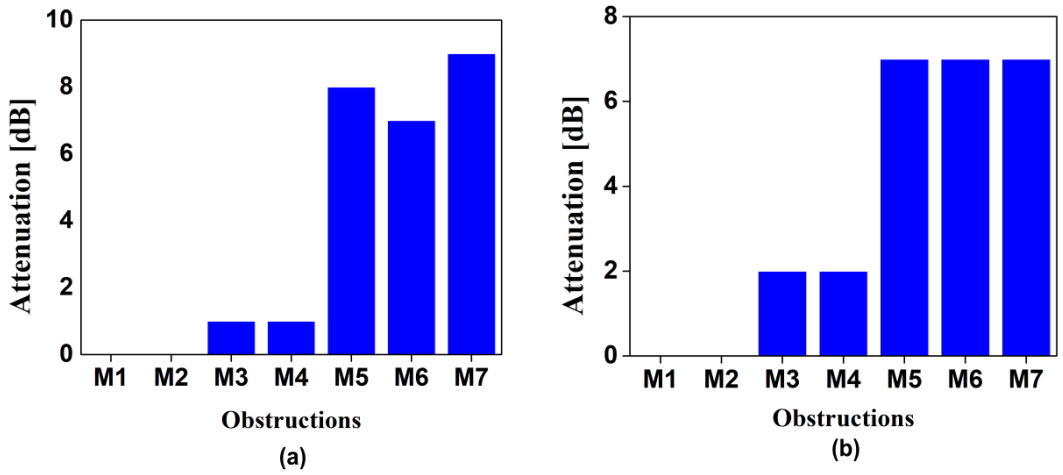

FIGURE 6.8: a) When the obstructions are stable, b) When the obstructions are in movement. The obstructions are cardboard (M1), Thermocol (M2), Book (M3), Wood (M4), Stainless steel (M5), Copper (M6), Human (M7).

As depicted in Fig. 6.8a and 6.8b, two different cases were considered with seven different materials to analyze the attenuation in received power. In both cases when the obstructions are stable and unstable, no attenuation for cardboard and Thermocol, around 1 to 2 dB attenuation is observed for book and wood. When it comes to conductors and humans a maximum of almost the same attenuation in the two cases around 7 to 9 dB is observed. The maximum attenuation noted is for humans and metals, whereas this simple sensing mechanism can be utilized in contactless continuous security based applications.

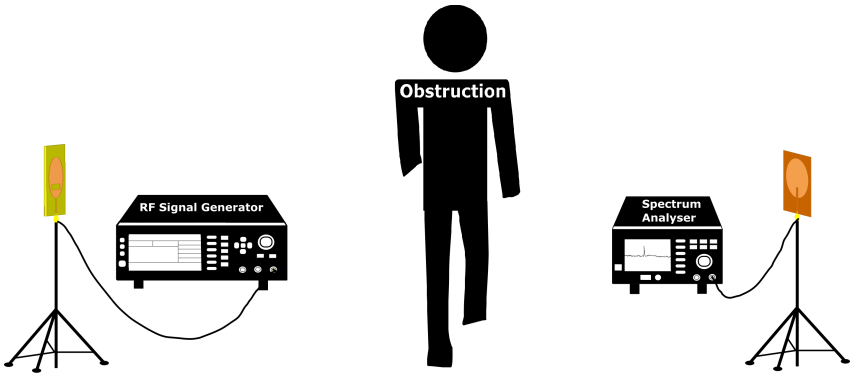

FIGURE 6.9: Communication and sensing mechanism for human motion sensing.

As shown in the Fig. 6.9 each of the six individuals (H1 – H6) with heights ranging from 155 cm to 165 cm and ages ranging from 25 to 35 years were assisted to examine the received power relative to height and area. From Fig. 6.10 the attenuation of received

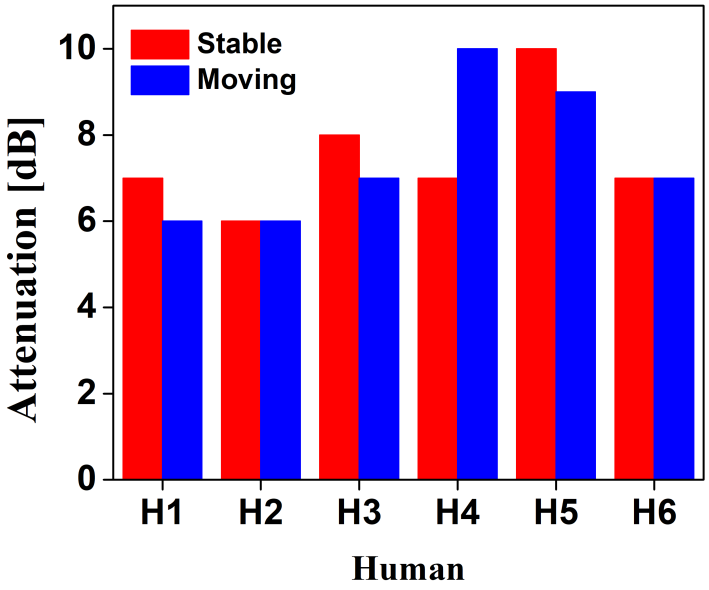

FIGURE 6.10: When the obstruction is human while stable and in movement.

power specifically for humans is noted around 6 dB to 10 dB. The variation in attenuation differs for each human due to the difference in height and structural area as per the radar cross-section. The range of attenuation observed for humans is supportive in switching circuits for making smart IoT applications simple and efficient.

6.4 Summary

Here, a novel antenna-based wireless motion sensor is proposed to expand the smart sensing technology through wireless communication. The measured results of attenuated power at the receiving antenna show the detection of obstructions when stable and in movement, where in both cases the attenuation is almost the same. The experimental received power range observed for human motion detection is around 7-9 dB. This proves the antenna can be used as a smart motion sensor for short-range indoor applications.

Chapter 7

A 2D Nanomaterial-Based Sixteenth-Mode Flexible SIW Antenna

7.1 Introduction

In recent decades, the rise of attention is more towards developing flexible electronics by utilizing various novel metallic and non-metallic nanomaterials. Especially in the microwave domain, the invention of flexible antennas paved the way for creating numerous integrable, wearable, and implantable devices [246]. From the literature, diverse flexible antennas, such as monopole, dipole, MPA and RFID tags were developed for conformal applications [19], [247]–[249]. Due to their flexible nature, when attached to the object or device, there are certain challenges, such as radiation losses, conductor losses, and frequency detuning, that affect the performance of the antenna [15]. The degradation of the antenna can be due to the materials considered or the structural design of the antenna. Therefore, there is a necessity for a planar, low-loss, less bulky flexible antenna that can withstand adverse conditions along with its suitability for industry, academic, and biomedical applications.

The development of substrate-integrated waveguide (SIW) technology can resolve the challenges to some extent related to the performance parameters of the flexible antenna. SIW offers notable advantages, including a high-quality factor, less conductor losses, and the ability to be easily integrated or attached to any device due to its planar structure [250]. Using shorted vias as cavity side walls with a complete ground plane tends to confine more EM field inside the cavity, providing a high-quality factor to the SIW antenna

[251]. This notable quality factor offers stability to the antenna parameters in rigorous conditions and leads to the efficient performance of the antenna.

Numerous works have been published on rectangular SIW cavity-backed antenna [252], [253]. However, the numbers of works on circular cavity SIW antennas are scant [254]–[257]. In [254], a dual-band antenna is designed for body-centric communication. In [255], the ring-slot, placed at upper layer, is fed by another SIW structure placed below. Split-ring is being used in [256] to obtain multiband. In [257], wideband has been achieved using cylindrical cavity along with dual substrate layer. So far, the SIW antennas were created in various desirable structures and operational principles which were manufactured using hard materials depending on the applications [258], [259].

Lately, there is a high necessity for conformal and sensing applications where the conventional SIW structures are incompatible and are not adaptable to the structure of the device under consideration. As an alternative, textile-based SIWs were created using copper plated textile [260] and conductive fabrics [261], where brass eyelets are used as vias which reduces the flexibility of the antenna. Subsequently, a textile-integrated waveguide (TIW), including vias is made of conductive threads and is fully integrated into the textile [262]. However, the performance of the TIW antenna falls short because of its weaving method. As a result, the requirement for flexible, mechanically deformable, and highly efficient materials as a substrate and conducting patch were necessary for the adaptability of SIW technology with flexibility-based applications.

Here in our study, as far as the authors' knowledge goes, the first flexible nanomaterial-based SIW antenna prototype is manufactured entirely using materials that are suitable for flexible electronics. Along with the substrate and conducting part, vias also play an important role in providing flexibility to the SIW antenna. The materials selected for the ground, substrate, patch, and vias are Copper tape, PDMS, MXene, and silver paste. The utilization of PDMS for substrate makes the device more flexible, deformable, and semi-transparent, while the conducting parts, which include copper, silver, and MXene, help support the performance of the antenna. The antenna is designed by collecting the parameters of the chosen materials, then fabricated and verified experimentally. The measured and simulated results show that the flexible sixteenth-mode antenna resonates at 3.5 GHz with a measured gain of – 3.39 dBi. The proposed SIW antenna is completely flexible and is useful for wireless communication applications such as IoT.

7.2 Device Fabrication

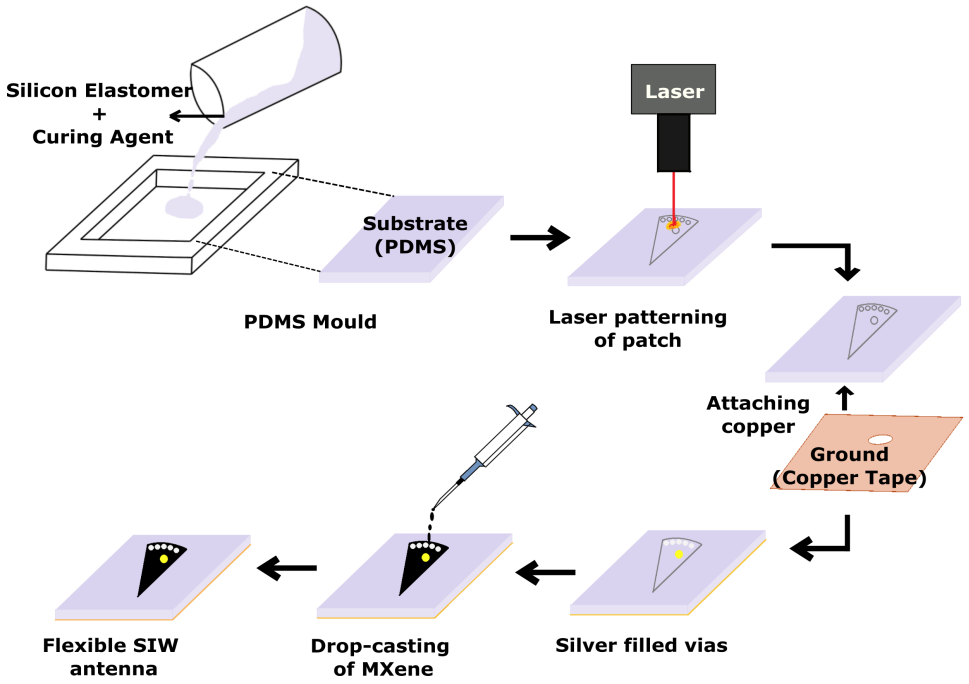

FIGURE 7.1: Fabrication process for sixteenth-mode flexible SIW antenna.

The presented flexible sixteenth-mode SIW antenna comprises a PDMS substrate sandwiched between copper tape as the ground plane and drop-casted MXene as a conductive patch on the top. The PDMS utilized here is from sylgard 184 silicon elastomer kit by Dow Corning Dowsil having $\varepsilon_r = 2.68$ and loss tangent = 0.0375 [23]. Fig. 7.1 depicts the fabricating procedure of the flexible SIW antenna. In the first step, the acrylic mask is prepared with the dimensions of the substrate having a thickness of 1.57mm is considered to make a block of PDMS substrate. PDMS is a widely used material and is produced by the combination of two solvents-silicone elastomer along with the curing agent with a mass ratio of 10:1. The prepared PDMS is kept in a desiccator for degassing until the removal of bubbles. Then the PDMS mould is made by placing the PDMS-filled mask in the oven at 80 ^{0}C for 2 hours. Laser patterning of the patch is done on the PDMS mould using a CO_2 laser machine (Universal®Laser Systems). A slotted copper tape is attached to the backside of the mould as a ground. Then the SMA connecter is connected to the antenna, and the vias were filled with silver paste, which is kept in the oven for 1 hour. Finally, the synthesized MXene with a conductivity of 2.89 $\times$ 10^5 S/m is drop-casted onto the patterned surface and is placed in the oven for an hour. The presented sixteenth-mode flexible SIW antenna patch is fabricated using the synthesized MXene. The synthesis

and chemical characterizations of MXene nanomaterial is comprehensively discussed in chapter 4 - Fig. 4.1a, Fig. 4.2 and Fig. 4.3

7.3 Design

7.3.1 Circular SIW Cavity at 10 GHz

The presented antenna in Fig. 7.2 radiates at 10 GHz. The antenna without the slot acts as a cylindrical cavity with a negligible height. The cavity side wall is generated by placing metallic via-holes periodically around the circumference of the cylindrical cavity. The proposed antenna is being fed by a coaxial probe. Since the cavity is a cylindrical one, its working principle and design frequency could be estimated from the solution of the wave equation in a cylindrical cavity along with some modification due to the discontinuous sidewall. If the leakage from the sidewall is negligible, the resonant frequency of TM_{npq} mode of a cylindrical cavity, having radius a and height d, can be expressed as Eqn. (7.1),

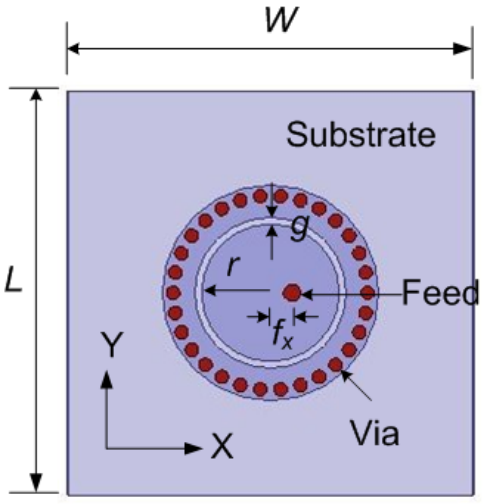

FIGURE 7.2: The proposed circular SIW antenna [W = 30, L = 30, r = 5.1, g = 0.5, f_X= 1.6 (all are in mm)].

$$f_r = \frac{c}{2\pi\sqrt{\mu_r \varepsilon_r}}\sqrt{\left(\frac{X_{np}}{a}\right)^2 + \left(\frac{q\pi}{d}\right)^2} \tag{7.1}$$

where, X_{np} is the p-th zero of the n-th order Bessel function of the first kind. Fig. 7.3a shows that, when there is no annular slot, the resonant frequencies of TM_{010} and TM_{110} modes of the SIW cavity are obtained at 8.32 and 14.7 GHz, respectively, which can be

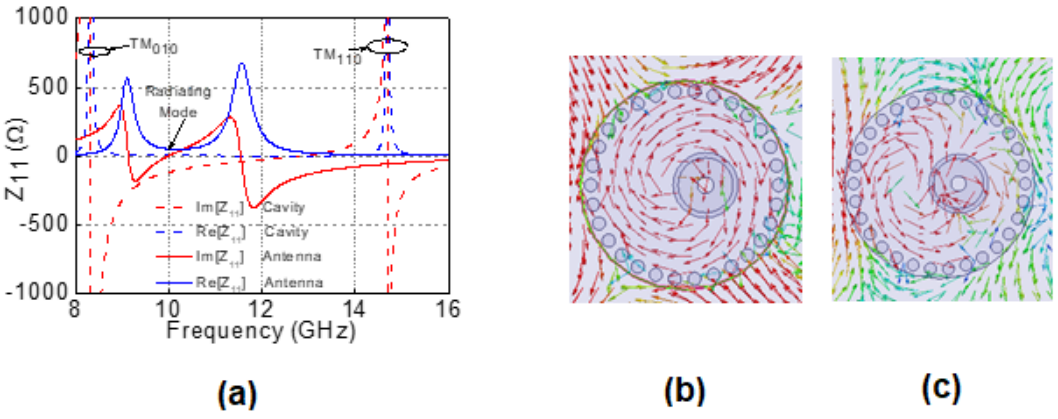

FIGURE 7.3: a) Z_{11} parameters for cavity and antenna, b) H-field distribution within the cavity at 8.32 GHz and c) 14.7 GHz.

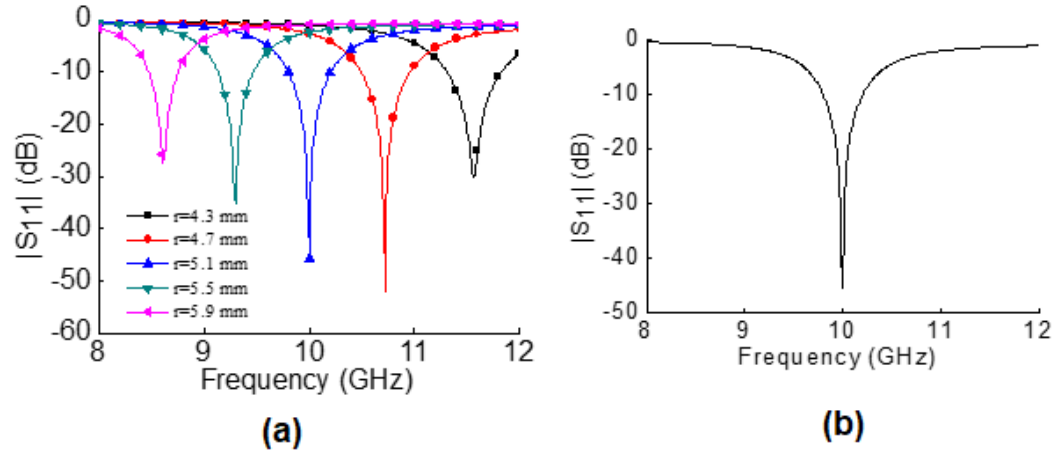

FIGURE 7.4: a) Variation of $|S_{11}|$ parameters for different values of r, b) $|S_{11}|$ parameter of the proposed antenna.

approximately obtained from Eqn. (7.1), with some modification due to the discontinuous side wall. This fact is supported by the vector H-field distribution within the cavity given in figure 3, where the distribution of H-field in Fig. 7.3b is that of TM_{010} and in Fig. 7.3c is that of TM_{110} mode. When the annular slot is introduced, the field within the substrate is perturbed and consequently a radiating mode is obtained due to the loading effect of the annular slot. The parametric study shows that the resonant frequency of the antenna can be tuned by varying the radius of the ring-shaped slot. This tenability is very much advantageous from the aspect of the antenna designer. Moreover, Fig. 7.4a shows that by judiciously choosing the slot radius, radiation could be obtained at any frequency over the X-band.

7.3.2 Sixteenth-Mode SIW Antenna at 3.5 GHz

The development of half-mode SIW technology resulted in an exponential reduction in the antenna size without affecting its performance [263]. By further extending this concept, the geometry of the sixteenth-mode SIW antenna is obtained as shown in Fig. 7.5a. The one-sixteenth part of the SIW cavity has the same resonant frequency of 3.5 GHz as of full mode, but the overall size is reduced significantly. From the vector H-Field distribution shown in Fig. 7.5b, the mode existing in the sixteenth-mode SIW antenna is identical to the circular SIW cavity, i.e., TM_{010} mode. To obtain a resonant frequency of 3.5 GHz from the proposed sixteenth-mode antenna, the radius of the full-mode is slightly modified. A simulated operating band of 130 MHz is observed for SIW antenna.

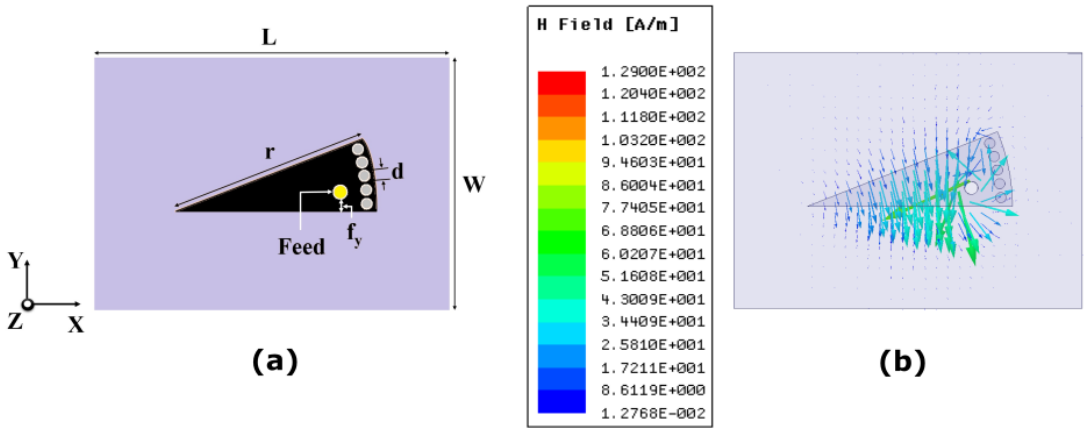

FIGURE 7.5: a) The proposed sixteenth mode SIW flexible antenna [L = 33, W = 25, r = 19.4, d = 1, f_y = 1.165 (all the dimensional values are in mm)] b) Vector H-Field distribution of the proposed SIW antenna at 3.5 GHz.

7.4 Results & Discussion

The antenna design and performance parameters are investigated using HFSS V.15.0. Fig. 7.6a presents the simulated and measured $|S_{11}|$ parameter of the flexible SIW antenna at 3.5 GHz resonant frequency. The Z-parameter in Fig. 7.6b shows the occurrence of resonance at 3.5 GHz. Fig. 7.7 illustrates the plot of radiation patterns in XZ & YZ planes at a resonant frequency of 3.5 GHz. The measured operating band of the presented antenna for $|S_{11}|$ < -10 dB is around 1800 MHz. The presented SIW antenna portrays a unidirectional radiation pattern from the plots with a gain of -3.39 dBi. The proposed antenna also provides a 15.5 dB difference between co-polarization and cross-polarization

levels in the direction of maximum radiation. The difference in $|S_{11}|$ parameter bandwidth and gain reduction can be due to the inhomogeneity of the MXene material as a conducting patch and its low conductivity compared to conventional materials. The wide band of the measured $|S_{11}|$ parameter is also a result of the limitation in the simulation environment, fabrication tolerance, and connector loss.

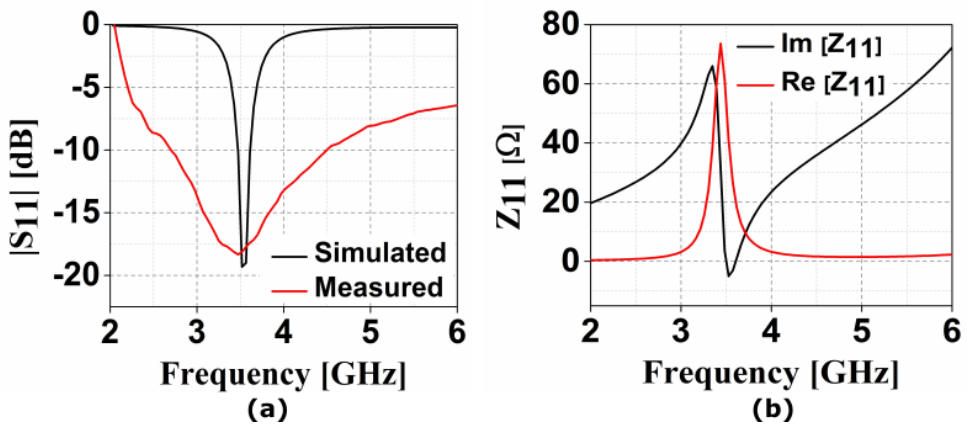

FIGURE 7.6: a) $|S_{11}|$ parameter b) Z parameter of flexible SIW antenna.

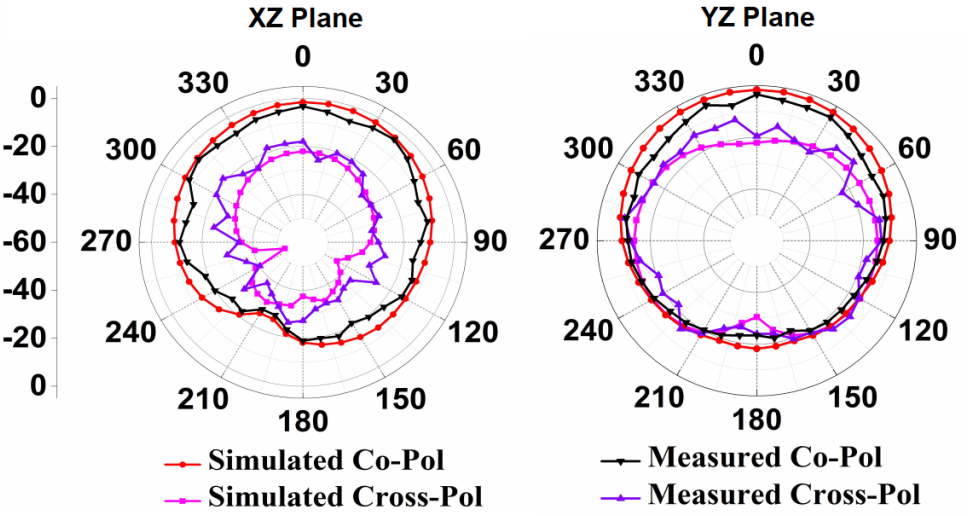

FIGURE 7.7: 2-D Radiation patterns of flexible SIW at 3.5 GHz.

7.5 Flexibility Demonstration

The materials used in designing and fabricating the antenna are flexible, which makes the SIW antenna completely suitable for conformal applications. In accordance with their structure and conformability, the presented SIW antenna can be mounted on a variety of

objects, as shown in Fig. 7.8. As a proof of concept, the SIW antenna is strained inward and outward in Fig. 7.8a and 7.8b and attached to different objects as shown in Fig. 7.8c and 7.8d, demonstrating that it can even be affixed on a curved surface.

FIGURE 7.8: Demonstration of SIW antenna's flexibility. a) Inward bent position, b) Outward bent position, c) Placed on a bottle, d) Placed on an object.

To further study the conformal response of the SIW antenna, the resonant frequency at various bending angles and radiation patterns at flat and bent state were analyzed. From the Fig. 7.9a, a shift in the resonant frequency is observed by varying the bending angles from 0^0 to 40^0 and after a 40^0 bend, the performance of the antenna degrades majorly due to its impedance mismatch and geometrical distortion. Fig. 7.9b depicts that as the bent angle increases, the normalized resonant frequency increases respectively. A comparison of radiation patterns of the antenna in its flat state and bent at an angle of 20^0 is shown in Fig. 7.9c. As per the measured values obtained, not much difference is observed between the two except the direction of maximum radiation is tilted and is obtained at approximately 10^0. The significant change of frequency while bending can be mostly due to the morphological structural changes in the nanomaterial utilized, which is also previously discussed in our recent works [29].

7.6 State of the Art

Recently, SIW technology is progressing towards wearable and textile-based miniaturized antennas for body-centric applications as presented in Table 7.1. The miniaturization of the SIW antenna is highly feasible by exploiting the EM field of the cavity. Several wearable antennas with single-band or dual-band behaviour were developed by utilizing various fabrics [264]–[266]. Paper-based SIW antenna is also proposed as a part of the multi-layered configuration [267]. The vias of these SIW antennas are made of metal eyelets, which tends to effect the flexibility of the SIW antenna. Consequently, developing a completely flexible SIW antenna as a part of microwave components in planar form is

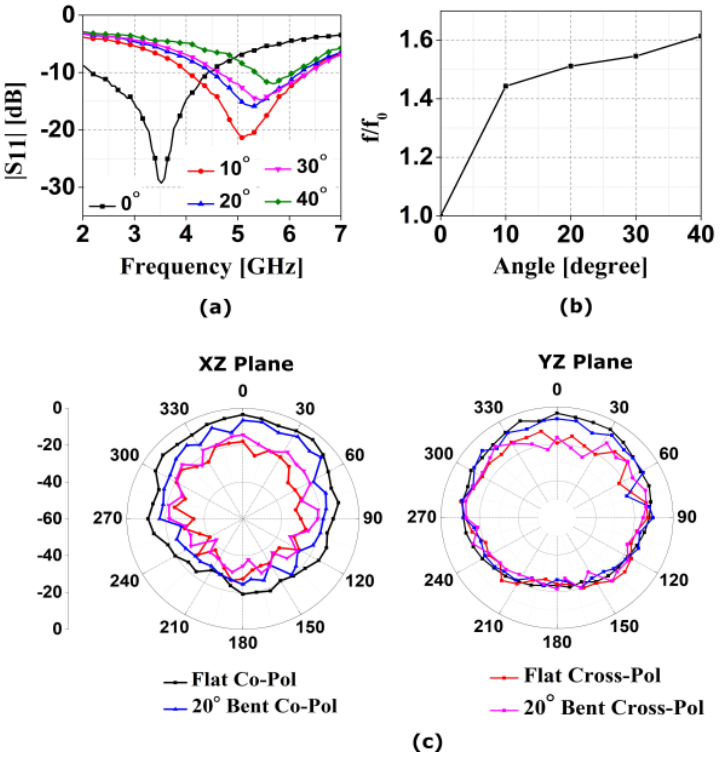

FIGURE 7.9: Bending analysis of SIW antenna. a) Resonant frequency at different bending angles, b) Normalized resonant frequency with respect to the bent angles, c). Radiation patterns of SIW antenna at flat and 20° bent position.

necessary for the progress of wireless applications. Here, a nanomaterial-based flexible miniaturized SIW antenna is presented for conformal applications, which can also be extended to IoT applications.

TABLE 7.1: Parametric comparison table for flexible SIW antennas

Substrate/Patch	**Electrical Dimensions**	**Gain [dBi]**	**Flexibility Level**	**Reference**
Photo paper/Silver Nano-particle ink	2.11 λ_0× 0.44 λ_0 (Approx.)	- 1.8 (Approx.)	Low	[267]
Wool Felt/ShieldIt super conductive textile	0.61 λ_0 × 0.39 λ_0	5.35	Low	[264]
Rubber foam/Copper-coated non-woven PET fabric	0.37 λ_0 × 0.38 λ_0 @ 0.867 GHz 0.35 λ_0 × 0.36 λ_0 @ 0.915 GHz	- 1.3 @ 0.867 GHz - 0.6 @ 0.915 GHz	Low	[265]
Jeans/Self-adhesive shieldit electro textiles	0.458 λ_0× 0.458 λ_0	5	Moderate	[266]
PET, PES/Shieldex yarns	0.5 λ_0× 0.466 λ_0	- 4.9	High	[262]
PDMS/MXene	**0.38 λ_0× 0.29 λ_0**	**- 3.39**	**High**	**This Paper**

7.7 Summary

A novel flexible nanomaterial-based sixteenth-mode SIW antenna for its utilization in conformal applications is presented. The characterizations of the chosen materials are explained, from which the design parametric values were considered. From the circular SIW cavity, a one-sixteenth part is designed as a sixteenth-mode SIW antenna at 3.5 GHz frequency. Due to the sixteenth-mode design, the proposed SIW antenna is reduced in size compared to all the other higher-order modes. The simulation and measured result are compared and a notable difference in bandwidth is observed in the $|S_{11}|$-parameter, but both are having a resonance at 3.5 GHz. The performance of the antenna can be significantly improved by enhancing the conductivity of the nanomaterial while maintaining the homogeneity of the material. In addition, the antenna has undergone flexibility demonstration, showing its adaptability toward IoT applications.

Chapter 8

Conclusion

This work presents the design and analysis of conformal/flexible microstrip antennas along with material selection and its synthesis, characterization, and fabrication procedure. Here, the flexible antennas are mainly utilized for sensing applications. The selection criteria for dielectric and conducting materials are considered based on the requirements of the antenna for sensing applications. This study involved expanding antenna-based sensors utilizing different dielectric and nanomaterials to enhance the sensing capabilities of the antenna. An added advantage of nanomaterials is their ability to react quickly to changes in electrochemical characteristics, which makes them suitable for wireless communication applications, especially antenna-based sensing. These antennas with nanomaterials as sensing elements have exhibited significant changes in their EM response corresponding to the changes in the applied physical quantity.

8.1 Summary of the Work Done

8.1.1 Antenna Sensor Analysis

- Different nanomaterial-based radiating elements and their effect on antenna parameters were studied for the antenna to act as a sensor with an enhanced sensing response. The electrochemical properties of these nanomaterials are highly responsive to any external changes applied. As a result, the EM properties of the antenna swiftly change with respect to the properties of the nanomaterials.

- A LIG-printed antenna sensor is presented for compressive and tensile strain sensing. The material characteristics of LIG were studied to observe its morphology and chemical composition. The device is fabricated using a single-step fabrication process. Then, the antenna is analyzed for strain sensing by exploiting the reflection parameter while bending and folding.
- The MXene-coated paper on polyimide is used as a flexible rectangular microstrip patch antenna for pressure and level sensing applications. The main idea of this work is to utilize a single antenna-based sensor for multiple applications, as presented separately for both pressure and level sensing. In both cases, the shift in the resonant frequency is observed due to the change in the effective physical parameters of the MXene and the polyimide.

8.1.2 Transient Antenna

For the transient nature of the antenna, a dielectric material like wax is chosen that disappears while heat is given as an external trigger. Materials sensitive to the applied and derived physical qualities are a requirement, as discussed, for the better sensing operation of the antenna. Utilizing nanomaterial like $NiSe_2$ as a conducting patch for the antenna also gave an efficient sensitivity when applied pressure. Additionally, theoretical analysis is performed to prove the effect of effective dielectric constant on the resonant frequency with the application of pressure on the antenna.

8.1.3 Contactless Sensing

Two separate antennas for transmitting and receiving the RF signal were considered in the presence of the obstructions for contactless wireless motion detection. Here, the operating principle lies in detecting the attenuated power of the received RF signal at the receiving antenna in the presence of obstruction. The attenuation of the received power is varied according to the size and structural area of the object, the material of the object, and the amount of the emitted energy from the object.

8.1.4 Flexible SIW Antenna

A miniaturized flexible nanomaterial-based SIW antenna prototype is manufactured entirely using flexile materials. The use of PDMS as a dielectric material makes the device more flexible, deformable, and semi-transparent, while the conducting parts, which include copper, silver, and MXene for ground, vias, and patch, respectively, help support the performance of the antenna. Due to the miniaturization, facile fabrication, and low conductivity, the antenna performance got affected, but it still can be used for short-range communication applications.

Consequently, this work concludes by presenting the antenna for flexible applications and sensing purposes, where the antenna sensors are developed for contact-based, contactless, and short-term sensing applications toward short-range communication.

8.2 Future Scope

- Due to the rise in the necessity for flexible applications, we may further explore innovative materials, designs, and fabrication techniques for antenna-based sensors and wireless communication applications.
- We may also look for suitable nanomaterials that provide better conductivity. An antenna with higher conductivity will exhibit a narrowband, which is more convenient for S-parameter-based sensing applications.
- The combination of low conductive nanomaterials and thin, flexible substrates offers lower gain than the conventional antennas and, hence, is suitable for only short-range communications. To find out suitable nanomaterial and substrate combinations, which will offer higher gain and hence could be used for long-range communication, may be a topic of further study.
- In our work, the S-parameters and the received power level are used as the sensing parameters. We can continue to explore the other antenna parameters that provide a good sensitivity, too.
- Here, the transient antenna is presented in its traditional planar shape. However, the transient antennas can also be designed for conformal applications.
- In all our works, we have designed the isolated antenna-based sensors. In future, a complete antenna-based sensing system with sufficient sensitivity can be developed.

Bibliography

[1] J. Zhu and H. Cheng, "Recent development of flexible and stretchable antennas for bio-integrated electronics," *Sensors*, vol. 18, no. 12, p. 4364, 2018.

[2] M. A. Monne, X. Lan, and M. Y. Chen, "Material selection and fabrication processes for flexible conformal antennas," *International Journal of Antennas and Propagation*, vol. 2018, 2018.

[3] S. G. Kirtania, B. A. Younes, A. R. Hossain, T. Karacolak, and P. K. Sekhar, "Cpw-fed flexible ultra-wideband antenna for iot applications," *Micromachines*, vol. 12, no. 4, p. 453, 2021.

[4] A. Mansour, M. Azab, and N. Shehata, "Flexible paper-based wideband antenna for compact-size iot devices," in *2017 8th IEEE Annual Information Technology, Electronics and Mobile Communication Conference (IEMCON)*, IEEE, 2017, pp. 426–429.

[5] A. Priya, A. Kumar, and B. Chauhan, "A review of textile and cloth fabric wearable antennas," *International Journal of Computer Applications*, vol. 116, no. 17, 2015.

[6] Z. Li, S. K. Sinha, G. M. Treich, *et al.*, "All-organic flexible fabric antenna for wearable electronics," *Journal of Materials Chemistry C*, vol. 8, no. 17, pp. 5662–5667, 2020.

[7] U. Ali, S. Ullah, B. Kamal, L. Matekovits, and A. Altaf, "Design, analysis and applications of wearable antennas: A review," *IEEE Access*, 2023.

[8] N. A. Malik, P. Sant, T. Ajmal, and M. Ur-Rehman, "Implantable antennas for bio-medical applications," *IEEE Journal of Electromagnetics, RF and Microwaves in Medicine and Biology*, vol. 5, no. 1, pp. 84–96, 2020.

[9] M. Al-Haddad, N. Jamel, and A. N. Nordin, "Flexible antenna: A review of design, materials, fabrication, and applications," in *Journal of Physics: Conference Series*, IOP Publishing, vol. 1878, 2021, p. 012 068.

[10] C. Du, X. Li, and S. Zhong, "Compact liquid crystal polymer based tri-band flexible antenna for wlan/wimax/5g applications," *IEEE Access*, 2019.

[11] A. Ghaffar, W. A. Awan, N. Hussain, S. Ahmad, and X. J. Li, "A compact dual-band flexible antenna for applications at 900 and 2450 mhz," *Prog. Electromagn. Res. Lett*, vol. 99, pp. 83–91, 2021.

[12] S. Ahmed, F. A. Tahir, A. Shamim, and H. M. Cheema, "A compact kapton-based inkjet-printed multiband antenna for flexible wireless devices," *IEEE Antennas and Wireless Propagation Letters*, vol. 14, pp. 1802–1805, 2015.

[13] Y. Zhang, S. Li, Z.-Q. Yang, X.-Y. Qu, and W.-H. Zong, "A coplanar waveguide-fed flexible antenna for ultra-wideband applications," *International Journal of RF and Microwave Computer-Aided Engineering*, vol. 30, no. 8, e22258, 2020.

[14] X. Qian, Z. Li, Z. Meng, N. Gao, and Z. Zhang, "Flexible rfid tag for sensing the total minerals in drinking water via smartphone tapping," *IEEE Sensors Journal*, vol. 21, no. 21, pp. 24 749–24 758, 2021.

[15] M. El Gharbi, R. Fernández-García, S. Ahyoud, and I. Gil, "A review of flexible wearable antenna sensors: Design, fabrication methods, and applications," *Materials*, vol. 13, no. 17, p. 3781, 2020.

[16] H. Huang, "Antenna sensors in passive wireless sensing systems," *Handbook of Antenna Technologies*, pp. 2795–2838, 2016.

[17] K. Kang, Y. Cho, and K. J. Yu, "Novel nano-materials and nano-fabrication techniques for flexible electronic systems," *Micromachines*, vol. 9, no. 6, p. 263, 2018.

[18] M. T. Islam, M. Cho, M Samsuzzaman, and S Kibria, "Compact antenna for small satellite applications [antenna applications corner]," *IEEE Antennas and Propagation magazine*, vol. 57, no. 2, pp. 30–36, 2015.

[19] Y. Wang, C. Yan, S.-Y. Cheng, *et al.*, "Flexible rfid tag metal antenna on paper-based substrate by inkjet printing technology," *Advanced Functional Materials*, vol. 29, no. 29, p. 1 902 579, 2019.

[20] O. P. Falade, S. F. Jilani, A. Y. Ahmed, *et al.*, "Design and characterisation of a screen-printed millimetre-wave flexible metasurface using copper ink for communication applications," *Flexible and Printed Electronics*, vol. 3, no. 4, p. 045 005, 2018.

[21] K.-Y. Shin, J.-Y. Hong, and J. Jang, "Micropatterning of graphene sheets by inkjet printing and its wideband dipole-antenna application," *Advanced materials*, vol. 23, no. 18, pp. 2113–2118, 2011.

[22] N Sundararajan, S. Joshi, and E. Armstrong, "Robust controller synthesis for a large flexible space antenna," *Journal of Guidance, Control, and Dynamics*, vol. 10, no. 2, pp. 201–208, 1987.

[23] G. Washington, "Smart aperture antennas," *Smart Materials and Structures*, vol. 5, no. 6, p. 801, 1996.

[24] S. M. Joshi, E. S. Armstrong, and N Sundararajan, "Application of the lqg/ltr technique to robust controller synthesis for a large flexible space antenna," Tech. Rep., 1986.

[25] M. Tabata, K. Yamamoto, T. Inoue, T. Noda, and K. Miura, "Shape adjustment of a flexible space antenna reflector," *Journal of intelligent material systems and structures*, vol. 3, no. 4, pp. 646–658, 1992.

[26] D. Grieg and H. Engelmann, "Microstrip-a new transmission technique for the klilomegacycle range," *Proceedings of the IRE*, vol. 40, no. 12, pp. 1644–1650, 1952.

[27] J. E. Butler and N. P. S. M. CA, "Design of strip transmission line systems and antennas," Ph.D. dissertation, Naval Postgraduate School, 1955.

[28] G. A. Deschamps, "Microstrip microwave antennas," in *Proceedings of the Third Symposium on the USAF Antenna Research and Development Program, Oct*, 1953, pp. 18–22.

[29] J. Bernhard, P. Mayes, D Schaubert, and R. Mailloux, "A commemoration of deschamps' and sichak's 'microstrip microwave antennas': 50 years of development, divergence, and new directions," in *Proc. of the 2003 Antenna Applications Symp*, 2003, pp. 189–230.

[30] R. Munson, "Microstrip phased array antennas," in *1973 EIC 11th Electrical Insulation Conference*, IEEE, 1973, pp. 281–283.

[31] F. K. Schwering and A. C.-E. C. F. M. NJ, "Millimeter wave antennas for avionics," *In AGARD Microwave Antennas for Avionics 8 p (SEE N87-23859 17-32)*, vol. 1, 1987.

[32] J Verpoorte, H. Schippers, and G Vos, "Technology for conformal load-bearing antennas on aircraft structures," 2000.

[33] C Krowne, "Cylindrical-rectangular microstrip antenna," *IEEE Transactions on Antennas and Propagation*, vol. 31, no. 1, pp. 194–199, 1983.

[34] K.-M. Luk, K.-F. Lee, and J. S. Dahele, "Analysis of the cylindrical-rectangular patch antenna," *IEEE Transactions on Antennas and Propagation*, vol. 37, no. 2, pp. 143–147, 1989.

[35] S. D. A. Fonseca and A. Giarola, "Analysis of microstrip wraparound antennas using dyadic green's functions," *IEEE Transactions on Antennas and Propagation*, vol. 31, no. 2, pp. 248–253, 1983.

[36] T. Kashiwa, T. Onishi, and I. Fukai, "Analysis of microstrip antennas on a curved surface using the conformal grids fd-td method," *IEEE transactions on antennas and propagation*, vol. 42, no. 3, pp. 423–427, 1994.

[37] E Tanabe, A McEuen, C. Norris, P Fessenden, and T. Samulski, "A multi-element microstrip antenna for local hyperthermia," in *1983 IEEE MTT-S International Microwave Symposium Digest*, IEEE, 1983, pp. 183–185.

[38] S. Jacobsen, P. R. Stauffer, and D. G. Neuman, "Dual-mode antenna design for microwave heating and noninvasive thermometry of superficial tissue disease," *IEEE Transactions on Biomedical Engineering*, vol. 47, no. 11, pp. 1500–1509, 2000.

[39] P. Salonen, L Sydanheimo, M. Keskilammi, and M. Kivikoski, "A small planar inverted-f antenna for wearable applications," in *Digest of papers. Third international symposium on wearable computers*, IEEE, 1999, pp. 95–100.

[40] P. Salonen, M. Keskilammi, J. Rantanen, and L. Sydanheimo, "A novel bluetooth antenna on flexible substrate for smart clothing," in *2001 IEEE International Conference on Systems, Man and Cybernetics. e-Systems and e-Man for Cybernetics in Cyberspace (Cat. No. 01CH37236)*, IEEE, vol. 2, 2001, pp. 789–794.

[41] P. Salonen and L Hurme, "A novel fabric wlan antenna for wearable applications," in *IEEE Antennas and Propagation Society International Symposium. Digest. Held in conjunction with: USNC/CNC/URSI North American Radio Sci. Meeting (Cat. No. 03CH37450)*, IEEE, vol. 2, 2003, pp. 700–703.

[42] M. Tanaka and J.-h. Jang, "Wearable patch antenna," *IEICE Proceedings Series*, vol. 10, no. 1A4-3, 2002.

[43] T. Yang, W. A. Davis, T. G. Campbell, and C. Reddy, "A low-profile antenna design approach for conformal space suit and other wearable applications," *NOTICE AND SIGNATURE PAGE*, p. 418, 2010.

[44] T. F. Kennedy, P. W. Fink, A. W. Chu, and G. F. Studor, "Potential space applications for body-centric wireless and e-textile antennas," 2007.

[45] S. Zhu and R. Langley, "Dual-band wearable textile antenna on an ebg substrate," *IEEE transactions on Antennas and Propagation*, vol. 57, no. 4, pp. 926–935, 2009.

[46] A. Tronquo, H. Rogier, C. Hertleer, and L. Van Langenhove, "Robust planar textile antenna for wireless body lans operating in 2.45 ghz ism band," *Electronics letters*, vol. 42, no. 3, p. 1, 2006.

[47] P. Salonen, Y. Rahmat-Samii, H. Hurme, and M. Kivikoski, "Effect of conductive material on wearable antenna performance: A case study of wlan antennas," in *IEEE Antennas and Propagation Society Symposium, 2004.*, IEEE, vol. 1, 2004, pp. 455–458.

[48] E. Apaydin, *Microfabrication techniques for printing on PDMS elastomers for antenna and biomedical applications*. The Ohio State University, 2009.

[49] S Holzwarth, J Kassner, R Kulke, and D Heberling, "Planar antenna arrays on ltcc-multilayer technology," 2001.

[50] G DeJean, R Bairavasubramanian, D Thompson, G. Ponchak, M. Tentzeris, and J Papapolymerou, "Liquid crystal polymer (lcp): A new organic material for the development of multilayer dual-frequency/dual-polarization flexible antenna arrays," *IEEE Antennas and Wireless Propagation Letters*, vol. 4, pp. 22–26, 2005.

[51] P. J. Burke, S. Li, and Z. Yu, "Quantitative theory of nanowire and nanotube antenna performance," *IEEE transactions on nanotechnology*, vol. 5, no. 4, pp. 314–334, 2006.

[52] H. Rmili, J.-L. Miane, H. Zangar, and T. Olinga, "Design of microstrip-fed proximity-coupled conducting-polymer patch antenna," *Microwave and Optical Technology Letters*, vol. 48, no. 4, pp. 655–660, 2006.

[53] A. C. Patel, M. P. Vaghela, H. Bajwa, and P. K. Patra, "Conformable patch antenna array for energy harvesting," *MRS Online Proceedings Library (OPL)*, vol. 1205, pp. 1205–L09, 2009.

[54] J. M. Jornet and I. F. Akyildiz, "Graphene-based nano-antennas for electromagnetic nanocommunications in the terahertz band," in *Proceedings of the Fourth European Conference on Antennas and Propagation*, IEEE, 2010, pp. 1–5.

[55] K. Khorsand Kazemi, S. Hu, O. Niksan, *et al.*, "Low-profile planar antenna sensor based on ti3c2tx mxene membrane for voc and humidity monitoring," *Advanced Materials Interfaces*, vol. 9, no. 13, p. 2 102 411, 2022.

[56] F. A. Tahir and A. Javed, "A compact dual-band frequency-reconfigurable textile antenna for wearable applications," *Microwave and Optical Technology Letters*, vol. 57, no. 10, pp. 2251–2257, 2015.

[57] S. Masihi, M. Panahi, D. Maddipatla, *et al.*, "Development of a flexible tunable and compact microstrip antenna via laser assisted patterning of copper film," *IEEE Sensors Journal*, vol. 20, no. 14, pp. 7579–7587, 2020.

[58] S. Kanaparthi, V. R. Sekhar, and S. Badhulika, "Flexible, eco-friendly and highly sensitive paper antenna based electromechanical sensor for wireless human motion detection and structural health monitoring," *Extreme Mechanics Letters*, vol. 9, pp. 324–330, 2016.

[59] A. Kiourti and J. L. Volakis, "Stretchable and flexible e-fiber wire antennas embedded in polymer," *IEEE Antennas and wireless propagation letters*, vol. 13, pp. 1381–1384, 2014.

[60] X. Gao, Z. Shen, and C. Hua, "Conformal vhf log-periodic balloon antenna," *IEEE Transactions on Antennas and Propagation*, vol. 63, no. 6, pp. 2756–2761, 2015.

[61] M Padmanabharaju, B. Madhav, D. P. Kishore, and P. D. Prasad, "Conductive fabric material based compact novel wideband textile antenna for wireless medical applications," *Materials Research Express*, vol. 6, no. 8, p. 086 327, 2019.

[62] F. Xu, L. Yao, D. Zhao, M. Jiang, and Y. Qiu, "Effect of weaving direction of conductive yarns on electromagnetic performance of 3d integrated microstrip antenna," *Applied Composite Materials*, vol. 20, pp. 827–838, 2013.

[63] A. Arriola, J. Sancho, S. Brebels, M. Gonzalez, and W. De Raedt, "Stretchable dipole antenna for body area networks at 2.45 ghz," *IET microwaves, antennas & propagation*, vol. 5, no. 7, pp. 852–859, 2011.

[64] L. Song, A. C. Myers, J. J. Adams, and Y. Zhu, "Stretchable and reversibly deformable radio frequency antennas based on silver nanowires," *ACS applied materials & interfaces*, vol. 6, no. 6, pp. 4248–4253, 2014.

[65] R. A. Liyakath, A. Takshi, and G. Mumcu, "Multilayer stretchable conductors on polymer substrates for conformal and reconfigurable antennas," *IEEE Antennas and Wireless Propagation Letters*, vol. 12, pp. 603–606, 2013.

[66] G. J. Hayes, J.-H. So, A. Qusba, M. D. Dickey, and G. Lazzi, "Flexible liquid metal alloy (egain) microstrip patch antenna," *IEEE transactions on Antennas and Propagation*, vol. 60, no. 5, pp. 2151–2156, 2012.

[67] W. Yang, H. Sun, Z. Guo, and X. Zhao, "Printable silver nano ink for bendable ultrawideband antenna with triple-notch characteristics," *ACS Applied Nano Materials*, 2023.

[68] S. Wang, T. Chinnasamy, M. A. Lifson, F. Inci, and U. Demirci, "Flexible substrate-based devices for point-of-care diagnostics," *Trends in biotechnology*, vol. 34, no. 11, pp. 909–921, 2016.

[69] J. S. Lee, M. Kim, J. Oh, *et al.*, "Platinum-decorated carbon nanoparticle/polyaniline hybrid paste for flexible wideband dipole tag-antenna application," *Journal of Materials Chemistry A*, vol. 3, no. 13, pp. 7029–7035, 2015.

[70] L. Mo, Z. Guo, Z. Wang, *et al.*, "Nano-silver ink of high conductivity and low sintering temperature for paper electronics," *Nanoscale research letters*, vol. 14, pp. 1–11, 2019.

[71] S. Z. Sajal, B. D. Braaten, and V. R. Marinov, "A microstrip patch antenna manufactured with flexible graphene-based conducting material," in *2015 IEEE international symposium on antennas and propagation & USNC/URSI National Radio Science meeting*, IEEE, 2015, pp. 2415–2416.

[72] Y. Zhou, Y. Bayram, F. Du, L. Dai, and J. L. Volakis, "Polymer-carbon nanotube sheets for conformal load bearing antennas," *IEEE Transactions on Antennas and Propagation*, vol. 58, no. 7, pp. 2169–2175, 2010.

[73] R. Asmatulu, P. K. Bollavaram, V. R. Patlolla, I. M. Alarifi, and W. S. Khan, "Investigating the effects of metallic submicron and nanofilms on fiber-reinforced composites for lightning strike protection and emi shielding," *Advanced Composites and Hybrid Materials*, vol. 3, pp. 66–83, 2020.

[74] D. Tang, Q. Wang, Z. Wang, *et al.*, "Highly sensitive wearable sensor based on a flexible multi-layer graphene film antenna," *Science Bulletin*, vol. 63, no. 9, pp. 574–579, 2018.

[75] S. Dhariwal, V. K. Lamba, and A. Kumar, "Simulation and performance analysis of carbon nano-materials based patch antennas," *Indian Journal of Science and Technology*, vol. 9, no. 4, pp. 1–8, 2016.

[76] A. Watanabe, A. Rahman, J. Cai, and M. Aminuzzaman, "Antenna sensors prepared by laser direct writing based on graphene hybrid materials," *Journal of Photopolymer Science and Technology*, vol. 33, no. 2, pp. 159–163, 2020.

[77] L. Song, B. Wu, X. Zhang, and B. Huang, "Demonstration of wireless gas sensor using reduced graphene oxide loaded patch antenna," in *2018 IEEE International Conference on Computational Electromagnetics (ICCEM)*, IEEE, 2018, pp. 1–3.

[78] H. Jeon, S. Jin, and K.-Y. Shin, "Highly flexible, high-performance radio-frequency antenna based on free-standing graphene/polymer nanocomposite film," *Applied Surface Science*, vol. 582, p. 152 455, 2022.

[79] X. Guo, Y. Huang, C. Wu, *et al.*, "Flexible and reversibly deformable radio-frequency antenna based on stretchable swcnts/pani/lycra conductive fabric," *Smart Materials and Structures*, vol. 26, no. 10, p. 105 036, 2017.

[80] R. R. Hasan, A. M. Saleque, A. B. Anwar, M. A. Rahman, and Y. H. Tsang, "Multiwalled carbon nanotube-based on-body patch antenna for detecting covid-19-affected lungs," *ACS omega*, vol. 7, no. 32, pp. 28 265–28 274, 2022.

[81] S. Ali, A. Hassan, S. Khan, and A. Bermak, "Flexible coplanar waveguide strain sensor based on printed silver nanocomposites," *SN Applied Sciences*, vol. 1, pp. 1–8, 2019.

[82] N. Lakshmi and T. Sreeja, "Dual nanocomposite materials that enhance the radiation characteristics of flexible circular antenna," *AEU-International Journal of Electronics and Communications*, vol. 170, p. 154 839, 2023.

[83] M. Wagih, O. Malik, A. S. Weddell, and S. Beeby, "E-textile breathing sensor using fully textile wearable antennas," *Engineering Proceedings*, vol. 15, no. 1, p. 9, 2022.

[84] M. El Gharbi, R. Fernández-García, and I. Gil, "Embroidered wearable antenna-based sensor for real-time breath monitoring," *Measurement*, vol. 195, p. 111 080, 2022.

[85] M. El Gharbi, R. Fernández-García, and I. Gil, "Wireless communication platform based on an embroidered antenna-sensor for real-time breathing detection," *Sensors*, vol. 22, no. 22, p. 8667, 2022.

[86] M. K. El Abbasi, M. Madi, H. F. Jelinek, and K. Y. Kabalan, "Wearable blood pressure sensing based on transmission coefficient scattering for microstrip patch antennas," *Sensors*, vol. 22, no. 11, p. 3996, 2022.

[87] M. K. ElAbbasi, M. Madi, K. Kabalan, and H. Jelinek, "Beat to beat continuous blood pressure estimation using transmission coefficient of on-body antennas," 2022.

[88] S. Saha, H. Cano-Garcia, I. Sotiriou, *et al.*, "A glucose sensing system based on transmission measurements at millimetre waves using micro strip patch antennas," *Scientific reports*, vol. 7, no. 1, p. 6855, 2017.

[89] R. B. Khadase, A. Nandgaonkar, B. Iyer, and A. Wagh, "Multilayered implantable antenna biosensor for continuous glucose monitoring: Design and analysis," *Progress In Electromagnetics Research C*, vol. 114, pp. 173–184, 2021.

[90] M. E. Gharbi, R. Fernández-García, and I. Gil, "Textile antenna-sensor for in vitro diagnostics of diabetes," *Electronics*, vol. 10, no. 13, p. 1570, 2021.

[91] V. V. Deshmukh and S. S. Chorage, "Microstrip antennas used for noninvasive determination of blood glucose level," in *2020 4th International conference on intelligent computing and control systems (ICICCS)*, IEEE, 2020, pp. 720–725.

[92] K. Sen, S. Anand, *et al.*, "Design of microstrip sensor for non invasive blood glucose monitoring," in *2017 International Conference on Emerging Trends & Innovation in ICT (ICEI)*, IEEE, 2017, pp. 5–8.

[93] E. Cheng, M Fareq, A. Shahriman, *et al.*, "Development of microstrip patch antenna sensing system for salinity and sugar detection in water," *Int. J. Mech. Mechatronics Eng*, vol. 15, no. 5, pp. 31–36, 2014.

[94] M. N. Rahman, M. T. Islam, and M. Samsuzzaman Sobuz, "Salinity and sugar detection system using microstrip patch antenna," *Microwave and Optical Technology Letters*, vol. 60, no. 5, pp. 1092–1096, 2018.

[95] M. T. Islam, M. N. Rahman, M. S. J. Singh, and M. Samsuzzaman, "Detection of salt and sugar contents in water on the basis of dielectric properties using microstrip antenna-based sensor," *IEEE Access*, vol. 6, pp. 4118–4126, 2018.

[96] S. Njokweni and P Kumar, "Salt and sugar detection system using a compact microstrip patch antenna," *International Journal on Smart Sensing and Intelligent Systems*, vol. 13, no. 1, pp. 1–9, 2020.

[97] R. Nilavalan, I. Craddock, A. Preece, J Leendertz, and R. Benjamin, "Wideband microstrip patch antenna design for breast cancer tumour detection," *IET Microwaves, Antennas & Propagation*, vol. 1, no. 2, pp. 277–281, 2007.

[98] C. J. Shannon, E. Fear, and M Okoniewski, "Dielectric-filled slotline bowtie antenna for breast cancer detection," *Electronics Letters*, vol. 41, no. 7, pp. 388–390, 2005.

[99] D. N. Elsheakh, R. A. Mohamed, O. M. Fahmy, K. Ezzat, and A. R. Eldamak, "Complete breast cancer detection and monitoring system by using microwave textile based antenna sensors," *Biosensors*, vol. 13, no. 1, p. 87, 2023.

[100] J. Lai, J. Wang, K. Zhao, *et al.*, "Design of a dual-polarized omnidirectional dielectric resonator antenna for capsule endoscopy system," *IEEE Access*, vol. 9, pp. 14 779–14 786, 2021.

[101] G.-b. Wang, X.-w. Xuan, D.-l. Jiang, K. Li, and W. Wang, "A miniaturized implantable antenna sensor for wireless capsule endoscopy system," *AEU-International Journal of Electronics and Communications*, vol. 143, p. 154 022, 2022.

[102] H. Jiang, J. Sanders, J. Yao, and H. Huang, "Patch antenna based temperature sensor," in *Nondestructive Characterization for Composite Materials, Aerospace Engineering, Civil Infrastructure, and Homeland Security 2014*, SPIE, vol. 9063, 2014, pp. 398–406.

[103] F. M. Tchafa and H Huang, "Microstrip patch antenna for simultaneous temperature sensing and superstrate characterization," *Smart Materials and Structures*, vol. 28, no. 10, p. 105 009, 2019.

[104] M. Bhattacharjee, F. Nikbakhtnasrabadi, and R. Dahiya, "Printed chipless antenna as flexible temperature sensor," *IEEE Internet of Things Journal*, vol. 8, no. 6, pp. 5101–5110, 2021.

[105] J. Zhang, C. Li, Y. Gao, J. Tan, F. Xuan, and X. Ling, "Flexible multimode antenna sensor with strain and humidity sensing capability for structural health monitoring," *Sensors and Actuators A: Physical*, vol. 347, p. 113 960, 2022.

[106] H. Kou, Q. Tan, Y. Wang, G. Zhang, S. Su, and J. Xiong, "A wireless slot-antenna integrated temperature-pressure-humidity sensor loaded with csrr for harsh-environment applications," *Sensors and Actuators B: Chemical*, vol. 311, p. 127 907, 2020.

[107] R. Verma, K Said, J Salim, *et al.*, "Carbon nanotube-based microstrip antenna gas sensor," in *2013 IEEE 56th International Midwest Symposium on Circuits and Systems (MWSCAS)*, IEEE, 2013, pp. 724–727.

[108] J. P. C. do Nascimento, F. F. do Carmo, A. J. M. Sales, *et al.*, "A novel wireless oxygen gas sensor based on silver film loaded on a patch antenna," *Materials Chemistry and Physics*, vol. 299, p. 127 513, 2023.

[109] Y. J. Mao, Q. Xu, X. Shi, and M. S. Tong, "A novel sensor based on microstrip patch antenna for detecting different gases in circular pipe," in *2019 IEEE International Conference on Microwaves, Antennas, Communications and Electronic Systems (COMCAS)*, IEEE, 2019, pp. 1–5.

[110] S. Costanzo and V. Cioffi, "Preliminary sar analysis of textile antenna sensor for non-invasive blood-glucose monitoring," in *Information Technology and Systems: Proceedings of ICITS 2020*, Springer, 2020, pp. 607–612.

[111] I. I. Labiano and A. Alomainy, "Fabric antenna for temperature sensing over ism frequency band," in *2019 IEEE International Symposium on Antennas and Propagation and USNC-URSI Radio Science Meeting*, IEEE, 2019, pp. 1567–1568.

[112] W. Wang, X.-W. Xuan, W.-Y. Zhao, and H.-K. Nie, "An implantable antenna sensor for medical applications," *IEEE Sensors Journal*, vol. 21, no. 13, pp. 14 035–14 042, 2021.

[113] A. R. Eldamak and E. C. Fear, "Conformal and disposable antenna-based sensor for non-invasive sweat monitoring," *Sensors*, vol. 18, no. 12, p. 4088, 2018.

[114] V. Satam, C. Kulkarni, and A. Kholapure, "Microstrip antenna as a temperature sensor for iot applications," in *2022 IEEE Microwaves, Antennas, and Propagation Conference (MAPCON)*, IEEE, 2022, pp. 944–947.

[115] J.-H. Low, P.-S. Chee, and E.-H. Lim, "Deformable liquid metal patch antenna for air pressure detection," *IEEE Sensors Journal*, vol. 20, no. 8, pp. 3963–3970, 2019.

[116] H. Huang, F. Farahanipad, and A. K. Singh, "A stacked dual-frequency microstrip patch antenna for simultaneous shear and pressure displacement sensing," *IEEE Sensors Journal*, vol. 17, no. 24, pp. 8314–8323, 2017.

[117] J Yao, C. Xu, A Mears, M Jaguan, S Tjuatja, and H Huang, "Pressure sensing using low-cost microstrip antenna sensor," in *Sensors and Smart Structures Technologies for Civil, Mechanical, and Aerospace Systems 2015*, SPIE, vol. 9435, 2015, pp. 919–923.

[118] B. Nie, R. Huang, T. Yao, *et al.*, "Textile-based wireless pressure sensor array for human-interactive sensing," *Advanced Functional Materials*, vol. 29, no. 22, p. 1 808 786, 2019.

[119] K. Wang, F. Lin, D. T. Lai, *et al.*, "Soft gold nanowire sponge antenna for battery-free wireless pressure sensors," *Nanoscale*, vol. 13, no. 7, pp. 3957–3966, 2021.

[120] X. Zhou, Y. He, and J. Zeng, "Liquid metal antenna-based pressure sensor," *Smart Materials and Structures*, vol. 28, no. 2, p. 025 019, 2019.

[121] P. Lopato and M. Herbko, "A circular microstrip antenna sensor for direction sensitive strain evaluation," *Sensors*, vol. 18, no. 1, p. 310, 2018.

[122] A. Daliri, A. Galehdar, S. John, W. Rowe, and K. Ghorbani, "Circular microstrip patch antenna strain sensor for wireless structural health monitoring," in *Proceedings of the world congress on engineering*, vol. 2, 2010, p. 1173.

[123] F. Nikbakhtnasrabadi, H. El Matbouly, M. Ntagios, and R. Dahiya, "Textile-based stretchable microstrip antenna with intrinsic strain sensing," *ACS Applied Electronic Materials*, vol. 3, no. 5, pp. 2233–2246, 2021.

[124] I Mohammad, V Gowda, H Zhai, and H Huang, "Detecting crack orientation using patch antenna sensors," *Measurement Science and Technology*, vol. 23, no. 1, p. 015 102, 2011.

[125] S. Xue, Z. Yi, L. Xie, G. Wan, and T. Ding, "A passive wireless crack sensor based on patch antenna with overlapping sub-patch," *Sensors*, vol. 19, no. 19, p. 4327, 2019.

[126] Q. Pang, G. Dong, and X. Yang, "Metal crack detection sensor based on microstrip antenna," *IEEE Sensors Journal*, vol. 23, no. 8, pp. 8375–8384, 2023.

[127] C.-H. Su and H.-W. Wu, "An antenna sensor to identify finger postures," in *2019 IEEE Eurasia Conference on IOT, Communication and Engineering (ECICE)*, IEEE, 2019, pp. 571–574.

[128] U. Hasni and E. Topsakal, "Wearable antennas for on-body motion detection," in *2020 IEEE USNC-CNC-URSI North American Radio Science Meeting (Joint with AP-S Symposium)*, IEEE, 2020, pp. 1–2.

[129] C. Li, T. Djerafi, E. Villeneuve, and K. Wu, "Planar antenna sensor with thermal stability for detection of ice formation," *Sensors and Actuators A: Physical*, vol. 341, p. 113 576, 2022.

[130] R. Kozak, K. Khorsand, T. Zarifi, K. Golovin, and M. H. Zarifi, "Patch antenna sensor for wireless ice and frost detection," *Scientific Reports*, vol. 11, no. 1, p. 13 707, 2021.

[131] L. Zhu, N. Alsaab, M. M.-C. Cheng, and P.-Y. Chen, "A zero-power ubiquitous wireless liquid-level sensor based on microfluidic-integrated microstrip antenna," *IEEE Journal of Radio Frequency Identification*, vol. 4, no. 3, pp. 265–274, 2020.

[132] M. T. Khan, X. Q. Lin, Z. Chen, F. Xiao, Y. H. Yan, and A. K. Memon, "Design and analysis of a microstrip patch antenna for water content sensing," in *2019 16th International Computer Conference on Wavelet Active Media Technology and Information Processing*, IEEE, 2019, pp. 438–442.

[133] Q. Shi, X.-W. Xuan, H.-K. Nie, Z.-Y. Wang, and W. Wang, "Antenna sensor based on amc array for contactless detection of water and ethanol in oil," *IEEE Sensors Journal*, vol. 21, no. 19, pp. 21 503–21 510, 2021.

[134] P. Soontornpipit, C. M. Furse, Y. C. Chung, and B. M. Lin, "Optimization of a buried microstrip antenna for simultaneous communication and sensing of soil moisture," *IEEE transactions on antennas and propagation*, vol. 54, no. 3, pp. 797–800, 2006.

[135] A. P. Priyaa, A. Mohammed, C Ambili, *et al.*, "Microwave sensor antenna for soil moisture measurement," in *2015 Fifth International Conference on Advances in Computing and Communications (ICACC)*, IEEE, 2015, pp. 258–262.

[136] P. Kumar and A. Chaturvedi, "Design and development of single & dual resonant frequency antennas for moisture content measurement," *Wireless Personal Communications*, vol. 114, pp. 565–582, 2020.

[137] S. Jain, P. K. Mishra, J. Mishra, and V. V. Thakare, "Design and analysis of h-shape patch sensor for rice quality detection," *Materials Today: Proceedings*, vol. 29, pp. 581–586, 2020.

[138] S. Jain, P. K. Mishra, and V. V. Thakare, "Design and analysis of dual frequency microwave moisture sensor based on rectangular microstrip antenna," *Materials Today: Proceedings*, vol. 47, pp. 6441–6448, 2021.

[139] M. T. Islam, F. B. Ashraf, T. Alam, N. Misran, and K. B. Mat, "A compact ultrawideband antenna based on hexagonal split-ring resonator for ph sensor application," *Sensors*, vol. 18, no. 9, p. 2959, 2018.

[140] J.-I. Kim, Z. Ding, S.-N. Lee, J.-G. Yook, B. Ziaie, and D. Peroulis, "Hydrogel-based integrated antenna-ph sensor," in *SENSORS, 2007 IEEE*, IEEE, 2007, pp. 695–698.

[141] A. Bouchalkha and R. Karli, "Planar microstrip antenna sensor for ph measurements," in *2019 International Conference on Electrical and Computing Technologies and Applications (ICECTA)*, IEEE, 2019, pp. 1–5.

[142] M. Nie, Y.-H. Xia, and H.-S. Yang, "A flexible and highly sensitive graphene-based strain sensor for structural health monitoring," *Cluster Computing*, vol. 22, no. 4, pp. 8217–8224, 2019.

[143] U Tata, H Huang, R. Carter, and J. Chiao, "Exploiting a patch antenna for strain measurements," *Measurement Science and Technology*, vol. 20, no. 1, p. 015 201, 2008.

[144] I. Ibanez-Labiano, M. S. Ergoktas, C. Kocabas, A. Toomey, A. Alomainy, and E. Ozden-Yenigun, "Graphene-based soft wearable antennas," *arXiv preprint arXiv:2005.09558*, 2020.

[145] P. Sambandam, M. Kanagasabai, R. Natarajan, M. G. N. Alsath, and S. Palaniswamy, "Miniaturized button like wban antenna for off body communication," *IEEE Transactions on Antennas and Propagation*, 2020.

[146] J. Zhang, R. Song, X. Zhao, *et al.*, "Flexible graphene-assembled film-based antenna for wireless wearable sensor with miniaturized size and high sensitivity," *ACS Omega*, 2020.

[147] T. Leng, X. Huang, K. Chang, J. Chen, M. A. Abdalla, and Z. Hu, "Graphene nanoflakes printed flexible meandered-line dipole antenna on paper substrate for low-cost rfid and sensing applications," *IEEE Antennas and Wireless Propagation Letters*, vol. 15, pp. 1565–1568, 2016.

[148] Z. Jing, Z. Guang-Yu, and S. Dong-Xia, "Review of graphene-based strain sensors," *Chinese Physics B*, vol. 22, no. 5, p. 057 701, 2013.

[149] P. Avouris and C. Dimitrakopoulos, "Graphene: Synthesis and applications," *Materials today*, vol. 15, no. 3, pp. 86–97, 2012.

[150] R. Song, Q. Wang, B. Mao, *et al.*, "Flexible graphite films with high conductivity for radio-frequency antennas," *Carbon*, vol. 130, pp. 164–169, 2018.

[151] R. Song, G.-L. Huang, C. Liu, *et al.*, "High-conductive graphene film based antenna array for 5G mobile communications," *International Journal of RF and Microwave Computer-Aided Engineering*, vol. 29, no. 6, e21692, 2019.

[152] P. Rewatkar, A. Kothuru, and S. Goel, "Pdms-based microfluidic glucose biofuel cell integrated with optimized laser-induced flexible graphene bioelectrodes," *IEEE Transactions on Electron Devices*, vol. 67, no. 4, pp. 1832–1838, 2020.

[153] A. Kothuru and S. G. Goel, "Laser induced graphene on phenolic resin and alcohol composite sheet for flexible electronics applications," *Flexible and Printed Electronics*, 2020.

[154] Z. Wan, N. T. Nguyen, Y. Gao, and Q. Li, "Laser induced graphene for biosensors," *Sustainable Materials and Technologies*, e00205, 2020.

[155] Y. Yu, P. C. Joshi, J. Wu, and A. Hu, "Laser-induced carbon-based smart flexible sensor array for multiflavors detection," *ACS applied materials & interfaces*, vol. 10, no. 40, pp. 34 005–34 012, 2018.

[156] F. Tehrani, M. Beltrán-Gastélum, K. Sheth, *et al.*, "Laser-induced graphene composites for printed, stretchable, and wearable electronics," *Advanced Materials Technologies*, vol. 4, no. 8, p. 1 900 162, 2019.

[157] D. S. Bergsman, B. A. Getachew, C. B. Cooper, and J. C. Grossman, "Preserving nanoscale features in polymers during laser induced graphene formation using sequential infiltration synthesis," *Nature communications*, vol. 11, no. 1, pp. 1–8, 2020.

[158] H. Kapton, *Polyimide film*, ASTM D-5213 [Online]; Wilmington, U.S, 2016, [accessed August, 2020], Wilmington, U.S., 2016.

[159] C. A. Balanis, *Antenna Theory: Analysis and Design*, 3rd ed. John Wiley & Sons, 2014, ch. 14.

[160] J. Lin, Z. Peng, Y. Liu, *et al.*, "Laser-induced porous graphene films from commercial polymers," *Nature communications*, vol. 5, no. 1, pp. 1–8, 2014.

[161] L. Groo, J. Nasser, L. Zhang, K. Steinke, D. Inman, and H. Sodano, "Laser induced graphene in fiberglass-reinforced composites for strain and damage sensing," *Composites Science and Technology*, vol. 199, p. 108 367, 2020.

[162] R. Ye, D. K. James, and J. M. Tour, "Laser-induced graphene: From discovery to translation," *Advanced Materials*, vol. 31, no. 1, p. 1 803 621, 2019.

[163] S.-G. Kim, O.-K. Park, J. H. Lee, and B.-C. Ku, "Layer-by-layer assembled graphene oxide films and barrier properties of thermally reduced graphene oxide membranes," *Carbon Letters (Carbon Lett.)*, vol. 14, no. 4, pp. 247–250, 2013.

[164] V. H. Pham, T. V. Cuong, S. H. Hur, *et al.*, "Chemical functionalization of graphene sheets by solvothermal reduction of a graphene oxide suspension in n-methyl-2-pyrrolidone," *Journal of Materials Chemistry*, vol. 21, no. 10, pp. 3371–3377, 2011.

[165] S Hyun and K Char, "Effects of strain on the dielectric properties of tunable dielectric $SrTio_3$ thin films," *Applied Physics Letters*, vol. 79, no. 2, pp. 254–256, 2001.

[166] T. Schimizu, "The effect of strain on the permittivity of SrTio3 from first-principles study," *Solid state communications*, vol. 102, no. 7, pp. 523–527, 1997.

[167] J. Zhu, J. J. Fox, N. Yi, and H. Cheng, "Structural design for stretchable microstrip antennas," *ACS applied materials & interfaces*, vol. 11, no. 9, pp. 8867–8877, 2019.

[168] A. H. Hamad and A. Mian, "Radio frequency response of flexible microstrip patch antennas under compressive and bending loads using multiphysics modeling approach," *International Journal of RF and Microwave Computer-Aided Engineering*, vol. 29, no. 3, e21649, 2019.

[169] S. Govindhasamy, V. Ramaswamy, A. Perumal, and D. Selvaraj, "A flexible microstrip antenna for health monitoring application in wireless body area network," *International Journal of Scientific and Technology Research*, vol. 9, pp. 7088–7092, Apr. 2020.

[170] N. Sakib, S. N. Ibrahim, M. I. Ibrahimy, M. S. Islam, and M. H. Mahfuz, "Design of microstrip patch antenna on rubber substrate with DGS for WBAN applications," 2020 IEEE Region 10 Symposium (TENSYMP), 2020, pp. 1050–1053.

[171] Q. Chen, Q. Gao, X. Wang, D. W. Schubert, and X. Liu, "Flexible, conductive, and anisotropic thermoplastic polyurethane/polydopamine/mxene foam for piezoresistive sensors and motion monitoring," *Composites Part A: Applied Science and Manufacturing*, vol. 155, p. 106 838, 2022.

[172] W. Zhang, C. Ma, L.-Z. Huang, *et al.*, "Stretchable, antifreezing, non-drying, and fast-response sensors based on cellulose nanocomposite hydrogels for signal detection," *Macromolecular Materials and Engineering*, vol. 306, no. 12, p. 2 100 549, 2021.

[173] A. Al-Fuqaha, M. Guizani, M. Mohammadi, M. Aledhari, and M. Ayyash, "Internet of things: A survey on enabling technologies, protocols, and applications," *IEEE communications surveys & tutorials*, vol. 17, no. 4, pp. 2347–2376, 2015.

[174] G. Breed *et al.*, "The fundamentals of patch antenna design and performance," *High frequency electronics*, vol. 3, no. 12, pp. 49–51, 2009.

[175] F. Shahzad, M. Alhabeb, C. B. Hatter, *et al.*, "Electromagnetic interference shielding with 2d transition metal carbides (mxenes)," *Science*, vol. 353, no. 6304, pp. 1137–1140, 2016.

[176] Q. Gao, Y. Pan, G. Zheng, C. Liu, C. Shen, and X. Liu, "Flexible multilayered mxene/thermoplastic polyurethane films with excellent electromagnetic interference shielding, thermal conductivity, and management performances," *Advanced Composites and Hybrid Materials*, vol. 4, pp. 274–285, 2021.

[177] B. Anasori and Y. Gogotsi, "Introduction to 2d transition metal carbides and nitrides (mxenes)," *2D Metal Carbides and Nitrides (MXenes) Structure, Properties and Applications*, pp. 3–12, 2019.

[178] M. Han, Y. Liu, R. Rakhmanov, *et al.*, "Solution-processed ti3c2tx mxene antennas for radio-frequency communication," *Advanced Materials*, vol. 33, no. 1, p. 2 003 225, 2021.

[179] H. Cheng, Y. Pan, X. Wang, *et al.*, "Ni flower/mxene-melamine foam derived 3d magnetic/conductive networks for ultra-efficient microwave absorption and infrared stealth," *Nano-Micro Letters*, vol. 14, no. 1, p. 63, 2022.

[180] Y.-Z. Zhang, Y. Wang, Q. Jiang, J. K. El-Demellawi, H. Kim, and H. N. Alshareef, "Mxene printing and patterned coating for device applications," *Advanced Materials*, vol. 32, no. 21, p. 1 908 486, 2020.

[181] M. Han, C. E. Shuck, R. Rakhmanov, *et al.*, "Beyond ti3c2t x: Mxenes for electromagnetic interference shielding," *ACS nano*, vol. 14, no. 4, pp. 5008–5016, 2020.

[182] A. Sarycheva, A. Polemi, Y. Liu, K. Dandekar, B. Anasori, and Y. Gogotsi, "2d titanium carbide (mxene) for wireless communication," *Science advances*, vol. 4, no. 9, eaau0920, 2018.

[183] L. Pu, J. Zhang, N. K. L. Jiresse, *et al.*, "N-doped mxene derived from chitosan for the highly effective electrochemical properties as supercapacitor," *Advanced Composites and Hybrid Materials*, pp. 1–14, 2022.

[184] Y. Guo, D. Wang, T. Bai, *et al.*, "Electrostatic self-assembled nife2o4/ti3c2tx mxene nanocomposites for efficient electromagnetic wave absorption at ultralow loading level," *Advanced Composites and Hybrid Materials*, vol. 4, no. 3, pp. 602–613, 2021.

[185] H. Cheng, Y. Pan, Q. Chen, *et al.*, "Ultrathin flexible poly (vinylidene fluoride)/mxene/silver nanowire film with outstanding specific emi shielding and high heat dissipation," *Advanced Composites and Hybrid Materials*, vol. 4, pp. 505–513, 2021.

[186] Y. Jia, Y. Pan, C. Wang, *et al.*, "Flexible ag microparticle/mxene-based film for energy harvesting," *Nano-Micro Letters*, vol. 13, pp. 1–12, 2021.

[187] C. Ma, M.-G. Ma, C. Si, X.-X. Ji, and P. Wan, "Flexible mxene-based composites for wearable devices," *Advanced Functional Materials*, vol. 31, no. 22, p. 2 009 524, 2021.

[188] Z. Yu, W. Feng, W. Lu, *et al.*, "Mxenes with tunable work functions and their application as electron-and hole-transport materials in non-fullerene organic solar cells," *Journal of Materials Chemistry A*, vol. 7, no. 18, pp. 11 160–11 169, 2019.

[189] F. Xie, F. Jia, L. Zhuo, *et al.*, "Ultrathin mxene/aramid nanofiber composite paper with excellent mechanical properties for efficient electromagnetic interference shielding," *Nanoscale*, vol. 11, no. 48, pp. 23 382–23 391, 2019.

[190] Y. Wan, P. Xiong, J. Liu, *et al.*, "Ultrathin, strong, and highly flexible ti3c2t x mxene/bacterial cellulose composite films for high-performance electromagnetic interference shielding," *ACS nano*, vol. 15, no. 5, pp. 8439–8449, 2021.

[191] J.-Y. Li, Y.-H. Li, F. Zhang, Z.-R. Tang, and Y.-J. Xu, "Visible-light-driven integrated organic synthesis and hydrogen evolution over 1d/2d cds-ti3c2tx mxene composites," *Applied Catalysis B: Environmental*, vol. 269, p. 118 783, 2020.

[192] J. Halim, M. R. Lukatskaya, K. M. Cook, *et al.*, "Transparent conductive two-dimensional titanium carbide epitaxial thin films," *Chemistry of Materials*, vol. 26, no. 7, pp. 2374–2381, 2014.

[193] S. J. Kim, H.-J. Koh, C. E. Ren, *et al.*, "Metallic ti3c2t x mxene gas sensors with ultrahigh signal-to-noise ratio," *ACS nano*, vol. 12, no. 2, pp. 986–993, 2018.

[194] A Rozmysłowska-Wojciechowska, T Wojciechowski, W Ziemkowska, L Chlubny, A Olszyna, and A. Jastrzębska, "Surface interactions between 2d ti3c2/ti2c mxenes and lysozyme," *Applied Surface Science*, vol. 473, pp. 409–418, 2019.

[195] V. Presser, M. Naguib, L. Chaput, A. Togo, G. Hug, and M. W. Barsoum, "First-order raman scattering of the max phases: Ti2aln, ti2alc0. 5n0. 5, ti2alc,(ti0. 5v0. 5) 2alc, v2alc, ti3alc2, and ti3gec2," *Journal of Raman Spectroscopy*, vol. 43, no. 1, pp. 168–172, 2012.

[196] S. Elumalai, M. Yoshimura, and M. Ogawa, "Simultaneous delamination and rutile formation on the surface of ti3c2tx mxene for copper adsorption," *Chemistry–An Asian Journal*, vol. 15, no. 7, pp. 1044–1051, 2020.

[197] M. Hu, Z. Li, T. Hu, S. Zhu, C. Zhang, and X. Wang, "High-capacitance mechanism for ti3c2 t x mxene by in situ electrochemical raman spectroscopy investigation," *ACS nano*, vol. 10, no. 12, pp. 11 344–11 350, 2016.

[198] B. Wang, T. Shi, Y. Zhang, C. Chen, Q. Li, and Y. Fan, "Lignin-based highly sensitive flexible pressure sensor for wearable electronics," *Journal of Materials Chemistry C*, vol. 6, no. 24, pp. 6423–6428, 2018.

[199] Y. Ma, N. Liu, L. Li, *et al.*, "A highly flexible and sensitive piezoresistive sensor based on mxene with greatly changed interlayer distances," *Nature communications*, vol. 8, no. 1, p. 1207, 2017.

[200] D. M. Pozar, *Microwave Engineering*, 4th ed. John Wiley & Sons, Inc., 2011.

[201] Y. Cao and L. An, "Anomalous piezo-dielectricity of a polymer-derived amorphous silicoaluminum oxycarbide (sialco)," *Ceramics International*, vol. 44, no. 2, pp. 1467–1470, 2018.

[202] K. Guerchouche, E. Herth, L. E. Calvet, N. Roland, and C. Loyez, "Conductive polymer based antenna for wireless green sensors applications," *Microelectronic Engineering*, vol. 182, pp. 46–52, 2017.

[203] Q. Liu, T. Le, S. He, and M. M. Tentzeris, "Button-shaped radio-frequency identification tag combining three-dimensional and inkjet printing technologies," *IET Microwaves, Antennas & Propagation*, vol. 10, no. 7, pp. 737–741, 2016.

[204] A. Kumar, H. Saghlatoon, T.-G. La, *et al.*, "A highly deformable conducting traces for printed antennas and interconnects: Silver/fluoropolymer composite amalgamated by triethanolamine," *Flexible and Printed Electronics*, vol. 2, no. 4, p. 045 001, 2017.

[205] Z Hamouda, J.-L. Wojkiewicz, A. A. Pud, L. Koné, S. Bergheul, and T. Lasri, "Magnetodielectric nanocomposite polymer-based dual-band flexible antenna for wearable applications," *IEEE Transactions on Antennas and Propagation*, vol. 66, no. 7, pp. 3271–3277, 2018.

[206] T. A. Elwi and A. M. Al-Saegh, "Further realization of a flexible metamaterial-based antenna on indium nickel oxide polymerized palm fiber substrates for rf energy harvesting," *International Journal of Microwave and Wireless Technologies*, vol. 13, no. 1, pp. 67–75, 2021.

[207] J. W. Sanders, J. Yao, and H. Huang, "Microstrip patch antenna temperature sensor," *IEEE sensors journal*, vol. 15, no. 9, pp. 5312–5319, 2015.

[208] W. B. Han, J. H. Lee, J.-W. Shin, and S.-W. Hwang, "Advanced materials and systems for biodegradable, transient electronics," *Advanced Materials*, vol. 32, no. 51, p. 2 002 211, 2020.

[209] B. Yalagala, S. Khandelwal, J Deepika, and S. Badhulika, "Wirelessly destructible mgo-pvp-graphene composite based flexible transient memristor for security applications," *Materials Science in Semiconductor Processing*, vol. 104, p. 104 673, 2019.

[210] T. A. Elwi, "Novel uwb printed metamaterial microstrip antenna based organic substrates for rf-energy harvesting applications," *AEU-International Journal of Electronics and Communications*, vol. 101, pp. 44–53, 2019.

[211] T. A. Elwi, Z. A. Abdul Hassain, and O. A. Tawfeeq, "Hilbert metamaterial printed antenna based on organic substrates for energy harvesting," *IET Microwaves, Antennas & Propagation*, vol. 13, no. 12, pp. 2185–2192, 2019.

[212] W. Seo and S. T. Phillips, "Patterned plastics that change physical structure in response to applied chemical signals," *Journal of the American Chemical Society*, vol. 132, no. 27, pp. 9234–9235, 2010.

[213] Y. H. Jung, T.-H. Chang, H. Zhang, *et al.*, "High-performance green flexible electronics based on biodegradable cellulose nanofibril paper," *Nature communications*, vol. 6, no. 1, p. 7170, 2015.

[214] F. Xu, H. Zhang, L. Jin, *et al.*, "Controllably degradable transient electronic antennas based on water-soluble pva/tio2 films," *Journal of materials science*, vol. 53, no. 4, pp. 2638–2647, 2018.

[215] S.-W. Hwang, J.-K. Song, X. Huang, *et al.*, "High-performance biodegradable/transient electronics on biodegradable polymers," *Advanced Materials*, vol. 26, no. 23, pp. 3905–3911, 2014.

[216] S.-W. Hwang, X. Huang, J.-H. Seo, *et al.*, "Materials for bioresorbable radio frequency electronics," *Advanced Materials*, vol. 25, no. 26, pp. 3526–3531, 2013.

[217] R. Li, H. Qi, Y. Ma, *et al.*, "A flexible and physically transient electrochemical sensor for real-time wireless nitric oxide monitoring," *Nature communications*, vol. 11, no. 1, p. 3207, 2020.

[218] Y. Guo, M. Zhong, Z. Fang, P. Wan, and G. Yu, "A wearable transient pressure sensor made with mxene nanosheets for sensitive broad-range human–machine interfacing," *Nano letters*, vol. 19, no. 2, pp. 1143–1150, 2019.

[219] C. Dagdeviren, S.-W. Hwang, Y. Su, *et al.*, "Transient, biocompatible electronics and energy harvesters based on zno," *small*, vol. 9, no. 20, pp. 3398–3404, 2013.

[220] D.-H. Kim, S. Wang, H. Keum, *et al.*, "Thin, flexible sensors and actuators as 'instrumented'surgical sutures for targeted wound monitoring and therapy," *Small*, vol. 8, no. 21, pp. 3263–3268, 2012.

[221] R. Bhattacharyya, C. Floerkemeier, and S. Sarma, "Low-cost, ubiquitous rfid-tag-antenna-based sensing," *Proceedings of the IEEE*, vol. 98, no. 9, pp. 1593–1600, 2010.

[222] S. H. Ghadeer, S. K. A. Rahim, M. Alibakhshikenari, *et al.*, "An innovative fractal monopole mimo antenna for modern 5g applications," *AEU-International Journal of Electronics and Communications*, vol. 159, p. 154 480, 2023.

[223] M. M. Ismail, T. A. Elwi, and A. Salim, "A miniaturized printed circuit crlh antenna-based hilbert metamaterial array," *Journal of Communications Software and Systems*, vol. 18, no. 3, pp. 236–243, 2022.

[224] M. R. Abdul-Aziz, S. A. Mohassieb, N. A. Eltresy, *et al.*, "Enhancing the performance of polygon monopole antenna using graphene/tmdcs heterostructures," *IEEE Transactions on Nanotechnology*, vol. 19, pp. 269–273, 2020.

[225] T. A. Elwi, D. A. Jassim, and H. H. Mohammed, "Novel miniaturized folded uwb microstrip antenna-based metamaterial for rf energy harvesting," *International Journal of Communication Systems*, vol. 33, no. 6, e4305, 2020.

[226] S. Krishnan, X. He, F. Zhao, Y. Zhang, S. Liu, and R. Xing, "Dual labeled mesoporous silica nanospheres based electrochemical immunosensor for ultrasensitive detection of carcinoembryonic antigen," *Analytica Chimica Acta*, vol. 1133, pp. 119–127, 2020.

[227] S. Mani, S. Ramaraj, S.-M. Chen, B. Dinesh, and T.-W. Chen, "Two-dimensional metal chalcogenides analogous nise2 nanosheets and its efficient electrocatalytic performance towards glucose sensing," *Journal of colloid and interface science*, vol. 507, pp. 378–385, 2017.

[228] N. Vishnu, P. Sahatiya, C. Y. Kong, and S. Badhulika, "Large area, one step synthesis of nise2 films on cellulose paper for glucose monitoring in bio-mimicking samples for clinical diagnostics," *Nanotechnology*, vol. 30, no. 35, p. 355 502, 2019.

[229] N. Bokka, V. Adepu, A. Tiwari, S. Kanungo, and P. Sahatiya, "A detailed comparative performance analysis of the transition metal di-chalcogenides (tmds) based strain sensors through experimental realisations and first principle calculations," *FlatChem*, vol. 32, p. 100 344, 2022.

[230] N. Bokka and P. Sahatiya, "Heat and light triggered mechanical destruction of 2d materials based electronic devices fabricated on wax substrate," *FlatChem*, vol. 35, p. 100 423, 2022.

[231] D. Lu, Y. Yan, R. Avila, *et al.*, "Bioresorbable, wireless, passive sensors as temporary implants for monitoring regional body temperature," *Advanced Healthcare Materials*, vol. 9, no. 16, p. 2 000 942, 2020.

[232] N. Bokka, D. Som, S. Kanungo, and P. Sahatiya, "Investigation of the transduction mechanism of few layer sns for pressure and strain sensing- experimental correlation with first principles study," *IEEE Sensors Journal*, vol. 21, no. 15, pp. 17 254–17 261, 2021.

[233] S. QuantumATK, *Quantumatk*, quantumwise website, [Online - accessed November, 2022], version 2021.06.

[234] D. Cholakova and N. Denkov, "Rotator phases in alkane systems- in bulk, surface layers and micro/nano-confinements," *Advances in colloid and interface science*, vol. 269, pp. 7–42, 2019.

[235] M. Ahadi, M. Roudjane, M.-A. Dugas, A. Miled, and Y. Messaddeq, "Wearable sensor based on flexible sinusoidal antenna for strain sensing applications," *Sensors*, vol. 22, no. 11, p. 4069, 2022.

[236] L. Zhu, W. Li, X. Han, and Y. Peng, "Microfluidic flexible substrate integrated microstrip antenna sensor for sensing of moisture content in lubricating oil," *International Journal of Antennas and Propagation*, vol. 2020, pp. 1–9, 2020.

[237] I. Ibanez-Labiano and A. Alomainy, "Dielectric characterization of non-conductive fabrics for temperature sensing through resonating antenna structures," *Materials*, vol. 13, no. 6, p. 1271, 2020.

[238] X. Lin, B.-C. Seet, and F. Joseph, "Wearable humidity sensing antenna for ban applications over 5g networks," in *2018 IEEE 19th Wireless and Microwave Technology Conference (WAMICON)*, IEEE, 2018, pp. 1–4.

[239] M. P. McGrath, R. N. Sabouni, and A.-V. H. Pham, "Development of nanobased resonator gas sensors for wireless sensing systems," *Nanosensing: Materials and Devices*, vol. 5593, pp. 62–72, 2004.

[240] K. S. Kiran, A. O. Asok, S. G. Nath, and S. Dey, "Microwave imaging with modified stack type pifa antenna utilizing sar algorithm," in *2022 IEEE Microwaves, Antennas, and Propagation Conference (MAPCON)*, IEEE, 2022, pp. 1899–1902.

[241] R. Bharadwaj, S. Swaisaenyakorn, C. G. Parini, J. Batchelor, and A. Alomainy, "Localization of wearable ultrawideband antennas for motion capture applications," *IEEE Antennas and Wireless Propagation Letters*, vol. 13, pp. 507–510, 2014.

[242] M. A. Belen, P. Mahouti, F. Güneş, and H. P. PARTAL, "Design and implementation of doppler microwave motion sensor for indoor application," *Sigma Journal of Engineering and Natural Sciences*, vol. 36, no. 3, pp. 849–859, 2018.

[243] M. Bhavani and K Babulu, "Design and implementation of low cost microwave motion sensor based security system," *Int. J. Eng. Res. Technol.(IJERT)*, vol. 2, pp. 1696–1700, 2013.

[244] J.-Y. Lee, K.-B. Lee, and S.-H. Choi, "A design of motion detecting sensor using microwave," in *2007 Asia-Pacific Microwave Conference*, IEEE, 2007, pp. 1–4.

[245] A. Yin, C. Zhang, J. Luo, *et al.*, "A highly sensitive and miniaturized wearable antenna based on mxene films for strain sensing," *Materials Advances*, vol. 4, no. 3, pp. 917–922, 2023.

[246] S. G. Kirtania, A. W. Elger, M. R. Hasan, *et al.*, "Flexible antennas- a review," *Micromachines*, vol. 11, no. 9, p. 847, 2020.

[247] A. Hassan, S. Ali, J. Bae, and C. H. Lee, "All printed antenna based on silver nanoparticles for 1.8 ghz applications," *Applied Physics A*, vol. 122, pp. 1–7, 2016.

[248] J.-H. So, J. Thelen, A. Qusba, G. J. Hayes, G. Lazzi, and M. D. Dickey, "Reversibly deformable and mechanically tunable fluidic antennas," *Advanced Functional Materials*, vol. 19, no. 22, pp. 3632–3637, 2009.

[249] S. Cheng and Z. Wu, "A microfluidic, reversibly stretchable, large-area wireless strain sensor," *Advanced functional materials*, vol. 21, no. 12, pp. 2282–2290, 2011.

[250] A. O. Nwajana and E. R. Obi, "A review on siw and its applications to microwave components," *Electronics*, vol. 11, no. 7, p. 1160, 2022.

[251] D. Chaturvedi and S Raghavan, "Circular quarter-mode siw antenna for wban application," *IETE Journal of Research*, vol. 64, no. 4, pp. 482–488, 2018.

[252] S. Mukherjee, A. Biswas, and K. V. Srivastava, "Broadband substrate integrated waveguide cavity-backed bow-tie slot antenna," *IEEE Antennas and Wireless Propagation Letters*, vol. 13, pp. 1152–1155, 2014.

[253] S. Nandi and A. Mohan, "An siw cavity-backed self-diplexing antenna," *IEEE Antennas and Wireless Propagation Letters*, vol. 16, pp. 2708–2711, 2017.

[254] Z. G. Liu and Y. X. Guo, "Dual band low profile antenna for body centric communications," *IEEE Transactions on Antennas and Propagation*, vol. 61, no. 4, pp. 2282–2285, 2012.

[255] J. Lacik and T. Mikulasek, "Circular ring-slot antenna fed by siw for wban applications," in *2013 7th European Conference on Antennas and Propagation (EuCAP)*, IEEE, 2013, pp. 213–216.

[256] M. Dong, D. Shen, C. Ma, Z.-H. Ma, X. Li, and J. Su, "A novel split ring slot antenna with multiband characteristics based on siw," in *2016 11th International Symposium on Antennas, Propagation and EM Theory (ISAPE)*, IEEE, 2016, pp. 39–42.

[257] C.-M. Liu, S.-Q. Xiao, and K. Wu, "Wideband slot antenna backed by cylindrical substrate-integrated waveguide cavity," *IEEE Transactions on Antennas and Propagation*, vol. 67, no. 3, pp. 1509–1518, 2018.

[258] G. Q. Luo, Z. F. Hu, W. J. Li, X. H. Zhang, L. L. Sun, and J. F. Zheng, "Bandwidth-enhanced low-profile cavity-backed slot antenna by using hybrid siw cavity modes," *IEEE transactions on Antennas and Propagation*, vol. 60, no. 4, pp. 1698–1704, 2012.

[259] A. J. Martinez-Ros, J. L. Gómez-Tornero, and F. Quesada-Pereira, "Efficient analysis and design of novel siw leaky-wave antenna," *IEEE Antennas and Wireless Propagation Letters*, vol. 12, pp. 496–499, 2013.

[260] R. Moro, S. Agneessens, H. Rogier, and M. Bozzi, "Circularly-polarised cavity-backed wearable antenna in siw technology," *IET Microwaves, Antennas & Propagation*, vol. 12, no. 1, pp. 127–131, 2018.

[261] M. E. Lajevardi and M. Kamyab, "A low-cost wideband quasi-yagi siw-based textile antenna," *Progress in Electromagnetics Research Letters*, vol. 67, pp. 53–59, 2017.

[262] L. Alonso-González, S. Ver-Hoeye, M. Fernández-García, C. Vázquez-Antuña, and F. L.-H. Andrés, "On the development of a novel mixed embroidered-woven slot antenna for wireless applications," *IEEE Access*, vol. 7, pp. 9476–9489, 2019.

[263] J. Xu, W. Hong, H. Tang, Z. Kuai, and K. Wu, "Half-mode substrate integrated waveguide (hmsiw) leaky-wave antenna for millimeter-wave applications," *IEEE antennas and wireless propagation letters*, vol. 7, pp. 85–88, 2008.

[264] M. E. Lajevardi and M. Kamyab, "Ultraminiaturized metamaterial-inspired siw textile antenna for off-body applications," *IEEE antennas and wireless propagation letters*, vol. 16, pp. 3155–3158, 2017.

[265] G. A. Casula, G. Montisci, and G. Muntoni, "A novel design for dual-band wearable textile eighth-mode siw antennas," *IEEE Access*, vol. 11, pp. 11 555–11 569, 2023.

[266] R. M. Krishnan and G Kannan, "A compact dual-sense circularly polarized siw textile antenna for body-centric wireless communication," *AEU-International Journal of Electronics and Communications*, vol. 160, p. 154 523, 2023.

[267] R. Moro, S. Kim, M. Bozzi, and M. Tentzeris, "Inkjet-printed paper-based substrate-integrated waveguide (siw) components and antennas," *International Journal of Microwave and Wireless Technologies*, vol. 5, no. 3, pp. 197–204, 2013.

List of Publications Based on This Thesis

Journals

1. **B. Sindhu**, A. Kothuru, P. Sahatiya, S. Goel, and S. Nandi, “Laser-induced graphene printed wearable flexible antenna-based strain sensor for wireless human motion monitoring,” ***IEEE Transactions on Electron Devices***, vol. 68, no. 7, pp. 3189–3194, Jul. 2021.

2. **B. Sindhu**, V. Adepu, P. Sahatiya, and S. Nandi, “An MXene based flexible patch antenna for pressure and level sensing applications,” ***FlatChem***, vol. 33, p. 100367, May 2022.

3. **B. Sindhu**, N. Bokka, N. Bahadursha, S. Kanungo, P. Sahatiya, and S. Nandi, "Heat triggered Wax/$NiSe_2$ based transient microstrip antenna for pressure sensing application," ***Materials Science in Semiconductor Processing***, vol. 166, p.107730, 2023.

4. **B. Sindhu**, S. Siraj, P. Sahatiya, and S. Nandi, "MXene-Based Sixteenth-Mode Flexible SIW Antenna for Conformal Wireless Applications," ***Flexible and Printed Electronics***, (Under Review).

Conferences

1. **B. Sindhu** and S. Nandi, “A cavity-backed circular SIW antenna for X-band applications,” ***IEEE, Proc. URSI Regional Conf. Radio Sci.***, Varanasi, India, pp. 1–3, Feb. 2020.

2. **B. Sindhu**, Y. C. Gandhi, P. Sahatiya, and S. Nandi, "A study on contactless flexible antenna-based motion sensor for smart wireless communication," ***IEEE, Microwave, Antennas, and Propagation Conference (MAPCON)***, December 2023 [Presented].

Biographies

Candidate Biography

Battina Sindhu received the B.Tech. Degree in Electronics and Communication Engineering with specialization in Communications in 2017 from K L University, Vijayawada, and the M.Tech. Degree in Communication Engineering and Signal Processing in 2019 from Amrita Vishwa Vidyapeetham, Coimbatore. She is currently pursuing her Ph.D. from Birla Institute of Technology & Science (BITS), Pilani, Hyderabad Campus, and is working on flexible antennas for sensing applications. Her research interests include antenna theory and design, MIMO antenna, printable wearable flexible microstrip antennas, sensing applications, nanomaterials for RF devices, and SIW structures.

Supervisor Biography

Dr. Sourav Nandi completed his B. Tech in Electronics and Communication Engineering in 2010 from West Bengal University of Technology. He completed his M. Tech in Communication Engineering from the University of Kalyani, West Bengal, in 2013. He achieved a PhD in RF & Microwave Engineering in 2018 from the Indian Institute of Technology, Kharagpur. Presently, he is working in the Electrical and Electronics Engineering Department as an assistant professor at Birla Institute of Technology & Science (BITS), Pilani, Hyderabad Campus, India. His research area includes the design of antennas and other components for RF, microwave and millimetre wave applications. He has published 15 papers in international journals and 4 conference papers. He is a member of IEEE. He also serves as a reviewer of various reputed international journals, such as IEEE Open Journal of Antennas & Propagation, IEEE Transactions on Antennas & Propagation, IEEE Access, IEEE Sensors Journal, Frequenz etc.

Co-Supervisor Biography

Dr. Parikshit Sahatiya received his PhD degree from Indian Institute of Technology Hyderabad, India. Post PhD, he joined Redpine Signals Inc. as Research Scientist. Currently, he is an Assistant Professor in the Department of Electrical and Electronics Engineering, Birla Institute of Technology and Science (BITS) Pilani Hyderabad Campus. Dr. Sahatiya's research is very interdisciplinary which include 2D materials based flexible and wearable nanoelectronic devices and sensors. Some of applications which Dr. Sahatiya's lab have demonstrated include artificial skin, human motion monitoring, wireless keypad, sleep apnea diagnostics and posture analysis and smart bed etc. Further, Dr. Sahatiya's lab also focuses on understanding the transport of complex heterostructure (including monolayer 2D vdW vertical heterostructure) which have led to the development of broadband photodetectors. Recently, Dr. Sahatiya has been exploring memristors and trying to understand the physical mechanism of the same. Further, he is also working tow arms the device-circuit interface using memristor by developing data driven models for the memristors. Also, Dr. Sahatiya's lab has also been actively working in the field of Transient electronics and exploring different triggers for the destruction of the devices. Dr. Sahatiya has published more than 100 Journal articles, 5 patents and have delivered talks nationally and internationally. Dr. Sahatiya's lab is currently being funded by Government (SERB), DRDO and Industry grants and have a fully equipped lab for the development of various 2D materials based devices. Dr. Sahatiya serves as an Associate Editor for Nature Scientific Reports, Microelectronic Engineering Journal, IEEE Access, Chip, Materials Today: Electronics and Springer Nature Graphene and 2D Materials and Junior Editorial board member of IOP Journal of Mircomechanics and Microengineering. Dr. Sahatiya has received Young Scientist and Medal Lecture at ICLED 2023, Singapore. Dr. Sahatiya has served as a Visiting Assistant Professor at Purdue University and Tufts University, USA. Dr. Sahatiya is a member of the Royal Society of Chemistry and also Materials Research Society.